Development and regeneration of neuronal circuits in the vertebrate retina

Florence D. D'Orazi

A dissertation

submitted in partial fulfillment of the

requirements for the degree of

Doctor of Philosophy

University of Washington

2016

Reading Committee:

Rachel O. Wong, Chair

David Raible

Thomas Reh

Program Authorized to Offer Degree:

Neuroscience

University of Washington

Abstract

Development and regeneration of neuronal circuits in the vertebrate retina

Florence D. D'Orazi

Chair of the Supervisory Committee:

Professor Rachel O. Wong

Department of Biological Structure

Like in other parts of the central nervous system (CNS), information processing in the retina depends upon the exquisite organization of synaptic connectivity amongst diverse neuronal cell types. Assembly of neuronal circuits during retinal development is highly orchestrated. Recapitulating the precision of this process presents a major challenge for therapeutic efforts to repair the retina after injury or disease in mammals. Whereas mammals cannot replenish lost neurons in their retinas, zebrafish show an innate ability to regenerate their retinas. In this work, I sought to advance our understanding of the restorative potential of retinal regeneration. I capitalized on the native regenerative capacity of the zebrafish to provide some of the first insights into the fidelity of neuronal replacement and integration in the retina.

In Chapter 1, I review the factors and mechanisms that shape organized circuitry during retinal development, as well as summarize the current state of the field in teleost and mammalian retinal regeneration research. In Chapters 2 and 3, I investigate bipolar cells, interneurons that convey light signals from photoreceptors to the retinal output neurons. In Chapter 2, I explore the cellular strategies that functionally distinct bipolar cell types undertake during retinal development to attain their characteristic morphologies and dendritic wiring patterns. I use this knowledge in Chapter 3 as a framework to assess the ability of regenerated circuits to engage developmental mechanisms to re-establish their original patterning. I utilize a genetically targeted cell ablation technique to trigger regeneration of bipolar cells *in situ*, and investigate the precision with which regenerated cells integrate into a mature retinal network. In Chapter 4, I

examine the specificity of endogenous neuronal replacement by comparing the composition of regenerated cone photoreceptor populations after ablation of distinct cone types. Lastly, in Chapter 5 I summarize my findings and discuss future directions to address questions raised by this work.

TABLE OF CONTENTS

LIST OF FIGURES

LIST OF TABLES

ACKNOWLEDGEMENTS

As the saying goes, “it takes a village.” Many hands have guided my development as a neuroscientist over the years.

I owe a debt to my first advisor, Hwai-Jong Cheng, for introducing me to developmental neuroscience and setting me on my path toward research. I am also grateful for the massive support I received from Regina Faulkner Lemus during my tenure in HJ’s lab. I can now appreciate how chaotic the day of a graduate student can be, and it makes me appreciate even more the time that Regina spent teaching me, and her patience throughout. I would also like to acknowledge Kim McAllister, who was a mentor and role model to me. I thank Kim for encouraging me to pursue my love of research, but also for her honesty when she told me “Research is really hard, so you had better really love it.”

Through no real planning of my own, I found myself a member of Rachel’s Wong lab in 2011. Looking back, I can’t believe my good fortune in landing Rachel as an advisor. Rachel consistently gave me her attention and guidance throughout my graduate career. I am especially grateful to her for pushing me to advance myself not only as a scientist at the bench but also as a science communicator. I now know that few graduate students are afforded as many opportunities as Rachel provided me with to grow as both an author and an orator. I appreciate the kindness and patience that Rachel has showed me over the years, but even more so I appreciate the times that she set high expectations of me. Rachel pushed my standard of excellence, and thanks to her, I can look back on my time and work in graduate school with pride.

Rachel has also done an incredible job of recruiting some of the most brilliant yet humble people I know to her lab. Every member of the Wong lab has touched this work in some way, but I’d like to name a few people in particular. Above all, I have to thank Takeshi Yoshimatsu, who was my post-doc mentor, and like a second advisor to me. Takeshi provided the vast majority of my graduate school training at the bench. I am forever thankful to him for the willingness, and even eagerness, he showed in helping me battle problems in the lab. I think that there is no better nourishment for a new scientist than a lab environment that is friendly to questions, and Takeshi made sure I could always count on that. He also led by example; his passion for science, and the tenacity of his approach to answering research questions, is awe-inspiring. I am lucky to have had such a fantastic scientist as a mentor and a friend these past 5 years.

Special thanks to the past Wong lab members who supported me when I started with the Wong lab, especially Felice Dunn, Sachi Suzuki, Luca Della Santina, Haru Okawa, and Adam Bleckert. Each of them is a brilliant scientist in their own right, and had plenty to do, yet was willing to drop their own work at a moment’s notice to help me. They also each offered kind words of encouragement that boosted my energy and confidence as a floundering newbie. I will never forget their selflessness.

I have also benefited greatly from the comradery and mentorship of current Wong lab members. Thank you to Mrinalini Hoon, Chi Zhang, and Wan-Qing Yu for their advice and knowledge; their feedback in and out of lab meetings was critical to my progress. Thank you to Clare Gamlin

and Phil Mardoum, my fellow grad students, who were always available for a laugh or a beer when needed. I only wish you two had joined the lab earlier! Thank you to Kaori Oda, Mei Zhang, and John Campbell, for your reliable behind-the-scenes support. Kaori and Mei especially facilitated my work during the last critical stages by taking on the task of managing our fish colony, and I am extremely grateful to them for that.

Thank you to the past and present members of my thesis committee, Dave Raible, Tom Reh, Cecilia Moens, Jay Parrish, and Jon Cooper, for their thoughtful insight and support. I truly appreciate the time and care that each of you invested in my future. In particular I'd like to acknowledge Dave for steering the Developmental Biology Training Grant. Dave fostered a fantastic learning environment for myself and the other trainees. I am indebted to him and my fellow trainees for broadening my scientific perspective, and for providing me fundamental training on how to do rigorous research.

I am lucky to have made friends with a wonderful group of people in graduate school. There are too many to list altogether, but they each taught me to better enjoy science, as well as my life outside the lab. I must specifically thank Stephanie Seeman, Sweta Agrawal, Leah Bakst, Sarah Pickett, and Bethany Kondiles. You have each inspired me with your passion and quality of character. I look up to each of you, and I can't express how much your encouragement has meant to me. Sarah, along with Eric Thomas and Philia Gau, were my comrades in arms in zebrafish research, and they provided me with candid and helpful criticisms that made my work far better. But, I am most grateful to them for all times spent talking and laughing together outside the lab over beers or tea. And thank you to Anna, my oldest friend, whose sheer energy and enthusiasm helped propel me through the last and most difficult stages of my work.

I'd especially like to acknowledge the first two mentors I ever had, my mom and dad, Deborah and Terry D'Orazi. Both of my parents are models of the success that comes from hard work and fortitude. They each also instilled in me the joy that comes from setting and achieving high expectations of myself in my work, and their lessons forged my greatest strengths as a scientist. Mom and Dad, there are no words to express the gratitude I have for your guidance, and especially for your unwavering encouragement and love all these years.

Finally, I would like to recognize the incredible support I received from my husband and partner, Brian Turner. Brian kept me nourished through the culmination of this thesis. He fed me delicious meals, offered me his respect and thoughts in even the most stressful times, and always had me laughing. Brian also kept me motivated simply by being himself; his insatiable curiosity about the world around him inspires and challenges me every day. Brian, thank you for believing in me.

FD

Seattle, 2016

Chapter 1. Introduction

Information processing in the central nervous system (CNS) depends upon stereotypic patterns of synaptic wiring amongst diverse neuronal cell types. Because most CNS circuits in adult mammals do not spontaneously replace lost neurons, neuronal damage can result in debilitating dysfunction. The retina in particular is susceptible to a number of inherited and acquired neuronal degenerative diseases (Boye et al., 2013; Schmidt et al., 2008), which can lead to irreversible blindness. Much effort has thus been made towards repairing retinal circuits by transplanting cells or tissue into the damaged environment. Indeed, neurons introduced by cell transplantation can form synaptic contacts with intact host neurons in the retina (Barber et al., 2013; Hertz et al., 2014; MacLaren et al., 2006; Pearson et al., 2012; Singh et al., 2013; Venugopalan et al., 2016), and importantly, are capable of recovering some aspects of normal physiology within the undamaged (Venugopalan et al., 2016) or dysfunctional retina (Pearson et al., 2012). However, transplantation efforts have been met with several challenges, including limitations in transplantation efficiency and neuronal survival, and the potential for immune rejection.

To overcome the obstacles inherent in cell transplantation, there has been an increasing effort to replace lost neurons instead by stimulating endogenous production of cells *in situ* (Arlotta and Berninger, 2014; Becker and Becker, 2015). Unlike mammals, teleosts demonstrate an innate and robust ability to regenerate retinal neurons, making them an ideal model system for understanding the restorative potential of endogenous neuronal regeneration. Investigations in zebrafish revealed that their regenerative capacity stems from the latent neurogenic potential of glial cells in the retina (Bernardos et al., 2007; Fausett and Goldman, 2006; Fimbel et al., 2007; Ramachandran et al., 2010). Recent attempts to stimulate retinal regeneration in mammals have consequentially focused on glial cells; researchers successfully induced the production of new retinal neurons *in vivo* by stimulating resident glia after retinal injury in mice (Ueki et al., 2015). Nonetheless, progress in this field has fallen short of understanding the capacity of regenerated circuits to reinstate all of the elements of organized neuronal circuitry. Does endogenous retinal regeneration preserve cellular diversity, as well as the appropriate proportions of each neuronal population? Can regenerated neurons wire accurately with a mature, pre-existing retinal circuit?

Portions of Chapter 1 were published in Dendrites, Development and Disease by Springer Japan, which maintains copyrights for this material, and has been reprinted with permission: D'Orazi F.D. and Yoshimatsu, T. (2016). Development of synaptic input patterns on dendrites of retinal neurons. In Dendrites, Development and Disease, Emoto, K., Wong, R., Huang, E. Hoogenraad, C., eds. (Japan: Springer Japan).

Re-assembly of neuronal circuits during regeneration must to some degree recapitulate the steps taken during developmental assembly, including cell amplification, neuronal differentiation and morphogenesis, and synaptogenesis. Knowledge of the mechanisms that regulate each of these steps during CNS development thus provides a framework for investigating circuit assembly during regeneration. However, regenerated neurons face the additional challenge of integrating into a previously established network; the cellular composition and molecular environment of the mature CNS likely differ from that during initial development, when neuronal circuits are first assembled. Below, I review our current understanding of the mechanisms that regulate neuronal cell fate and composition, as well as stereotypic features of synaptic connectivity during development of the vertebrate retina. I also provide an overview of the regeneration process in zebrafish, and discuss the relevance of this knowledge to retinal repair in mammals.

1.1 Organization of vertebrate retinal circuits

The retina is an especially tractable neural circuit for dissecting the relationship between neurite structure, synaptic connections, and physiological function at the level of the individual neuron. As a consequence of the highly organized synaptic wiring between retinal neurons, important visual functions, from color vision to motion detection, arise in the retina. The retina hosts diverse neuronal cell types, and its layered organization facilitates relatively easy reconstruction of neuron morphology, as well as identification of synapses. Further, as a sensory system the retina offers access to neuronal output under physiological conditions.

The retina is populated by five major neuronal cell classes and a single glial cell class. The nuclei of different cell types are by and large organized into one of three nuclear layers, and the processes and synaptic connections of neurons are confined to synaptic laminae, the outer and inner plexiform layers (OPL and IPL), as schematized in Figure 1.1. Müller glia project their apical and basal processes to the outer and inner limiting membranes of the retina, respectively, and provide physical and metabolic support for the surrounding neurons (Bringmann et al., 2006). Two major photoreceptor classes populate the outer nuclear layer (ONL), and transduce light stimuli into an electrical signal via the phototransduction cascade (Arshavsky and Burns, 2012). Both photoreceptor types are excitatory, and release glutamate in the dark. Absorption of photons activates the phototransduction cascade, resulting in hyperpolarization of the

photoreceptor, and thus a decrease in glutamate release onto postsynaptic cells. Rod photoreceptors express opsins specialized to absorb photons in dim light, whereas cone photoreceptors possess opsins that function at high light levels and detect specific light wavelengths, thereby contributing to color vision. Humans have three cone types, which respond to long, medium, or short wavelengths (red, green, and blue, respectively), and zebrafish possess an additional cone type that is sensitive to ultraviolet (UV) wavelengths (Ebrey and Koutalos, 2001; Vihtelic et al., 1999)(Figure 1.2). Whereas cone photoreceptors are primarily restricted to the foveal area in humans, the four cone types in zebrafish populate the entire retina, and are organized in a non-random mosaic (Allison et al., 2010)(Figure 1.2).

Photoreceptor synapses are restricted to the OPL, where the neurites of their two postsynaptic partners intermingle: horizontal cells (HCs) and bipolar cells (BCs). HCs are lateral interneurons that provide inhibitory input, whereas BCs are excitatory and span the plexiform layers to convey light information to the projection neurons of the retina, retinal ganglion cells (RGCs). The soma of both BCs and HCs reside in the inner nuclear layer (INL). In addition to synapsing with RGCs in the IPL, BC axons form glutamatergic synapses with lateral interneurons called amacrine cells (ACs). BCs, ACs, and RGCs are generally categorized by how they encode changes in illumination: ON cells depolarize whereas OFF cells hyperpolarize in response to light increments. The functionally distinct ON and OFF neuron classes synapse in separate domains of the IPL, either the ON or OFF sublayer (Figure 1.1).

The ON and OFF visual pathways originate with BCs; BCs are able to encode photoreceptor input differently on the basis of their expression of either metabotropic (sign-inverting) or ionotropic (sign-preserving) glutamate receptors (mGluR or iGluR) (Euler et al., 2014). Mammalian BCs can be further distinguished by their dendritic connectivity. Cone BCs (CBCs) or rod BCs (RBCs) wire exclusively with either cones or rods (Euler et al., 2014), respectively, although recent evidence suggests that some OFF BCs may wire with a mix of cones and rods (Haverkamp et al., 2008; Mataruga et al., 2007; Tsukamoto and Omi, 2014). BC populations in adult zebrafish form one of nine distinct photoreceptor connectivity patterns, and this repertoire includes patterns of “mixed” inputs from both cones and rods (Li et al., 2012). Furthermore, zebrafish possess BCs that stratify in both the ON and OFF IPL domains (ON-OFF BCs) (Figure 1.1). Physiological recordings of ON-OFF BCs in zebrafish and other teleosts have been reported to behave either like an ON or an OFF BC in response to light (Connaughton and

Nelson, 2000), or sometimes show both ON and OFF components in their light response (Wong and Dowling, 2005).

In the vertebrate retina, photoreceptors and BCs typically exhibit graded potentials in response to sensory or excitatory input, rather than the all-or-nothing spikes associated with action potentials. These neurons utilize "ribbons," specialized presynaptic structures that respond to graded potentials, which are also optimized to rapidly encode visual signals with fast and tonic neurotransmitter release (Sterling and Matthews, 2005). Ribbons can be recognized by electron microscopy as electron-dense structures in the presynaptic zone, and the ribbon synapse is completed by the formation of characteristic arrangements of postsynaptic processes near the ribbon-anchoring site (Figure 1.3).

In the OPL, ribbon synapses are arranged as triads within the photoreceptor terminal. Triad synapses comprise a membrane-anchored ribbon in the photoreceptor terminal, and two HC processes as well as one to three BC dendrites that appose the presynaptic ribbon (Figure 1.3). Both ON BC dendrites and HC processes insert into the photoreceptor terminal, forming an invagination. The HC processes lie in closest proximity to the ribbon, which is hypothesized to allow them to regulate neurotransmitter flow from the photoreceptor to BC dendrites (Dowling, 1970). In contrast, in many vertebrates, the dendrites of OFF BCs form superficial, or "basal" synaptic contacts at the base of the photoreceptor terminal (Dowling, 1970). Basal contacts are located up to hundreds of nanometers away from the neurotransmitter release site, yet they still conduct glutamatergic signaling from the ribbon, albeit with slower responses compared to the deeply invaginating HCs (DeVries et al., 2006). It has been suggested that the difference in proximity to photoreceptor ribbons between invaginating and basal dendritic contacts may lead to different sensitivities and temporal frequency responses in ON and OFF BCs, respectively (Haverkamp et al., 2000).

Dyad ribbon synapses in the IPL comprise two postsynaptic dendrites from a combination of ACs and RGCs, which are positioned opposite the ribbon in the BC axon terminal (Figure 1.3). Although ribbons in the IPL are not surrounded by invaginations as in the OPL, the postsynaptic processes are still located in close proximity to the ribbon. In addition to ribbon synapses, there is an abundance of conventional synapses in the IPL, which lack ribbons but feature other synaptic components, including presynaptic vesicles and postsynaptic densities.

Most conventional synapses originate from inhibitory, GABAergic or glycinergic ACs synapsing onto BC axons, RGC dendrites, or other AC processes in the IPL.

1.2 Retinal neurogenesis and synapse assembly during development

Across vertebrate species, retinal cells are derived from multipotent, neuroepithelial progenitors (Turner and Cepko, 1987; Wetts and Fraser, 1988). Cell genesis, as well as synapse assembly, is an ordered process during vertebrate development. Although the absolute timing of cell genesis, lamination, and synaptogenesis is not conserved, the general theme that the inner retina is established before the outer retina holds true for most vertebrates. In zebrafish, cell genesis occurs in waves separated by about 10 hours. RGCs are born first at ~30 hours post-fertilization (hpf), followed by the cells of the INL (ACs, BCs, HCs, and Müller glia), and lastly the photoreceptors (~48 hpf) (Hu and Easter Jr., 1999; Peterson et al., 2001) (Figure 1.4). The dendrites of RGCs are the first processes to laminate in the IPL at ~50 hpf, followed by ACs and BCs at around ~60 hpf (Schmitt and Dowling, 1999). Whereas inner retinal lamination is apparent by 60 hpf, ribbon synaptogenesis does not commence until ~74 hpf, the first stage at which ribbons are observed in BC axons. In the outer retina, HC processes are the first to enter the OPL at ~50 hpf, followed by photoreceptor terminals at ~60 hpf, and finally BC dendrites by 74 hpf (Schmitt and Dowling, 1999)(Figure 1.4). Thus, although BCs are born prior to photoreceptors, the photoreceptors laminate more rapidly, and the BC dendrites must extend out to contact their presynaptic partners. Finally, photoreceptors form ribbon synapses just prior to the stage at which BC dendrites first enter the OPL. Zebrafish larvae display their first visually-evoked responses at about 70 hpf (Easter Jr and Nicola, 1996), the same stage at which the first ribbons appear in BC axons in the IPL (Schmitt and Dowling, 1999)(Figure 1.4). Zebrafish larvae display robust visually-guided behaviors by 4 days post-fertilization (dpf) (Easter Jr and Nicola, 1996), demonstrating that the zebrafish retina undergoes rapid functional maturation.

Although retinal assembly is largely complete by early larval stages in zebrafish, neurogenesis is ongoing after initial development. Zebrafish continue to grow from larval stages (<20 dpf) through adulthood (>6 months post-fertilization). As the retina expands, new cells are added to the peripheral retina. Such ongoing neurogenesis is supported by a stem cell niche in the periphery, the ciliary marginal zone (CMZ) (Lenkowski and Raymond, 2014; Raymond et al., 2006). The CMZ stem cells express many of the same molecular markers as retinal

progenitors during initial development (Raymond et al., 2006), and show similar proliferative behaviors as well (Wan et al., 2016). Further, new rod photoreceptors are seeded into central retinal regions throughout the lifetime of the zebrafish (Stenkamp, 2011). Unlike neurons born in the CMZ, late-born rods are generated from dedicated progenitors that derive from resident Müller glia (Bernardos et al., 2007).

1.3 Determination of cell fate and neuronal number in the retina

How an initially homogenous pool of progenitor cells can produce the diversity of cell types found in the retina (> 60 in mice) (Masland, 2012) remains unclear. However, investigators have gained insight from the observation that, across vertebrate species, different cell types are generated in a specific order during retinal development (described in section 1.2). This led to the initial hypothesis that an individual progenitor progresses through time periods of different competences, during which a specific cell type is generated (Figure 1.5A). Indeed, this appears to occur in the *Drosophila* CNS; neuroblasts express specific sets of transcription factors at different times, which determine the fates of their daughter cells (Isshiki et al., 2001; Pearson and Doe, 2003). Because of this, neuroblasts in the *Drosophila* CNS demonstrate reproducible, fixed cell lineages, or "family trees" comprised of specific cell types and cell numbers.

By contrast, lineage-tracing studies in vertebrates have reported that retinal progenitors display variability in their behavior, indicating that stochastic mechanisms may be at play. Clonal analysis in frogs, rats, and mice revealed that an individual progenitor could produce multiple cell types at a given time point during retinal development (Holt et al., 1988; Turner and Cepko, 1987; Turner et al., 1990; Wetts and Fraser, 1988) (Figure 1.5B). However, recent work in zebrafish has also revealed that there are progenitors dedicated to producing either horizontal cells or cone photoreceptors, providing evidence of restricted lineages (Godinho et al., 2007; He et al., 2012; Suzuki et al., 2013). Thus, the debate about the role of restricted lineage programs in regulating neuronal identity in the retina, and the extent to which stochastic mechanisms impinge upon cell fate choice, is ongoing (Boije et al., 2014).

Do neuronal progenitors in the retina follow a cell-intrinsic program to achieve their appropriate identity and number, or does extracellular signaling from the retinal environment guide neurogenesis? Early cell-mixing and transplantation experiments, in which young progenitors were exposed to cells from an older environment, showed that the donor cells

differentiated into the neuron types appropriate for their age (Belliveau et al., 2000; Rapaport et al., 2001; Watanabe and Raff, 1990). Similarly, clonal analysis of isolated progenitor cells grown *in vitro* revealed that the cultured progenitors generated clones whose composition resembled those grown *in vivo* despite experiencing a different environment (Austin et al., 1995; Cayouette et al., 2003; Gomes et al., 2011; Reh and Kljavin, 1989). Together these results support the hypothesis that the progenitor competence schedule is largely regulated by intrinsic programs, which have since been shown to include transcriptional regulation as well as epigenetic modification (Ohsawa and Kageyama, 2008; Rao et al., 2011; Yang et al., 2015).

However, regulation of cell fate and number is not entirely independent of extracellular signaling. Mitogenic factors can indirectly influence a cell's ultimate fate by regulating progenitor proliferation and the timing of cell cycle exit (Agathocleous and Harris, 2009). Additionally, extrinsic signaling has been demonstrated to direct progenitor cell fate without impacting proliferation; the secreted growth and differentiation factor GDF11 regulates the duration of the window during which progenitors are competent to produce RGCs (Kim et al., 2005). Thus, retinal neurogenesis is an elaborate process involving both autonomous and non-autonomous mechanisms. These mechanisms are undoubtedly interlinked, as intrinsic cell properties dictate the responsiveness of a cell to extracellular factors. Moreover, the availability of different extracellular signals may change with time and according to location; as new cells are born over time, they alter the molecular environment of the retina. Additionally, like in other layered neuronal networks such as the cerebral cortex, neuroepithelial cells in the retina undergo interkinetic migration, which exposes them to extrinsic signaling gradients (Del Bene et al., 2008). To date, the relative contributions of intrinsic and extrinsic signaling in regulating cell fate and number remain unclear. Nonetheless, a number of key mechanisms have been identified, which I will discuss briefly below.

Intrinsic control of cell fate specification is largely achieved by the interplay between basic helix loop helix (bHLH) and homeodomain transcription factors (Ohsawa and Kageyama, 2008). Some of the homeodomain transcription factors that initiate vertebrate retinal development persist into later stages. They repress the expression of proneural bHLH factors, thereby maintaining progenitor competence. For example, time-lapse imaging in transgenic zebrafish indicated that the homeodomain factor Vsx2/Chx10 maintains the multipotent progenitor pool by repressing the expression of *vsx1* and *atoh7*, genes required for the

differentiation of restricted BC and RGC lineages, respectively (Vitorino et al., 2009). Whereas some transcription factor genes act instructively to direct cell fate, others are permissive. *Nrl*, which encodes a basic motif-leucine zipper transcription factor, is necessary and sufficient to promote rod photoreceptor fate in mice (Mears et al., 2001; Oh et al., 2007). In contrast, the expression of bHLH genes alone is insufficient to promote cell fate; as such, bHLH factors often operate in combination with homeodomain factors during cell fate specification (Marquardt, 2003; Ohsawa and Kageyama, 2008). Such combinatorial signaling can allow a particular bHLH gene to promote different cell fates; co-expression of the bHLH factor *Neurod4/Math3* with *Chx10* promotes BC fate, whereas co-expression of *Math3* with *Pax6* or *Six3* promotes AC fate in mice (Hatakeyama et al., 2001; Inoue et al., 2002). Ultimately, a postmitotic cell's final commitment to becoming a particular cell type often involves negative regulatory signaling to enforce the cell fate biases established previously during specification. For example, the homeobox transcription factor Brn3b both promotes the differentiation of early-born RGC types and represses the expression of genes necessary for the differentiation of late-born RGCs, cones, ACs, and HCs in mice (Qiu et al., 2008).

Extracellular cues can originate from the retinal environment as well as newborn postmitotic cells, and may influence neuronal composition by positive, inductive signaling or via negative feedback. *In vitro* experiments in rat cell cultures revealed that taurine, an amino acid that is present at high levels during CNS development, specifically promotes rod photoreceptor differentiation (Altshuler et al., 1993). Addition of taurine at stages when cell division is largely complete increased the proportion of cells expressing rod photoreceptor markers, indicating that taurine directly instructs differentiation in postmitotic cells. Further examination of taurine's mechanism of action *in vivo* in mouse retina suggested that taurine may act both indirectly and directly to instruct cell fate; in addition to regulating cell fate in postmitotic cells, taurine inhibits progenitor proliferation by binding glycine receptor $\alpha 2$ (Young and Cepko, 2004). Unlike taurine, which acts as a positive regulator of rod differentiation, many other extrinsic signals provide inhibitory feedback to regulate progenitor competence or proliferation and the timing of neuronal differentiation. GDF11 is produced by already-differentiated RGCs to limit the duration of *Atoh7/Math5* expression in mouse retinal progenitors, a gene that confers RGC competence. Consequentially, GDF11 prevents the production of excess RGCs (Kim et al., 2005). Mouse RGCs also provide feedback to limit progenitor proliferation. Loss of Sonic hedgehog (SHH)

signaling causes progenitors to precociously exit the cell cycle, such that RGCs are overproduced at the expense of the progenitor pool size (Wang et al., 2005). The reduction of the progenitor population consequentially leads to decreased production of later-born cell types, such as BCs. Like in other parts of the CNS, Notch-mediated lateral inhibition amongst neuronal progenitors ensures progenitor heterogeneity across developmental stages in the retina (Agathocleous and Harris, 2009). Notch receptor activation promotes progenitor maintenance by reducing the expression of proneural bHLH genes, and conversely, reduced Notch receptor activation facilitates neuronal differentiation. As such, lateral inhibition via Notch signaling ensures that the entire retinal progenitor population does not exit the cell cycle simultaneously, and thus adopt the same cell fate(s).

1.4 Regulation of stereotypic features of neuronal connectivity in the retina

Synaptic partner selection

The stereotyped connectivity pattern of a retinal neuron is characterized by the identity of its synaptic partners, as well as by the number and distribution of synapses it makes with each of these partner types. How do neurons in the retina establish their unique patterns of connections? The laminar organization of the retina provides the first limitation on synaptic partner choice. For example, RGCs with dendrites stratifying in the ON layer of the IPL only encounter axons from the functionally matched ON BCs, rather than the entire BC population. Nonetheless, even within a synaptic layer, retinal neurons wire exclusively with a subset of available partner types. Different cell types may generate their connection patterns by employing various strategies, from targeted partner selection to developmental refinement of inappropriate connections. Below, I briefly discuss some of the known molecular mechanisms that direct lamination and instruct target specificity, as well as the roles that afferents play in regulating the wiring of postsynaptic cells.

The role of molecular signaling in guiding neurite arbor lamination in vertebrates is well established. Several membrane-associated molecules have been shown to regulate neurite stratification. These include repulsive guidance cues from the semaphorin/plexin family, as well as adhesion molecules, such as cadherins and immunoglobulin superfamily (IgSF) members, including Sidekicks, Dscam, and Contactins (Baier, 2013). In general, adhesive, membrane-

bound molecules constrain connectivity to the appropriate sublamina, ensuring that the processes of the appropriate presynaptic and postsynaptic cell types co-mingle.

A combinatorial code of molecular cues can specify and confine neurite targeting to the plexiform layers, yet structural refinement may also occur to achieve appropriate stratification (D'Orazi et al., 2014). In developing cat and ferret retinas, the dendrites of ON or OFF alpha and beta RGCs initially span the entire IPL (Bodnarenko and Chalupa, 1993; Maslim and Stone, 1986). As the retina matures, the dendrites of these RGCs are eliminated from inappropriate layers, such that the final stratification level is sculpted from an initially diffuse arbor (Bodnarenko et al., 1995). However, work examining the lamination of RGCs over time in zebrafish and mouse retina has demonstrated that RGCs do not always rely on selective pruning from inappropriate depths to achieve lamination (Kim et al., 2010; Mumm et al., 2006). In particular, most RGCs examined during time-lapse imaging of transgenic zebrafish retina initially form an arbor that is biased toward the correct laminar zone. Further, bistratified zebrafish RGCs sequentially added multiple arbors at different levels, rather than refining an initially diffuse arbor. Clearly, diverse strategies can be employed by retinal cells to achieve their final lamination, including different forms of laminar refinement as well as biased targeting and sequential addition of arbors.

To date, it is unclear why a particular neuron type employs its chosen stratification strategy. Attempts to understand the relationship between neural activity and laminar refinement have provided only further evidence of diverse mechanisms. Experiments to hyperpolarize ON BCs by chronic activation of mGluR6, effectively silencing input to ON RGCs, prevented the restriction of dendrites from ON alpha and beta RGCs to the appropriate IPL (Bodnarenko and Chalupa, 1993). Likewise, sensory deprivation experiments in mice found that an unusually high fraction of the RGC population had both ON and OFF responses, suggesting a failure to undergo refinement when neurotransmission is altered (Tian and Copenhagen, 2003). By contrast, when BC transmission is disrupted either in mGluR6 knockout mice or via tetanus toxin expression, RGCs arborize normally (Kerschensteiner et al., 2009). These results further highlight the need to study lamination and wiring with regard to potential differences across specific cell types, and by comparing the effects of different manipulations of neurotransmission (Bleckert and Wong, 2011).

Within a synaptic layer, the neurites of a retinal neuron synapse with only some of the partners available to them, and their partner selection is cell type-specific and stereotyped. Recent work in mouse retina provides some of the first evidence for molecular signaling that guides local synaptic specificity, effectively "matching" presynaptic and postsynaptic partners within a lamina. In the direction-selective circuit, type 5 and type 2 BCs synapse directly onto the ON or OFF dendritic arbors of the ON-OFF direction-selective ganglion cell, respectively. Each BC type expresses a different cadherin, Cadherin-8 (Cdh8) in type 2 BCs and Cadherin-9 (Cdh9) in type 5 BCs (Duan et al., 2014)(Figure 1.6A). Deletion of either cadherin gene led to misplacement of the BC axon terminals within the IPL, however, misplaced terminals still intermingled with the dendrites of ON-OFF ganglion cell (Figure 1.6A). Electrophysiological recording from the ganglion cell during optogenetic stimulation of single BCs in cadherin-deleted mice showed that BC transmission onto ganglion cell dendrites is severely reduced, suggesting a lack of functional synapse formation from both normally stratifying and misplaced BCs (Duan et al., 2014). Thus, cadherins may not only facilitate contact between appropriate partners, but directly impact synapse formation. Indeed, inappropriate expression of Cdh9 in type 2 BCs redirected their axons to the ON layer, and induced ectopic synapse formation with ON starburst amacrine cells (SACs) (Figure 1.6A).

However, synaptic partner choice does not appear to be molecularly "hardwired." Retinal cells show plasticity in their partner choice, thus necessitating a mechanism to prevent wiring with inappropriate partners during development. CBC dendrites form novel contacts with rods in 'coneless' mice, in which cones are ablated by the expression of diphtheria toxin during retinal development (Figure 1.6B). Similarly, RBC dendrites, as well as the axons of HCs, make new synapses with cones in 'rodless' mice, in which rod are re-specified to become cones (Keeley and Reese, 2010; Strettoi et al., 2004). Thus, BC dendritic connectivity is plastic, but neurotransmission from the preferred afferents is likely to be the cue that prevents dendrites from selecting novel partner types during normal development. In mice with impaired rod function due to a mutation in rhodopsin, RBCs form and maintain connections with cones, before all photoreceptors eventually degenerate (Cuenca et al., 2004; Peng et al., 2000). Likewise, in the *CNGA3* mutant mouse, which lacks a cation channel subunit necessary for cone function, CBC dendrites form contacts with rods (Haverkamp et al., 2006)(Figure 1.6B). Taken together with observations of rewiring in coneless and rodless mice, this indicates that neurotransmission from

the appropriate afferents is necessary to prevent dendritic selection of inappropriate partner types in the photoreceptor-BC circuit in mice.

In the IPL, elimination of all the preferred partners of a postsynaptic cell results in severe effects on dendritic connections, including alterations to dendrite stratification as well as partner preference. Elimination of all ON BCs via expression of diphtheria toxin in mouse retina results in ectopic elaboration of the alpha-ON-RGC's (A-ON-RGC) dendrites into the OFF layer of the IPL (Okawa et al., 2014). Remarkably, the OFF-stratifying dendrites selectively synapse with a specific OFF BC (type 2) within the layer. Thus, in the A-ON-RGC circuit, the preferred BC partner specifies RGC connectivity by restricting the RGC dendrites to the appropriate lamina, and by prohibiting synaptogenesis with functionally inappropriate cells. Unlike the photoreceptor-BC circuit, afferent control of partner selection is evidently exercised independently of neurotransmission from the RGC afferents; RGCs arborize appropriately even in retinas in which all ON BCs are silenced (Kerschensteiner et al., 2009). Moreover, blocking afferent neurotransmission alone does not affect dendritic partner specificity, because the A-ON-RGC retains synapses with silenced type 6 and 7 ON BCs, and still eliminates inappropriate contacts with silenced RBCs (Morgan et al., 2011).

The neurites of some neurons in the retina initially make "mismatched" connections with inappropriate partners, and thus developmental refinement is critical to generate the mature connectivity patterns of these neurons. Evidence for refinement of partner choice comes from work in both mouse and zebrafish. Early on, the dendrites of A-ON-RGCs in mouse retina wire with both ON CBCs and RBCs in the ON layer of the IPL. However, at later stages, A-ON-RGCs eliminate their synapse with RBCs to establish connectivity specifically with ON CBCs (Morgan et al., 2011). Similarly, in zebrafish retina, an HC subtype called H3 cells selectively synapse with UV and blue cones at maturity, but exhibit transient connections with red or green cones at immature stages (Yoshimatsu et al., 2014). In both cases, the developmental elimination of erroneous connections does not depend upon neurotransmission from the preferred partner types. A-ON-RGCs still lose their RBC connections when ON-BC neurotransmission is suppressed, and H3 HCs do not maintain red/green cone connections despite a reduction in either or both UV and blue cone transmission. Furthermore, although the majority of H3 HC dendritic connections are made with UV cones, the presence of this major partner is not required for H3 HC synaptic specificity. Despite elimination of the UV cone population from the retina at early

stages in the lots-of-rods mutant, H3 HC dendrites did not synapse with red or green cone types at maturity (Yoshimatsu et al., 2014). In the case of the H3 HCs, it is clear that the major partner type is unnecessary to prevent dendritic wiring with new partner types at maturity. Nonetheless, it remains to be seen whether transmission from the inappropriate afferents themselves induces elimination of their connections with H3 HCs during normal development.

Synapse number and density

In addition to choosing amongst synaptic partner types, the neurites of a cell often make a stereotyped number of connections with each of its partners to establish the cell's connectivity pattern. The first limitation on synapse number is often set by the size of the axonal or dendritic arbor. Numerous presynaptic or postsynaptic partners may still lie within the territory of a cell's neurite arbor, and the cell may make either a single or multiple synaptic contacts with an individual partner. How do neurons regulate the number of partners with which they synapse, and how are synapses allocated per partner type? As in the process of partner selection, different cell types variably employ synapse elimination to achieve their mature number of synapses.

Investigations of how neurons acquire their final number of connections during development in mouse and zebrafish retina have demonstrated that different cell types may employ different strategies (Dunn and Wong, 2012; Yoshimatsu et al., 2014). The H3 HC in zebrafish expands its dendritic arbor during development, and simultaneously increases its synapses with UV cones as more become available, so that it eventually contacts all of the available UV cones. BCs in mice engage diverse strategies to set their synapse number during development. Like H3 HCs, type 6 BCs continue to form synapses until they reach the mature number. In contrast, type 7 and 8 BCs exuberantly synapse with cones, only to reduce their total number of synapses after P13. Type 7 and 8 BCs also remodel the size of their dendritic fields over time. For all three BC circuits described, the BCs synapse with all of the afferents available to their dendrites, even in the case of type 7 and 8 BCs, which exuberantly add and eliminate synapses over time. These findings suggest that the number of available afferents may govern the number of connections on a retinal cell's dendritic arbor.

Experiments to alter retinal cell densities in multiple species have shown that the number of afferents lying within a dendritic arbor's territory often dictates the number of cells it contacts (Figure 1.7). For example, in mice, HC dendrites connect with a higher number of cones when

the density of cones across the retina is increased by re-specification of rods to the cone cell fate (Raven et al., 2007)(Figure 1.7A). Similar results were observed for zebrafish HCs; a morpholino antisense oligonucleotide (MO)-induced increase in the density of the predominant partner, UV cones, causes H3 HC dendrites to contact more UV cones compared to wildtype (Yoshimatsu et al., 2014)(Figure 1.7B). Neurons may also increase the number of presynaptic partners available to them by increasing dendritic growth (Poché et al., 2008). In the Lim1 conditional knockout mouse, HCs lacking neighboring HCs expand their dendritic territory, and thus come in proximity to an increased number of afferents. Ultimately, the expanded HCs connect with more cones than in wildtype retina. Neurons make more dendritic connections than normal in all of the experiments discussed above, providing evidence that many retinal neurons are free of cell-intrinsic limitations on synapse number.

However, retinal neurons do not always synapse with all of the preferred afferents available to them at maturity, as seen in circuits with 'biased' connectivity patterns. For example, H3 HCs in zebrafish only contact a fraction of their secondary partner, blue cones. Therefore, the availability of partners alone cannot regulate the number of connections formed with secondary partners, and the strategies that neurites employ to set their synapse number may depend upon the synaptic partner type.

There is accumulating evidence of homeostatic mechanisms to compensate for a reduction in afferent availability. One possible compensatory strategy for a loss of local partner availability is that the cell expands its axonal or dendritic territory to reach additional partners. This possibility was addressed by experiments to reduce, but not completely eliminate, the density of cones across the retina by genetic ablation in the coneless mouse, and by re-specification of cones to rods in the 'rodfull' mouse. Examination of HC connectivity in these mice revealed that HCs do not expand their dendritic territories compared to normal, nor do they acquire the normal number of connections (Raven et al., 2007; Reese et al., 2005). However, similar experiments in zebrafish demonstrated that retinal neurons may instead use a different homeostatic mechanism, increased synaptogenesis with a secondary partner, to compensate for a reduction in preferred partner availability (Yoshimatsu et al., 2014)(Figure 1.7B). When the density of UV cones is decreased in the lots-of-rods mutant, H3 HC dendrites allocate more synapses to blue cones. However, this compensation is only partial, as the H3 HC's total number of dendritic synapses is still reduced compared to normal. Nonetheless, results from

manipulations of HC afferents reveal another potential strategy whereby cells may compensate fully for lost connections. In both mice and zebrafish with reduced cone densities, the HC dendritic terminals that invaginate the remaining cone terminals are expanded in size (Reese et al., 2005; Yoshimatsu et al., 2014)(Figure 1.7A,B). Although it remains to be determined, it is possible that this phenotype represents an increase in the number or strength of synapses per afferent. Thus, under circumstances in which it is not possible to increase the local availability of afferents, cells may achieve their total number of synapses, or level of synaptic input, by increasing the number and/or strength of synapses per afferent.

Similarly, cells may increase the number of synaptic contacts they form per individual cell to maintain their total synapse number. Direct evidence of such comes from the A-ON-RGC circuit. Even when a majority of ON-BCs are ablated in mouse retina, A-ON-RGCs maintain the normal number of synapses on their dendrites (Okawa et al., 2014). Analysis of the synapse number per individual BC axon terminal for a given RGC revealed two compensatory strategies (Figure 1.7C). First, A-ON-RGC dendrites form more synapses per BC axon terminal. The remaining type 6 BCs expand their axons into the territories of their ablated neighbors, and the RGC forms more synapses with these expanded BCs. This increase in synaptogenesis matches axon territory expansion, such that the normal density of synapses onto the A-ON-RGC dendrites per type 6 BC terminal is maintained. Second, like the H3 HC, A-ON-RGCs increase the number of synapses with their secondary partner, the type 7 BCs. The type 7 BCs also increase their axon terminal territories, but differ from type 6 BCs in that they increase their density of synapses with RGCs. Thus, A-ON-RGCs maintain their normal synapse number when afferent availability is reduced by increasing the number of synapses formed with both their major and minor afferents.

How do presynaptic cells exert their control over the number of synapses on the postsynaptic cell's dendrites in the retina? Examination of ON-BC connections with the dendrites of A-ON-RGCs has provided strong evidence that neurotransmission from synaptic partners can directly impacts a cell's synaptogenesis, to the extent that the level of transmission dictates the number of synapses formed. In retinas in which ON-BCs are silenced by expression of tetanus toxin, preventing synaptic vesicle release, A-ON-RGCs show reduced numbers of glutamatergic synapses on their dendrites (Kerschensteiner et al., 2009)(Figure 1.7C). Conversely, elevated glutamate release from BCs increases the number of synapses on A-ON-

RGCs (Soto et al., 2012)(Figure 1.7C). Mutation of *Crx*, a transcription factor necessary for photoreceptor maturation (Freund et al., 1997; Furukawa et al., 1997), leads to a lack of functional photoreceptor input onto BC dendrites in mice. Consequentially, *Crx* mutation induces hyperactive, spontaneous transmission from BCs. Quantification of synapses on an RGC dendritic arbor over time revealed that the level of neurotransmission a dendrite receives directly impacts its rate of synaptogenesis, and thus synapse number. Time-lapse imaging of postsynaptic density protein-95 (PSD-95) clusters on A-ON-RGC dendrites when BC transmission is altered showed that neurotransmission specifically regulates the rate of synapse formation, but not the rate of synapse elimination (Kerschensteiner et al., 2009; Soto et al., 2012). Synaptogenesis is increased in retinas with increased spontaneous activity, and decreased in retinas with silenced ON-BCs, but altered neurotransmission yields no changes in the rate of synapse elimination on RGC dendrites.

Examinations of circuits in which connections are biased toward one input type provide further insights into how afferent neurotransmission influences the number of dendritic synapses formed per afferent type. In experiments to either increase or decrease ON-BC activity, only the number of RGC synapses specifically with type 6 BCs, but not type 7 BCs, is altered (Morgan et al., 2011; Soto et al., 2012)(Figure 1.7C). A possible explanation for this difference is that presynaptic activity from the major input type impacts synapse number with the postsynaptic partner. This is unlikely to be true in the cone-H3 HC circuit, however, because H3 HCs connect with the normal number of UV cones even when the UV cones themselves are silenced (Yoshimatsu et al., 2014). However, in this circuit, neurotransmission specifically from the major input can control the number of synapses made with the minor input. In zebrafish retina in which UV cones are silenced, H3 HC dendrites increase the number of blue cones they synapse with, but silencing blue cones did not alter connections with UV cones. This unidirectional control of synapse number in a convergent circuit is unique, because investigations in other neural systems had previously found evidence for activity-dependent regulation that relied upon competition between converging afferents (Hashimoto and Kano, 2013; Sanes and Lichtman, 1999).

Lastly, recent work in the mouse retina has demonstrated that the activity of the postsynaptic cell itself can ‘retrogradely’ regulate its dendritic synapse number (Johnson and Kerschensteiner, 2014). In experiments in which neurotransmitter release from axons is

abolished in a portion of the CBC population, the silenced CBCs have fewer cone connections on their dendrites, but only when the silenced cells are surrounded by active neighbors. Likewise, active CBCs increase their dendritic input number in regions where they are surrounded by silenced CBCs. Silenced CBC axons form fewer synapses regardless of their neighbors' status, and therefore do not compete for synapses. These results show that, first, the dendrites of CBCs in mice compete for input from the same partners and second, dendritic competition for synapses is surprisingly determined by the ability of CBCs to release neurotransmitter from their axons.

1.5 Retinal regeneration

Müller glia produce neuronal progenitors

Some of the earliest evidence to demonstrate that teleosts replace lost retinal neurons comes from surgical and chemical lesioning experiments in goldfish (Hitchcock et al., 1992; Maier and Wolburg, 1979; Negishi et al., 1991a, 1991b; Raymond et al., 1988). The application of mitotic labels such as bromodeoxyuridine (BrdU) or proliferating cell nuclear antigen (PCNA) after lesioning revealed that new neurons were generated via cell proliferation in the area of the injury. Importantly, measurements of the electrical responses of neuronal populations in the retina via electroretinography (ERG), as well as analysis of visually-guided behaviors revealed that teleosts recover general retinal function after neuronal regeneration (Mensinger and Powers, 1999; Sherpa et al., 2008). However, decreased spectral and contrast sensitivity in regenerated retinas has also been reported ((Lindsey and Powers, 2007), suggesting that recovery may not be complete.

Work in the chick retina provided the first evidence that Müller glia can act as sources of progenitors during neuronal regeneration (Fischer and Reh, 2001). Using transgenic reporters to temporarily or indelibly label the progeny of Müller glia, the Goldman, Hyde, and Raymond groups later showed that Müller glia similarly produce progenitors that differentiate into neurons during retinal regeneration in zebrafish (Bernardos et al., 2007; Fausett and Goldman, 2006; Fimbel et al., 2007; Ramachandran et al., 2010). Indelible lineage tracing in particular facilitated the ability of investigators to fate map Müller glial progeny, revealing that Müller glia-derived progenitors are capable of differentiating into each of the major neuronal classes in zebrafish (Ramachandran et al., 2010). As such, Müller glia are endogenous sources of multipotent progenitors in the teleost retina.

Cellular events and molecular signaling during regeneration in zebrafish

Since unmasking Müller glia as the source of regenerated neurons, investigators have focused heavily on understanding the molecular and cellular mechanisms that allow zebrafish to regenerate their retinal neurons. Much progress has been achieved to this end, uncovering a sequence of events that lead to neuronal replacement (summarized in Figure 1.8; reviewed in (Lenkowski and Raymond, 2014)). In brief, the regeneration response proceeds as follows:

1) Retinal injury and neuronal death activates Müller glia, leading them to 2) dedifferentiate and undergo a self-renewing, asymmetric cell division that produces a neuronal progenitor. Müller glia-derived progenitors 3) divide repeatedly to amplify the progenitor population which will eventually 4) become fate restricted and 5) terminally differentiate and migrate to the appropriate neuronal layer.

This sequence of cellular events is observed regardless of the lesioning paradigm, and generally initiates within days of retinal damage. However, the relative timing of each regeneration step, and the point at which regeneration is complete, may differ according to the injury. In general, selective elimination of photoreceptors (Bernardos et al., 2007; Nagashima et al., 2013; Thummel et al., 2008) stimulates the division of Müller glial cells and progenitors more rapidly than ablation of inner retinal neurons alone (Fimbel et al., 2007), or of all retinal layers (Fausett and Goldman, 2006). Below, I briefly discuss some of the general signaling pathways involved in each of the major regeneration steps.

The regeneration response is initiated rapidly after retinal injury, and several extracellular signaling pathways are associated with the response onset. Such extracellular cues can be translated into changes in gene expression because they activate receptor-associated signaling cascades that communicate to the nucleus, such as MAPK/ERK, JAK/STAT, and Gsk3β-β-catenin pathways (Goldman, 2014; Lenkowski and Raymond, 2014). To date, only a few molecules have been identified that are produced specifically by the dying neurons themselves (Battista et al., 2009; Nelson et al., 2013). Expression of tumor necrosis factor α (TNFα), a secreted pro-inflammatory cytokine, is increased in dying photoreceptors after light lesioning, as well as in dying inner retinal neurons after cytotoxic oubain treatment (Nelson et al., 2013). Blocking translation of TNFα protein by MO application before and after retinal injury significantly reduced the number of Müller glia and progenitors entering the cell cycle,

demonstrating that TNFα signaling is required for Müller cell and progenitor proliferation. TNFα likely functions as a general signal of neuronal cell death, rather than a signifier of the loss of specific neuron types. Several other secreted factors, including heparin-binding EGF-like growth factor (HB-EGF) (Wan 2012), ciliary neurotrophic factor (CNTF) (Kassen et al., 2009), and Wnts (Ramachandran et al., 2011) are upregulated after injury. However, they are expressed by Müller glia rather than dying neurons, and signal in an autocrine and paracrine fashion to prompt transcriptional changes that promote dedifferentiation and proliferation. Thus, whereas secreted factors from dying neurons activate the initial response to injury, Müller glia-derived signals sustain cell proliferation and recruit additional Müller glia to the regeneration response.

Many of the injury-associated signals discussed above converge to upregulate the expression of *achaete-scute complex homolog 1* (*ascl1*), a proneural bHLH transcription factor. Indeed, Ascl1 has emerged as the gatekeeper of retinal regeneration due to its position at the interface of injury cues and essential intrinsic signaling pathways (Goldman, 2014; Gorsuch and Hyde, 2014; Lenkowski and Raymond, 2014). Ascl1 expression is required for retinal regeneration in zebrafish (Fausett et al., 2008; Ramachandran et al., 2010), and it acts both to inhibit genetic programs that promote cellular differentiation and activate proliferation programs. For example, Ascl1 likely indirectly suppresses cellular differentiation by upregulating the RNA-binding protein Lin28. *In vitro* chromatin immunopreciptation (ChIP) assays revealed that Ascl1 directly binds the promoter of Lin-28, which is a repressor of *let-7*, a microRNA that normally maintains Müller glia quiescence (Ramachandran et al., 2010). Moreover, Ascl1 impinges on canonical signaling pathways involved in stem cell pluripotency and neuronal differentiation, including the Notch and Wnt pathways (Goldman, 2014; Gorsuch and Hyde, 2014; Lenkowski and Raymond, 2014). Ascl1 may also be involved in actively promoting a progenitor cell-like fate in Müller glia, as Ascl1a knockdown in zebrafish blocks the upregulation of *pax6*, a fundamental progenitor gene (Fausett et al., 2008).

After their activation, Müller glial cells exhibit interkinetic nuclear migration and undergo a single asymmetric division near the ONL to generate a progenitor (Bernardos et al., 2007; Nagashima et al., 2013). The Müller glia-derived progenitors resemble the transit-amplifying progenitors from other CNS networks in that they undergo several rounds of cell division to amplify their population size, but are ultimately limited in their division potential. The progenitors migrate along the Müller glia processes. Based on the timing of the expression

of specific cell lineage genes, it is hypothesized that progenitors commit to their final cell fate as they reach their terminal location (Fimbel et al., 2007; Gorsuch and Hyde, 2014; Thummel et al., 2008). Research into the factors that control the timing of Müller glia and progenitor cell cycle exit is still ongoing, but the transcriptional repressor Insulinoma-associated 1a (Insm1a) has been shown to play a role. The expression of several genes that are associated with cell cycle activation is increased during the stages when the progenitor population is amplified; the end of the progenitor proliferation period is associated with the upregulation of the cell cycle inhibitor $p57^{kip2}$ (Ramachandran et al., 2012). Morpholino-mediated knockdown of Insm1a expression during retinal injury in adult zebrafish led to an increase in pro-proliferation genes, as well as a decrease in $p57^{kip2}$ expression (Ramachandran et al., 2012). Thus, Insm1a appears to drive cell cycle exit during regeneration at least in part by suppressing the expression of cell cycle genes, as well as by indirectly inducing inhibitors of the cell cycle. Future research into the control of cell cycle exit may reveal mechanisms that keep progenitor proliferation in check in order to limit regeneration to only replacing the appropriate number of neurons.

Little known is about how the differentiation of Müller glial cell-derived progenitors is controlled. It is unclear whether the identity of the dying neuron population biases progenitor differentiation, a question of particular interest when only select neuronal cell types are damaged. Thus far, very few molecules have been identified that are associated with the regeneration of only a specific neuron type. Furthermore, it is unclear whether these candidates directly influence cell fate choice, or instead selectively control neuronal survival or the proliferation of fate-restricted precursors. For example, rod, but not cone regeneration is reduced in a transgenic zebrafish harboring a dominant negative *fgfr1* (Qin et al., 2011). *Fgfr1* encodes a transmembrane receptor tyrosine kinase, which is bound by fibroblast growth factor (Fgf) ligands. Qin et al. (2011) demonstrated that Fgf signaling is required specifically for the homeostasis of rod photoreceptors, and thus hypothesized that replacement rods likely underwent rapid degeneration in fish with inhibited Fgf signaling. Thus, the composition of regenerated neuron populations was likely shaped by the differential survival of newborn cells in the *fgfr1* dominant negative zebrafish.

Stimulating retinal regeneration in mammals

Müller glial cells are present in both mammals and zebrafish, and in the absence of neuronal injury, provide structural and trophic support to surrounding retinal neurons (Bringmann et al., 2006). However, their reaction to injury contrasts starkly between the two species. Mammalian Müller glia respond to injury by undergoing reactive gliosis, a neuroprotective process that involves morphological and biochemical changes to promote repair and to limit the extent of the injury. However, reactive gliosis can actually inflict further retinal damage. After a severe injury, mammalian Müller glia become proliferative, but do not replace lost neuronal populations (Bringmann and Wiedemann, 2012). Moreover, proliferation occurs at the expense of the health of surrounding neurons. Recent work has provided evidence that zebrafish similarly show gliotic potential (Thomas et al., 2016). Nonetheless, by and large, teleosts demonstrate a response that primarily serves to replace lost neuronal populations, rather than limit the extent of cell death and remodeling, as in mammals.

Why mammals and teleosts differ so greatly in their retinal injury response is still under investigation. In fact, Müller glial cells in mammals and fish have similar molecular profiles. Reactive Müller glia in mammals exhibit many of the same signaling pathways that are deployed during teleost retinal regeneration, including those related to the immune response, cell dedifferentiation, and cell proliferation (Bringmann et al., 2009; Lenkowski and Raymond, 2014). Moreover, serial analysis of gene expression (Blackshaw et al., 2004), as well as microarray analysis (Nelson et al., 2011; Roesch et al., 2008), has demonstrated that even quiescent Müller glia in the mature mammalian retina share molecular properties with progenitor cells. As such, mammalian Müller glial cells exhibit regenerative potential. Indeed, investigators have been able to stimulate Müller glia in rodents to generate new neurons in response to retinal damage, albeit of limited cell types and in low numbers. In one study, the application of mitogenic growth factors together with NMDA neurotoxic treatment in rats *in vivo* was reported to induce production of BCs and photoreceptors from Müller glia (Ooto et al., 2004). However, a later study in mice that similarly combined mitogenic and neurotoxic treatment found evidence only of newly generated AC types, as revealed by confocal imaging (Karl et al., 2008).

Mammalian glial cells fail to initiate regeneration at least in part because they are unable to activate the same transcriptional programs that support neuronal regeneration in teleosts. Whereas Ascl1 expression is rapidly upregulated after injury in fish, its expression is unaltered in

injured rodents after neurotoxic injury (Karl et al., 2008). However, recent attempts to force ASCL1 expression in Müller glia *in vitro* (Pollak et al., 2013) and *in vivo* (Ueki et al., 2015) have successfully provoked neuronal regeneration in mice. ChIP-qPCR revealed that forced ASCL1 expression via viral infection resulted in remodeling of chromatin at the promoters of progenitor genes in Müller glia, switching the chromatin from a repressed to active state. Moreover, the epigenetic status of the *Ascl1* promoter itself is altered upon ASCL1 infection in Müller glia (Pollak et al., 2013). Together these results suggest that epigenetic silencing of the promoters of *Ascl1* and other progenitor genes inhibits regeneration signaling pathways in mammalian Müller glia. By contrast, the promoters of pluripotency factors are hypomethylated in Müller glia from uninjured zebrafish retinas (Powell et al., 2013). Thus, Müller glial cells in either mammals or zebrafish are capable of activating progenitor gene programs that support neuronal regeneration. However, zebrafish Müller glia are better poised to initiate regeneration due to a reduced level of epigenetic silencing compared to mammalian cells.

1.6 Thesis overview

In the following thesis, I explored the accuracy of neuronal replacement and integration after regeneration in the mature vertebrate retina. First, I used confocal imaging to reconstruct *in toto* the morphology and connectivity of BCs across development and after regeneration of BC circuitry in larval zebrafish. I classified three functionally distinct BC types, and found that each forms a stereotypic dendritic wiring pattern, with distinct biases for particular cone types. I then examined the assembly of BC-photoreceptor connectivity and BC morphogenesis across stages of maturation. Having established this basis for comparison, I next investigated the ability of BCs to attain type-specific characteristics, and to establish appropriate connectivity after regenerating. Employing a genetically-targeted ablation technique to selectively eliminate BCs enabled me to assess the integration of regenerated BCs within the context of an otherwise intact circuit. Additionally, I attempted to gain insight into the specificity of endogenous neuronal replacement by eliminating distinct cone populations in the larval zebrafish retina. I compared the extent of neuronal replacement and the composition of the regenerated cone population across ablation conditions in order to assess the influence of neuronal identity and abundance on regeneration.

1.7 Figures

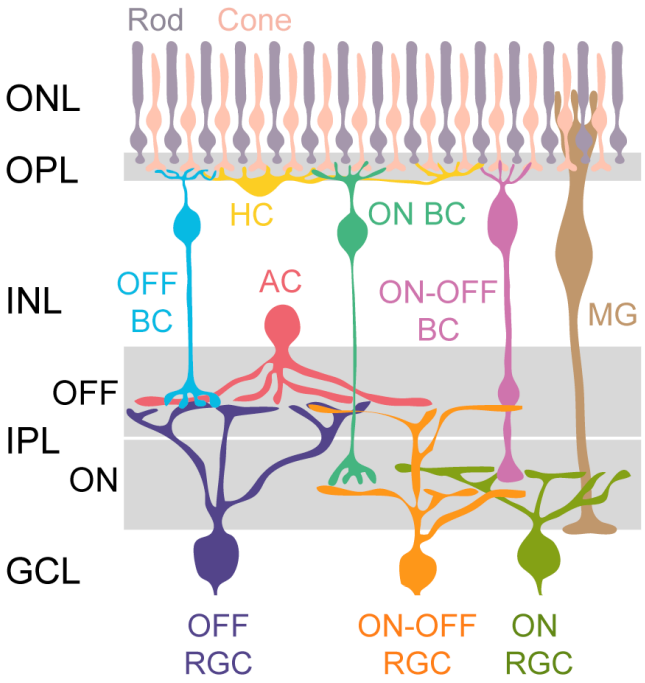

Figure 1.1 Organization of the vertebrate retinal circuit.

Schematic of the vertebrate retina. The major retinal neuronal cell classes are: cone and rod photoreceptors, bipolar cell (BC), horizontal cell (HC), amacrine cell (AC), and retinal ganglion cell (RGC). Müller glia (MG) are the major retinal glial cell class. Retinal cells are organized in laminae; cell bodies are located in the outer or inner nuclear layers (ONL or INL, respectively) or the ganglion cell layer (GCL). Neuronal synapses are distributed to the outer or inner plexiform layers (OPL or IPL). The IPL is further divided into OFF and ON sublaminae. Figure is adapted with permission from: D'Orazi F.D. and Yoshimatsu, T. (2016). Development of synaptic input patterns on dendrites of retinal neurons. In Dendrites, Development and Disease, Emoto, K., Wong, R., Huang, E. Hoogenraad, C., eds. (Japan: Springer Japan).

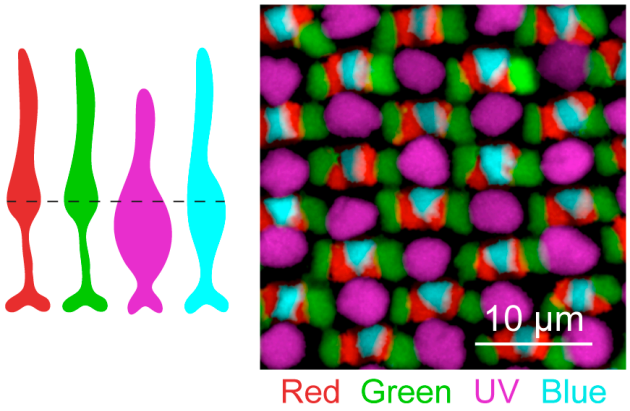

Figure 1.2 Specific cone types and their organization in the zebrafish retina.

(Left) Schematic showing a side view of the four cone types found in zebrafish, red, green, ultraviolet (UV), and blue cones. (Right) Confocal reconstruction showing an en face view of the cone photoreceptor mosaic in adult retina, at the level indicated in the side view. Distinct cone types were visualized using a quadruple transgenic fish. Here, fluorescent protein labeling is shown for red and blue cones, and green and UV cones are pseudo-colored. Image credit: Sachihiro Suzuki.

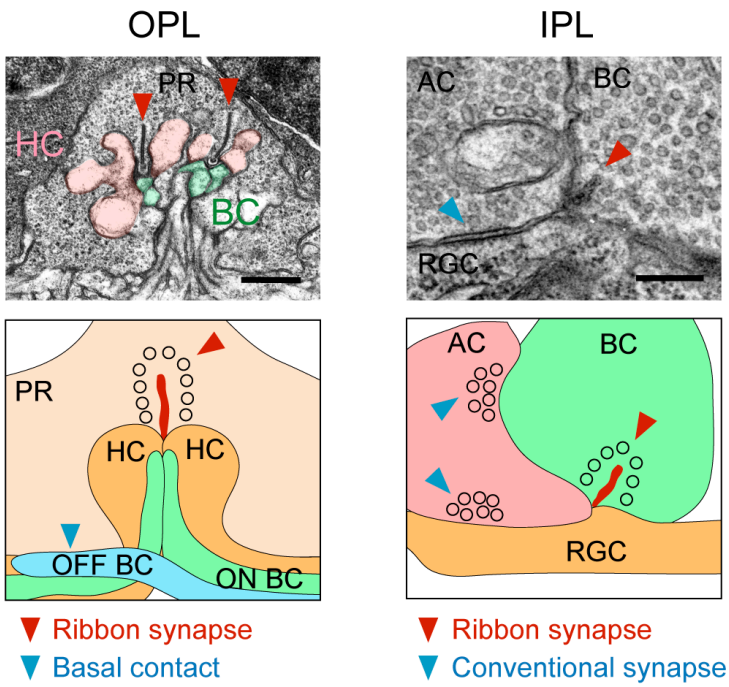

Figure 1.3 Subcellular synaptic organization in the retina.

Ultrastructure (top) and schematic (bottom) of the subcellular organization of ribbon synapses in the plexiform layers. **(OPL)** (Top) Electron micrograph of a triad synapse at a larval zebrafish cone terminal (from (Yoshimatsu et al 2014)). HC processes and BC dendrites invaginate the terminal at sites apposed to ribbon structures (red arrowhead) in the photoreceptor (PR) terminal. Scale bar is 0.5 µm. (Bottom) OFF-BC dendrites form basal contacts onto the cone terminal (blue arrowhead). **(IPL)** (Top) Electron micrograph of a dyad synapse at an adult mouse BC terminal (from (D'Orazi et al 2014)). ACs form feed-forward conventional synapses onto RGC dendrites (filled blue arrowhead), as well as reciprocal conventional synapses back onto BC axons (open blue arrowhead in schematic). Scale bar is 0.25 µm. Figure is reprinted with permission from: D'Orazi F.D. and Yoshimatsu, T. (2016). Development of synaptic input patterns on dendrites of retinal neurons. In Dendrites, Development and Disease, Emoto, K., Wong, R., Huang, E. Hoogenraad, C., eds. (Japan: Springer Japan).

Figure 1.4 Developmental time course of retinal synapse formation and lamination in the zebrafish retina.

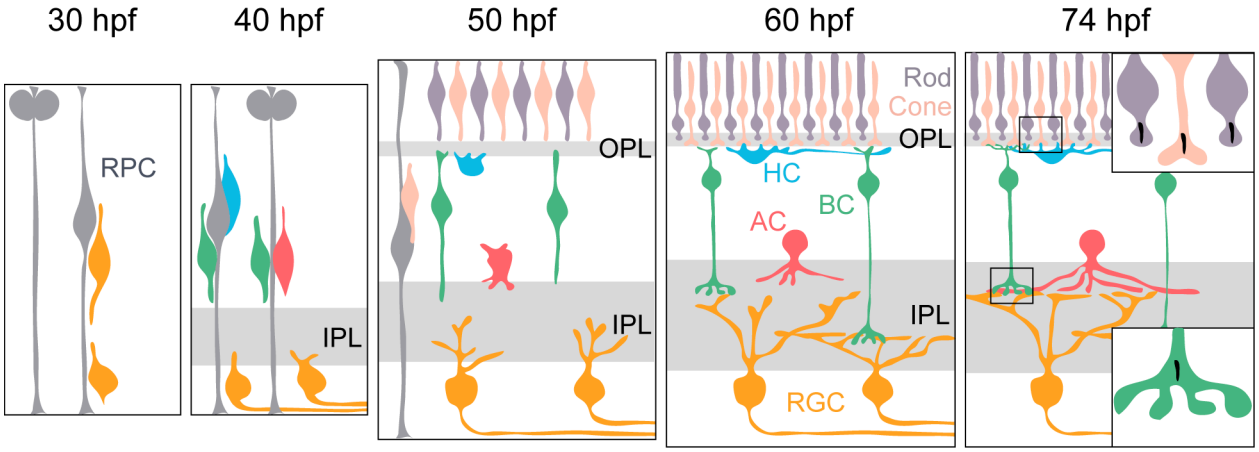

Illustration of the sequence of events during outer and inner plexiform layer (OPL and IPL) development in zebrafish retina, with approximate timing shown in hours post-fertilization (hpf)). Retinal ganglion cells (RGCs) are the first neurons to be produced from retinal progenitor cells (RPCs), at ~30 hpf. Bipolar cells (BCs), amacrine cells (ACs), and horizontal cells (HCs) are produced at ~40 hpf. At the same time, RGCs have begun to elaborate their dendrites within the IPL. Rod and cone photoreceptors are born at ~50 hpf, the time at which the OPL first appears as HC processes form. Photoreceptor terminals enter the OPL at ~60 hpf, as BC axons and AC processes begin to elaborate within the IPL. BC dendrites penetrate the OPL at around 74 hpf, a stage by which photoreceptor axons exhibit ribbon synapses, as do BC axons. Figure is adapted with permission from: D'Orazi F.D. and Yoshimatsu, T. (2016). Development of synaptic input patterns on dendrites of retinal neurons. In Dendrites, Development and Disease, Emoto, K., Wong, R., Huang, E. Hoogenraad, C., eds. (Japan: Springer Japan).

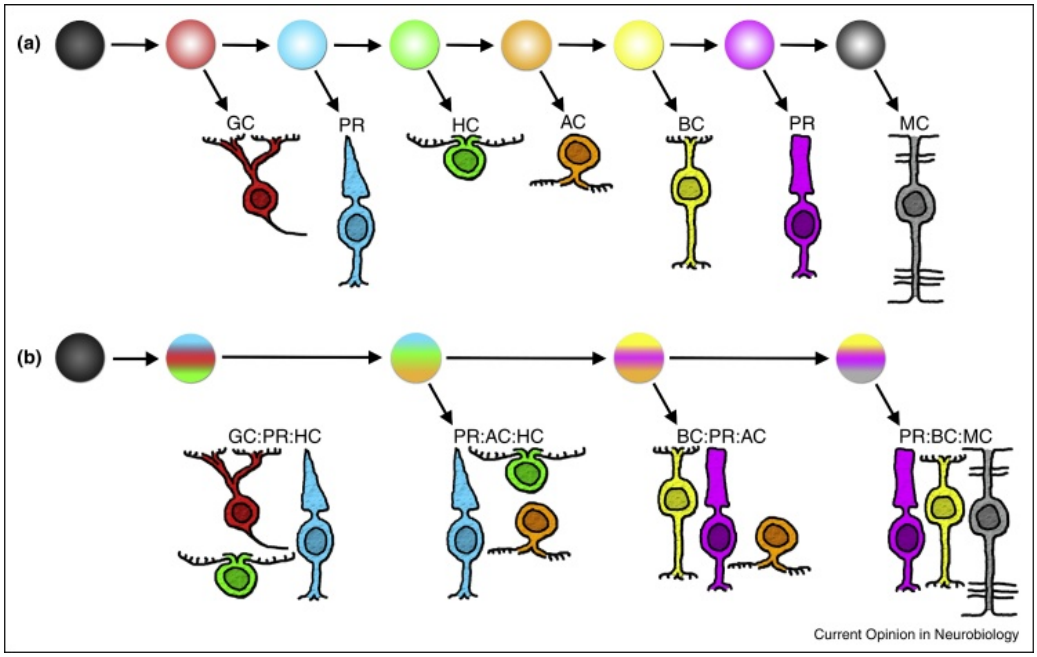

Figure 1.5 Models of progenitor competence during retinal development.

Schematic illustrating models of retinal progenitor cell competence. (**A**) The classic model posits that progenitor cells progress through distinct competence windows, during which a specific neuronal cell type is produced. (**B**) The currently accepted model suggests that progenitor cells choose from a subset of potential cell fates at a given stage in retinal development. Retinal ganglion cell (GC), photoreceptor (PR), horizontal cell (HC), amacrine cell (AC), bipolar cell (BC), Müller glia (MC). Figure is reprinted from (Boije et al., 2014) with permission (licensed under CC BY 3.0).

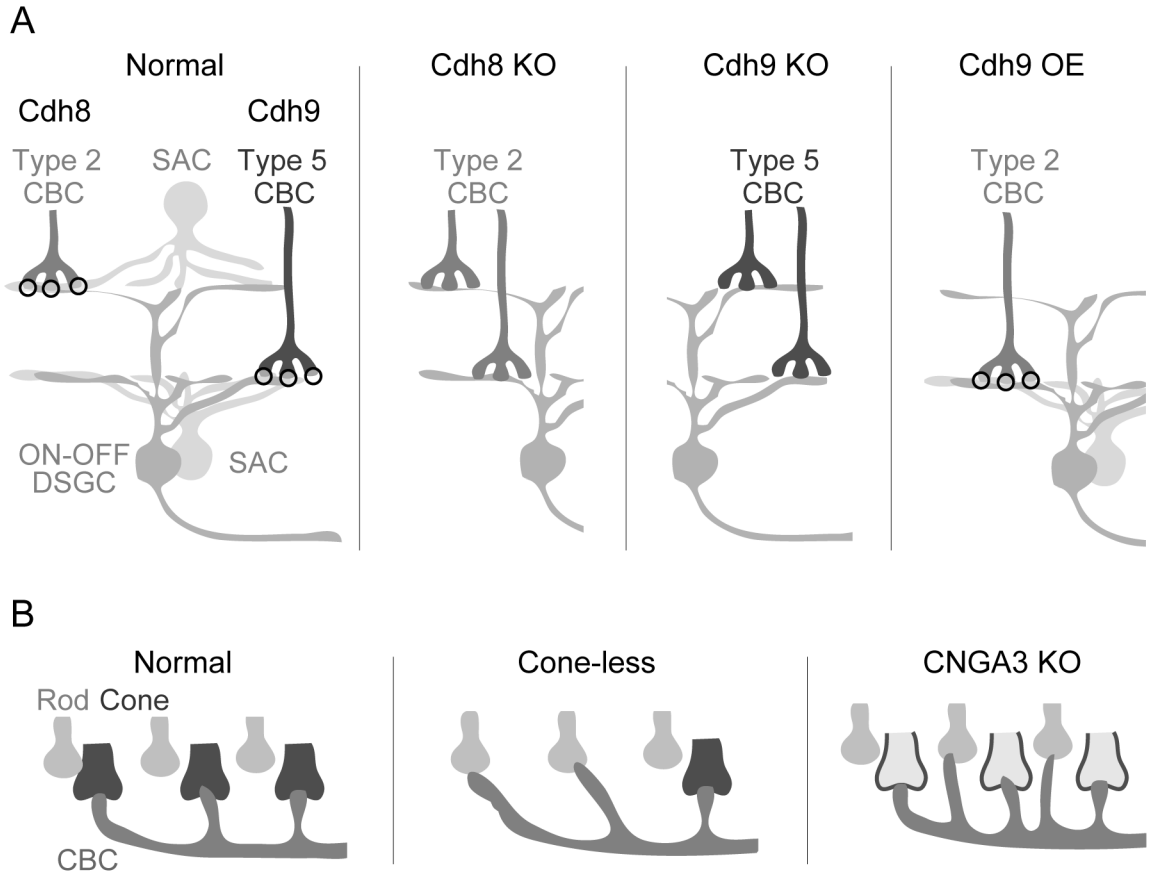

Figure 1.6 Molecular and afferent regulation of retinal neuron synapse specificity.

(A) Synaptic partner matching between cone bipolar cells (CBCs) and the dendrites of starburst amacrine cells (SACs) and direction-selective ganglion cells (DSGCs) in adult mouse retina. Cadherin-8 (Cdh8) and -9 (Cdh9) are normally expressed in type 2 and 5 cone bipolar cells (CBCs), respectively. Illustrations represent the differential effects of Cdh8 or Cdh9 knockout (KO) on Type 2 or 5 BC axon stratification and connectivity with ON-OFF DSGC dendrites. Cdh9 over-expression (OE) redirects type 2 CBCs axon terminals to stratify and make ectopic synapses with ON-SAC dendrites. **(B)** Schematics of changes to CBC dendritic partner selection in response to alterations in cone composition (in 'cone-less' mutant mice) or neurotransmission (in CNGA3 KO mice). Cones with disrupted neurotransmission are outlined. Figure is reprinted with permission from: D'Orazi F.D. and Yoshimatsu, T. (2016). Development of synaptic input patterns on dendrites of retinal neurons. In Dendrites, Development and Disease, Emoto, K., Wong, R., Huang, E. Hoogenraad, C., eds. (Japan: Springer Japan).

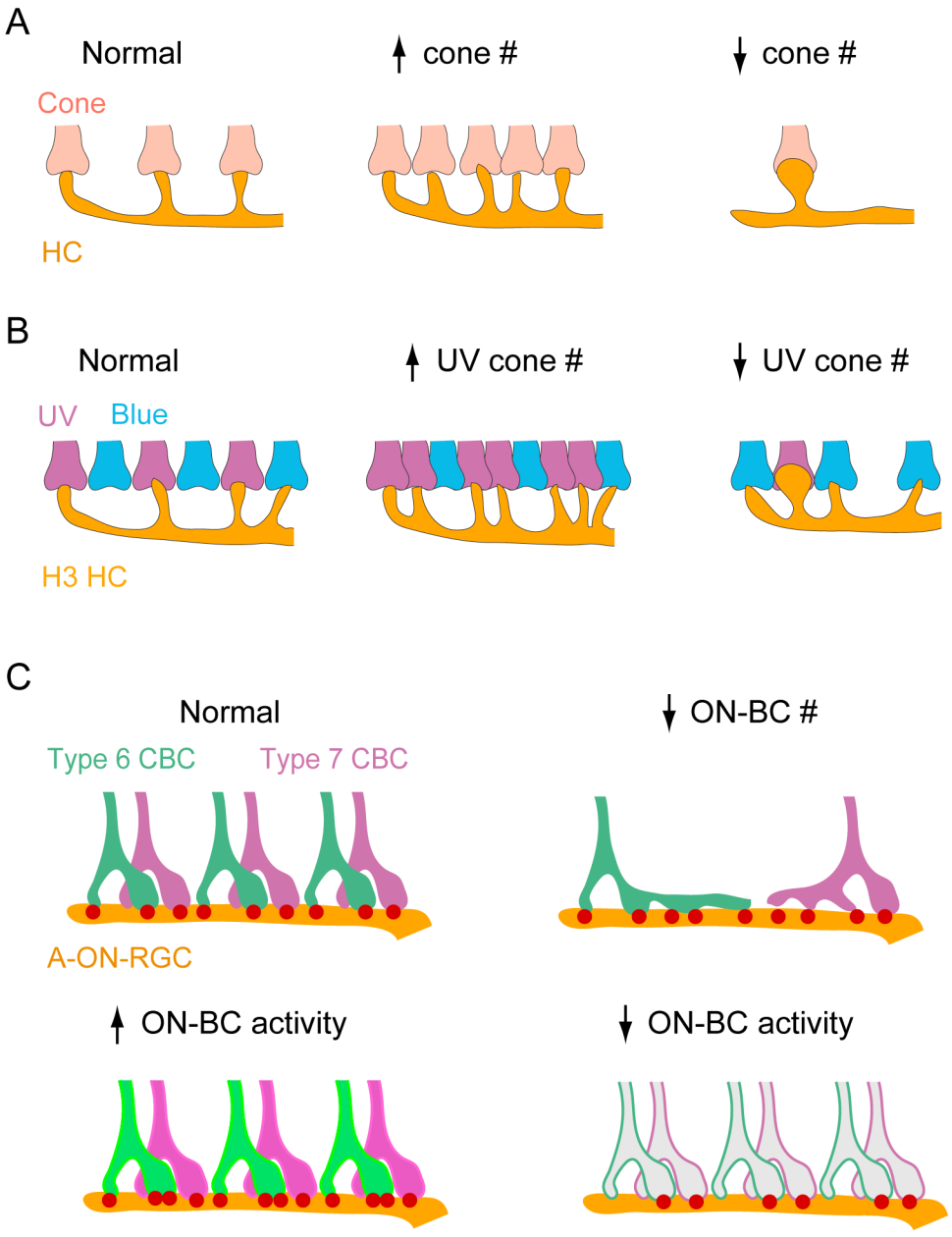

Figure 1.7 Regulation of dendritic synapse number by afferent availability and activity.

(A) Schematic of HC synaptic contact with cones after alteration of cone density in mouse retina (in 'conefull' and 'coneless' mutant mice). **(B)** H3 HCs in larval zebrafish retina connect with all the available UV cones (UV) within their dendritic fields, but only contact a fraction of the available blue cones (Blue). Schematics represent changes to H3 HC dendritic connections and morphology when UV cone numbers are altered by morpholino or in the *lots-of-rods* mutant. **(C)** (Top) alpha-like ON-stratifying retinal ganglion cells (A-ON-RGCs) normally receive the majority of their inputs from type 6 cone bipolar cells (CBCs), and minor input from type 7 CBCs. (Top right) Illustration of the effects of a decreased number of ON bipolar cells (ON-

BCs) on BC presynaptic territory size and synaptic density on A-ON-RGC dendrites. (Bottom) Representation of the differential effects of modified presynaptic neurotransmission on the number of A-ON-RGC dendritic synapses with its major and minor input partners. Hyperactive neurotransmission from ON-BCs in *Crx* mutant mice, and silencing of ON-BC neurotransmission by tetanus toxin expression. Figure is reprinted with permission from: D'Orazi F.D. and Yoshimatsu, T. (2016). Development of synaptic input patterns on dendrites of retinal neurons. In Dendrites, Development and Disease, Emoto, K., Wong, R., Huang, E. Hoogenraad, C., eds. (Japan: Springer Japan).

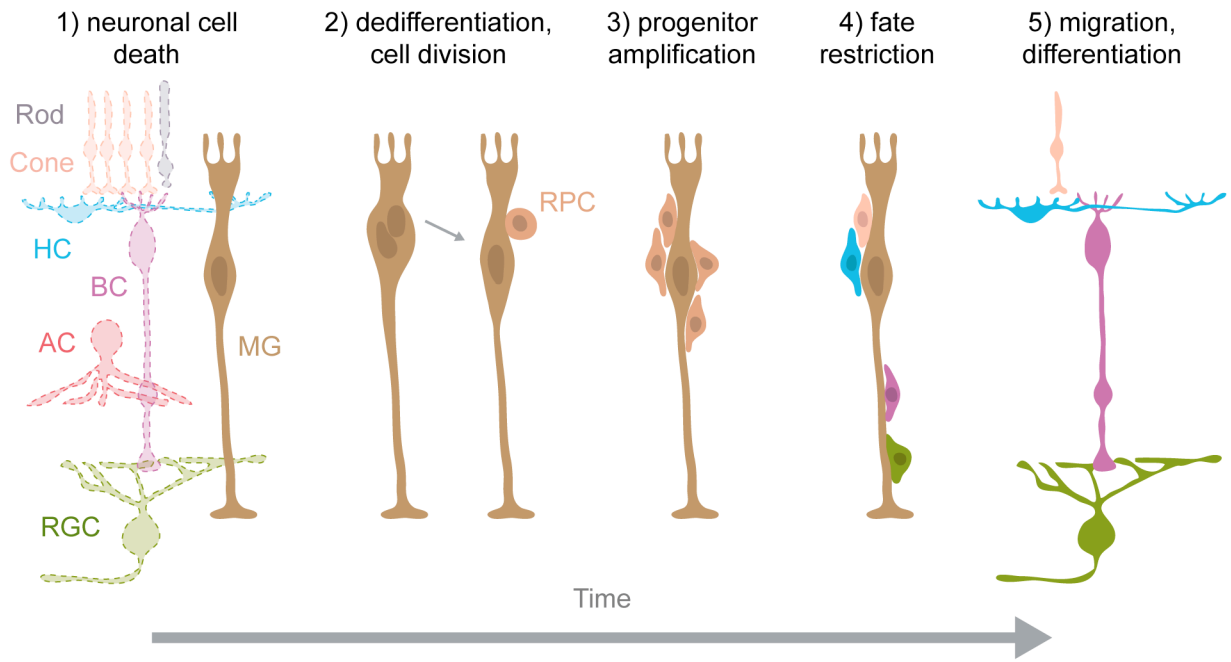

Figure 1.8 Sequence of major events during zebrafish retinal regeneration.

Schematic illustrating the sequence of major cellular events during retinal regeneration in zebrafish. 1) retinal injury and neuronal cell death activates resident Müller glia, which 2) dedifferentiate and undergo interkinetic nuclear migration toward the apical surface, where they divide once to produce a retinal progenitor cell. 3) The Muller glia-derived progenitor undergoes multiple cell divisions, and subsequently 4) become committed to a neuronal cell fate, 5) migrate to the appropriate layer and differentiate. Horizontal cell (HC), bipolar cell (BC), amacrine cell (AC), retinal ganglion cell (RGC), Müller glia (MG), retinal progenitor cell (RPC).

Chapter 2. Distinct neuronal populations assemble stereotypic wiring via preferential synaptogenesis in the larval zebrafish retina

2.1 Introduction

In the vertebrate central nervous system (CNS), the unique and stereotypic patterns of connectivity amongst different neuronal cell types generate a multitude of specialized circuit functions. Assembly of such wiring patterns is demanding because it requires selection of appropriate partner types amongst many potential partners, as well as control of the number of synapses with each partner type. Although the developmental mechanisms underlying precision in circuit assembly in the retina are becoming increasingly understood (reviewed in Chapter 1), little is known as to how well newborn neurons are able to reassemble their circuitry after retinal damage and cell replacement. Are mechanisms that enable neurons to wire precisely during development available to replacement cell populations in mature circuits that suffer neuronal loss due to injury or disease?

Here, we provide a framework for comparing the precision of synaptic wiring in developing versus replacement neuronal circuits. We assessed synaptic assembly in larval zebrafish because their retinas develop rapidly in order to support visually-guided behaviors, which are exhibited as early as 74 hours post-fertilization (hpf) (Easter Jr and Nicola, 1996). We specifically examined the connectivity of bipolar cells (BCs), interneurons that receive photoreceptor input at their dendrites in the outer plexiform layer (OPL), and transmit to retinal projection neurons via their axons in the inner plexiform layer (IPL) (Euler et al., 2014; Wässle, 2004). BCs are broadly classified according to how they encode changes in illumination: ON BCs depolarize in response to light increments, whereas OFF BCs depolarize in response to light decrements. An individual BC's response is shaped by its expression of specific neurotransmitter receptors and ion channels, and the number and properties of its presynaptic inputs (Euler et al., 2014; Wässle, 2004). In zebrafish, BCs have five potential presynaptic partners: rod photoreceptors and four cone photoreceptor types, which have peak sensitivity to red, green, ultraviolet (UV), or blue wavelengths (Fadool and Dowling, 2008). Whereas BCs in adult zebrafish form a number of distinct connectivity patterns with photoreceptors (Li et al., 2012), the precise axonal output patterns of these BCs have yet to be fully elucidated.

Portions of Chapter 2 were published in Current Biology, which maintains copyrights for this material, and has been reprinted with permission: D'Orazi F.D., Zhao X.-F., Wong R.O., Yoshimats T. Mismatch of synaptic patterns between neurons produced in regeneration and during development of the vertebrate retina. Curr. Bio., in press.

BCs are the last neurons to differentiate in the vertebrate retina, and must integrate into circuits that have already assembled (Schmitt and Dowling, 1999). Partner selectivity is especially challenging for BCs, which must select amongst potential input or output partners that intermingle within a layer. We first investigated the morphological maturation of three identified BC types, including two ON BCs and one OFF BC type, from early to late larval stages. Confocal reconstruction demonstrated that each BC type gained synaptic territory past early stages, and thus continued to mature beyond the onset of vision. Analysis of BC-cone connectivity at BC maturity revealed that each BC type formed type-specific dendritic wiring. Whereas the small-field ON BC synapses non-selectively with all cone types, the large-field ON and OFF BCs demonstrate biased connectivity, as they synapse primarily with red cones and secondarily with green cones. Tracking the input connectivity of these BCs further revealed that each BC type deployed the same strategy to acquire their disparate wiring patterns, preferential synaptogenesis with specific cone partners over time.

2.2 Methods

Transgenic zebrafish

All procedures were conducted in accordance with University of Washington Institutional Animal Care and Use Committee guidelines. Embryonic and larval fish were raised at 28°C in a room with a normal light cycle, lights on from 9:00 to 23:00. Embryos were maintained in system water until 12-24 hours post fertilization (hpf), at which point embryos were placed in system water containing 0.2 mM N-Phenylthiorurea (PTU) (Sigma P7629) to prevent pigmentation. Transgenic larvae were screened for FP expression after hatching. Screened larvae were removed from PTU-containing system water, and transferred to a University of Washington zebrafish facility where they were fed regularly. Zebrafish larvae were euthanized by MS-222 (Sigma A5040) overdose (200-500 mg/L)

All experiments were performed in the background of the enhancer trap transgenic *Tg(G4VP16; UAS:eGFP)*^{Ub43} (Zhao et al., 2009) crossed with *Tg(UAS:nfsB-mCherry)*^{c264} (Davison et al., 2007), which drives expression of NTR tagged with FP. Larvae were screened using the mCherry reporter, because eGFP was too dim for detection in nearly all *Tg(G4VP16; UAS:eGFP)*^{Ub43} animals. All transgenic fish were maintained in the *roy orbison* mutant background, in which the formation of iridophores is prevented, to facilitate visualization of FP during live imaging. See table below for a list of all the transgenic lines used.

Table. List of transgenic lines.

Transgenic	Source	Retinal Cells Labeled	Shorthand
Tg(G4VP16; UAS:eGFP; UAS:nfsBmCherry)	*Ub43* (Zhao et al., 2009)9) *; c264* (Davison et al., 2007)7)	bipolar cell subset	*xfz43*
Tg(thrb:Tomato)	*Q22* (Suzuki et al., 2013)3)	red cones	*trβ2*
Tg(thrb:MA-YFP)	*Q23* (Suzuki et al., 2013)3)	red cones	*trβ2*
Tg(-5.5opn1sw1:EGFP)	*kj9* (Takechi et al., 2003)3)	UV cones	*sws1*
Tg(-3.5opn1sw2:EGFP	*kj11* (Takechi et al., 2008)8)	blue cones	*sws2*
Tg(-3.2sws2:mCherry)	*mi2007* (Salbreux et al., 2012)2)	blue cones	*sws2*

Tg(Xla.Rho:EGFP)	*fl1* (Fadool, 2003)3)	rods	*xops*
Tg(Vsx1:MCerulean)	*Q19* (Randlett et al., 2013)3)	bipolar cell subset	*vsx1*

Plasmid injection

To visualize individual BCs, we injected pUAS:MYFP or pUAS:MmTFP1myc (Yoshimatsu et al., 2016) into single-cell stage embryos from the *xfz43* line. Plasmid was diluted in 1x Danieau's solution to a concentration of 50 ng/µL. Plasmid solution was loaded into a pulled-glass micropipette, mounted to a micromanipulator (Narishige), and pressure-injected via attachment to a Picospritzer II (Parker). Injections were made at 10 psi for durations from 100-200 ms.

Immunohistochemistry

After euthanasia, larvae were fixed in a solution of 4% paraformaldehyde and 3% sucrose in 0.1 M phosphate-buffered saline (PBS), pH 7.4 at room temperature, and retinas were dissected out within 1-3 days. Fixed, whole retinas were blocked in PBS containing 5% normal donkey serum and 0.5% TritonX-100 for 1-4 hours at room temperature. Tissue was incubated in primary antibody in blocking solution for 1-5 days at 4°C. After three washes in 0.5% TritonX-100 in PBS, samples were incubated in secondary antibody solution for 1 day at 4°C, followed by nuclear or actin staining for 1 hour at room temperature. Samples were washed three times in PBS, mounted in 0.7% agarose, and coverslipped in Vectashield (Vector Labs).

For nuclear staining, samples were washed in 50 mM Tris-HCl (pH 7.5) before immersion in Syto45 (1:1000, Life Technologies S11356) in Tris-HCl buffer for 1 hour at room temperature. For actin staining, samples were washed with PBS three times and immersed in Phalloidin-Alexa Fluor 647 (1:200, Life Technologies A22287) in PBS for 1 hour at room temperature. See tables below for lists of all primary and secondary antibodies used.

Table. List of primary antibodies.

Antibody	Host	Concentration	Source
anti-arrestin3a	mouse	1:100	ZIRC
anti-arrestin3b	chicken	1:250	Gift of Stephan Neuhauss

anti -DsRed	Rabbit	1:500	Clontech 632496
anti-GFP	Chicken	1:500	Abcam ab13970
anti-GFP	mouse	1:200	Neuromab 72-132
anti-GFP	rabbit	1:500	Abcam ab13970
anti-myc	mouse	1:100	DSHB 9E10
anti-PKC	mouse	1:500	Sigma P5704
anti-RibeyexA	chicken	1:200	Gift of Leon Lagnado*

* The Ribeye A antibody was produced by Cambridge Research Biochemicals and was raised in chicken against amino acids 82 to 97 [[C]-YNQGYLDRPDPRNIRK] of zebrafish ctbp2a transcript variant 1.

Table. List of secondary antibodies.

Antibody	Host	Concentration	Source
anti-chicken IgY DyLight488	goat	1:500	Jackson ImmunoResearch
anti-mouse IgG DyLight405	goat	1:500	Jackson ImmunoResearch
anti-mouse IgG DyLight488	donkey	1:500	Jackson ImmunoResearch
anti-mouse IgG DyLight649	goat	1:500	Jackson ImmunoResearch
anti-rabbit IgG DyLight488	donkey	1:500	Jackson ImmunoResearch
anti-rabbit IgG Alexa Fluor 568	donkey	1:500	Life Technologies

Confocal image acquisition

Image stacks were acquired on a confocal microscope (Olympus FV1000 or Leica TCS SP8) using a 1.35 numerical aperture (NA) 60x oil (Olympus), 63x oil (1.4 NA) (Leica), 20x oil (0.85 NA) (Olympus), or a 20x oil (0.75 NA) (Leica) objective lens. Images were acquired at the following resolutions: cone connectivity mapping, 0.07 µm per pixel XY and 0.15 µm Z step; BC morphology quantification, 0.07 µm per pixel XY and 0.3 µm Z step; whole retinas, between 0.1 and 0.4 µm per pixel XY, and 1 or 2 µm Z steps.

Image analysis

Image stacks were median filtered in Fiji (NIH) (Schindelin et al., 2012). Maximum intensity projections were generated in Amira (FEI). Three-dimensional (3D) image reconstructions were digitally sliced using the Amira slice functions. All measurements were made in Fiji. Image brightness, contrast, and hue were further adjusted in Photoshop (Adobe) or GIMP.

To assess BC axon stratification in the IPL and soma location in the INL, 3D reconstructions were digitally sliced to isolate the BC of interest, and oriented in a side view by rotating the plane of the OPL parallel to the viewing perspective. The IPL and INL were visualized by nuclear (Syto45) or actin (Phalloidin) staining. BC dendritic territory and axon terminal size were analyzed by digitally slicing away all of the BC around the dendritic arbor or axon terminal. *En face* views were generated by orienting the plane of the OPL or IPL at an orthogonal angle to the viewing perspective. To measure axon terminal sizes in images of *en face* axon terminals, BC axon terminal fluorescence was binarized by thresholding the image by eye. Pixels of the same brightness were then selected using the wand tool in Fiji, and the area of the selection was measured. See Figure 2.2 for more details about morphological analyses. Regenerated cells with displaced soma or abnormal axon trajectories were excluded from morphological comparisons.

Connectivity maps were obtained by identification of dendritic tip invaginations into photoreceptor axon terminals in 3D image reconstructions. Dendritic invaginations were examined by marching through a side view of the dendritic arbor and photoreceptor terminals in digitally-sliced thin sections. The location of each dendritic invagination, as well as the center of mass of each labeled photoreceptor terminal, was marked on a 2D maximum intensity projection of the BC dendritic arbor in Fiji or Illustrator (Adobe) (see Movie S1, Figure 2.3A). Sites at which dendritic tips were located without a labeled photoreceptor were marked as ‘other’ contacts. The numbers of dendritic tips and photoreceptor contacts were counted in Fiji. The percentage of available cones contacted was determined by comparing the number of cones contacted versus the number of cones lying within the BC dendritic territory. Cone terminals were counted as lying within the territory if their center of mass fell on or within the boundary of the polygon used to determine dendritic territory size (see Figures 2.2 and 2.6).

Statistical analysis

In Figure 2.3B and Figure 2.4C-D, a one-way ANOVA was used to test for differences in morphological or connectivity measurements across three ages for each BC type; pair-wise comparisons between ages were made using the Wilcoxon-Mann-Whitney rank sum test. In Figure 2.5C, a Chi-square test was used to test for differences in the proportion of contacts across all three partner types, as well as to make pair-wise comparisons. A Chi-square test was used in Figure 2.6 to test for differences in the proportion of available cells of each cone type that the BC contacted, as well as to make pair-wise comparisons. In Table 2.1, a one-way ANOVA was used to test for differences in morphological measurements across BC types, and pair-wise comparisons were made using the Wilcoxon-Mann-Whitney rank sum test. All statistical tests were performed using a significance level of 0.05.

Cluster analysis

We used K-means clustering with the Euclidean distance metric after normalizing all measures to the population mean in order to partition the population data from 20 dpf retinas.

2.3 Results

xfz43 comprises three BC types with characteristic anatomical and molecular features

The *xfz43* Gal4 enhancer trap line drives expression of reporter genes in a subpopulation of BCs residing in the central region of the zebrafish retina (Zhao et al., 2009), which corresponds to tissue generated during larval development. In order to distinguish the morphology of individual BCs in the larval *xfz43* line, we labeled a sparse population of cells with fluorescent protein (FP) by injecting pUAS:FP plasmid into the fertilized eggs of *xfz43* fish (see Methods) (Figure 2.1A). At 20 days post-fertilization (dpf), well after the function of larval retinal circuits is established (3 dpf) (Easter Jr and Nicola, 1996), we could identify three *xfz43* BC types based on several morphological features (Figure 2.2).

We observed that BCs in the *xfz43* BC population stratified within a thin layer in either the ON or OFF lamina of the IPL (Figure 2.1A). The axon terminals of ON *xfz43* BCs differentially expressed protein kinase C-alpha (PKC), an enzyme involved in modulating messenger pathways and a marker of ON BCs across species (Wood et al., 1997) (Figure 2.1B). Consequentially, we defined the PKC-positive ON BCs as ON Type 1 (ON T1), and the PKC-negative cells as ON Type 2 (ON T2) (Figure 2.1B). Cluster analysis of the population data revealed that the ON *xfz43* BCs also segregated into two groups by dendritic territory size, as well as by the location of their somata within the inner nuclear layer (INL) (Figure 2.1C, Table 2.1). Further, like the ON *xfz43* types, OFF *xfz43* BCs showed characteristic dendritic morphologies and somal locations (Figure 2.1C, Table 2.1).

xfz43 BCs attain their mature morphologies by progressive growth

To determine how *xfz43* BC types acquire their respective dendritic and axonal morphologies during development, we imaged *xfz43* fish at 5 and 15 dpf (Figure 2.3A). Quantification across cell types and ages demonstrated that the dendritic arbors of the small-field ON T1 BCs reached their mature size by 5 dpf, whereas the arbors of ON T2 and OFF BCs, the large-field BCs, continued to grow after this age (Figure 2.3B). Both ON types expanded their axonal terminals after 5 dpf, but OFF axon terminals remained relatively stable in size from this early age onwards (Figure 2.3B). Although fine scale morphological changes may occur in *xfz43* BCs prior to FP expression onset in the transgenic line (~3 dpf), our observation that the axonal

morphologies of these BCs were not refined over time contrasts with previous findings for other BC populations in larval zebrafish (Schroeter et al., 2006).

Stereotypic patterns of wiring with photoreceptors are established via selective synaptogenesis

In vertebrates, photoreceptor-BC synapses are characterized by the termination of a BC dendritic tip within the photoreceptor axon terminal (invaginating contact), or at the terminal base (basal contact) (Dowling, 2012). To establish the cone connectivity maps of each of the *xfz43* BC types, we reconstructed their more readily distinguishable invaginating contacts with photoreceptors at 20 dpf (Movie S1, Figure 2.4A-B). Across vertebrate species, invaginating contacts are generally formed by ON BCs, whereas basal contacts are made by OFF BCs (Dowling, 2012). However, our 3D confocal reconstructions here suggest that the *xfz43* OFF type makes invaginating synapses (Figure 2.4A, Figure 2.5A), and whether or not the OFF *xfz43* BCs form basal contacts remains to be elucidated. Each of the *xfz43* BC types largely contacted red and green cones (Figure 2.4A-B), but also contacted a few UV and blue cones, as well as rods (Figure 2.52A-B). Despite *xfz43* BCs contacting all photoreceptor types, each BC type exhibits a stereotypic pattern of connectivity with cones (Figure 2.4C-D). ON T1 BCs on average contacted a few more red and green cones than UV or blue cones, but they did not exhibit a strong bias for any particular cone type (Figure 2.5B). In contrast, for ON T2 and OFF BCs, connections with red and green cones together accounted for nearly 90% of the invaginating synapses (Figure 2.4D, Figure 2.5C). Moreover, both of these BC types biased their connectivity toward red cones specifically, and allocated their contacts amongst red and green cones in stereotypic ratios (ON T2 red/green cone contact: 2.97 ± 0.33 (mean ± SEM), n = 9 cells; OFF red/green cone contact: 2.34 ± 0.53, n = 10 cells) (Figure 2.4D).

It is possible that the distribution of BC dendritic contacts amongst preferred cone types is constrained by the relative abundance of each cone type. To address this possibility, we quantified the proportion of cones of each type that are present within the BC's dendritic territory of each *xfz43* population (Figure 2.6). We observed that ON T1 BCs contacted nearly all of the red, green, UV, and blue cones within their territory, and OFF BCs contacted all of the available red and green cones. ON T2 BCs similarly synapsed with all red cones within their field, but in contrast only contacted about 60% of the available green cones (Figure 2.6). Thus,

the relative abundances of red and green cones alone could not account for the input bias of ON T2 BCs.

To gain insight into the developmental strategies that *xfz43* BCs employ to acquire their stereotypic wiring patterns, we mapped their dendritic connectivity at earlier stages. All three *xfz43* BC types increased their total number of contacts with age (Figure 2.4C). ON T1 BCs specifically increased connections with photoreceptors other than red and green cones after 5 dpf (Figure 2.4D). ON T2 and OFF BCs already exhibited a preference for red and green cones over other types by 5 dpf, with red cones receiving the majority of connections (ON T2 red/green cone contact: 1.76 ± 0.34, n = 5 cells; OFF red/green cone contact: 2.57 ± 0.90, n = 6 cells) (Figure 2.4D). Over time, ON T2 and OFF BCs increased contact with red cones, their primary partner type (Figure 2.4D). Surprisingly, neither ON T2 nor OFF BCs gained additional contacts with their secondary partner, green cones, despite increasing contact with other partner types (Figure 2.4D). At least some of the late-formed contacts of *xfz43* BCs could be with rods (Figure 2.5A), because unlike cones (Hu and Easter Jr., 1999), rods are generated continuously in central retina (Stenkamp, 2011). Together, these results led us to conclude that *xfz43* BCs do not uniformly increase their number of contacts with each partner cone type. Instead, each BC type preferentially gains synapses with select cone types over time.

2.4 Discussion

Morphological differentiation of BCs during retinal development

BCs are the last neurons to differentiate in the retina during retinal development, and therefore must integrate rapidly into pre-existing circuits prior to the onset of vision (Schmitt and Dowling, 1999). After differentiation, the first step in BC integration requires that BCs stratify and elaborate their dendrites and axons within the appropriate plexiform layers. *xfz43* BC dendritic development shares similarities with that of mouse BCs; cells in both species can continue to elaborate their dendrites to contact photoreceptors beyond vision onset (Dunn and Wong, 2012). Because the size of the BC dendritic arbor corresponds to its sampling area of an image, these observations suggest that the visual function of BCs continues to be shaped after initial photoreceptor drive. Not all BCs show this extended growth period, however, implying that different BC types undergo maturation over different timelines, a feature also observed in mice (Dunn and Wong, 2012). In contrast to mice, we found that the dendritic arbors of *xfz43* BCs elaborate without evidence of gross remodeling. Thus, *xfz43* BCs do not employ exploratory growth to shape their dendritic and axonal arbors, although fine scale morphological changes may occur at stages prior to visual function (Schroeter et al., 2006) or between the ages we examined.

Acquisition of biased photoreceptor connectivity during BC development

The requirements developing neurons must fulfill to establish their specific synaptic patterns are two-fold: they must select appropriate synaptic partner types and establish connections in stereotypic numbers. Presynaptic partner selection is especially demanding for the retinal neurons that synapse in the outer retina, because their dendrites must select from several potential photoreceptor partners that intermingle within a single lamina. However, unlike horizontal cells (Li et al., 2009; Yoshimatsu et al., 2014), *xfz43* BCs are not strictly exclusive in their photoreceptor partner choices, because they synapse with each of the photoreceptor types. The connectivity of *xfz43* BCs is not random, however, because these cells allocate their synapses amongst photoreceptor partners differentially. How do *xfz43* BCs bias their synaptic connectivity towards a single or subset of cone types? A common developmental mechanism that shapes the stereotypic wiring of a neuron is the elimination of surplus synapses, or of contacts

with inappropriate partner types (D'Orazi et al., 2014; Sanes and Yamagata, 2009). This does not appear to occur for *xfz43* BCs, which showed no loss of synapses with any partner type over time, but instead preferentially increased synaptogenesis with their primary synaptic partner(s) with age. Such preferential synaptogenesis was also observed during the later developmental stages of the zebrafish the H3 horizontal cell (Yoshimatsu et al., 2014), but was preceded by a period of synapse pruning with inappropriate partners. Analysis at stages prior to vision onset will be necessary to determine whether or not, like these horizontal cells, BCs eliminate errant synapses before engaging in preferential synaptogenesis.

It may be that the distribution of *xfz43* BC synapses amongst partner types is shaped solely by the relative abundance of different cones types. Each of the cone photoreceptor populations is stable after cone genesis; thus, the loss or addition of different cone types cannot account for *xfz43* BC preferential synaptogenesis over time. However, although each cone type is uniformly distributed across the larval retina, the relative density of each cone type differs, forming a hierarchy of cell densities: red > green ~ UV > blue cones (Allison et al., 2010; Suzuki et al., 2013). Thus, the availability of red and green cones alone could conceivably account for the numbers of ON T1 and OFF BC synapses with each of these two cone types at maturity, as both of these BCs contact all of the red and green cones in the vicinity of their dendritic arbors. In contrast, ON T2 BCs do not contact all of their potential green cone partners. Manipulations of cone numbers previously demonstrated that H3 horizontal cells attain synaptic bias towards one cone type by employing a heterosynaptic mechanism; synaptogenesis with the primary input type suppressed synapse formation with the secondary input (Yoshimatsu et al., 2014). It is therefore possible that for ON T2 BCs, contact with red cones suppresses synaptogenesis with green cones. In the future, manipulations of the relative availability of red and green cones during development could confirm whether heterosynaptic control of synaptogenesis is at play in BC circuit assembly.

2.5 Figures

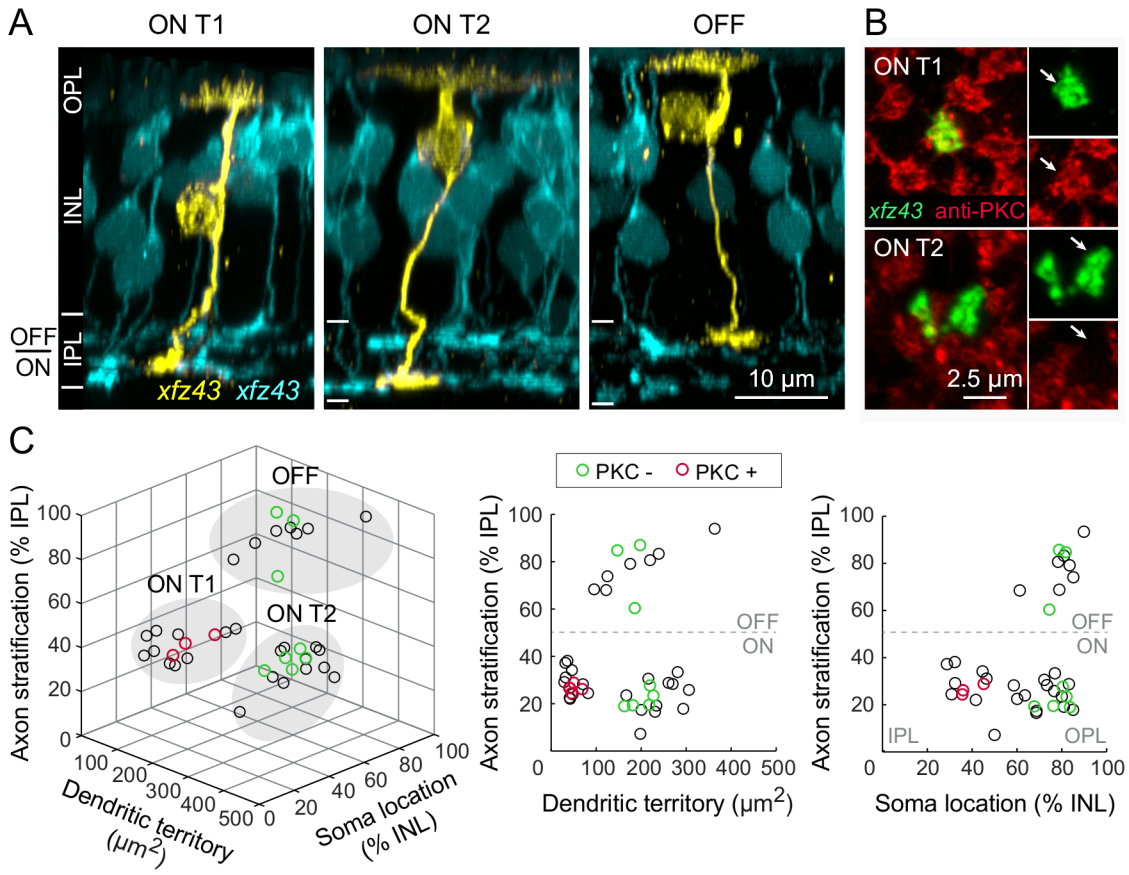

Figure 2.1 Morphology and classification of three *xfz43* BC types in larval zebrafish retina.

(**A**) Maximum intensity projections of confocal image stacks of individual *xfz43* BCs (yellow) together with the *xfz43* BC population (cyan) in 20 dpf tissue. Individual cells were visualized by transient fluorescent protein (FP) expression in *xfz43* transgenic fish (see Methods). The dendrites of BCs target the outer plexiform layer (OPL) while their axons project to the inner plexiform layer (IPL), and BC nuclei reside in the inner nuclear layer (INL). ON Type 1 (ON T1) and ON Type 2 (ON T2) populations stratify their axon terminals in the inner half of the IPL (ON), whereas a third population stratifies in the outer half (OFF). (**B**) *En face* views of ON T1 and T2 BC axon terminals with antibody labeling against PKC. Arrows mark the BC axon terminal. (**C**) Scatter plots show population data for the morphology and PKC expression of individually labeled cells (see Methods and Figure 2.2 for details on morphological analyses). Each open circle represents a single cell, $n = 39$ cells. Cells that were analyzed for PKC expression are green (PKC-negative) or red (PKC-positive). Filled, gray ovals depict the groups by which cells were classified as ON T1, ON T2, or OFF types using the K-means clustering algorithm. All measurements were made in 20 dpf *xfz43* larvae.

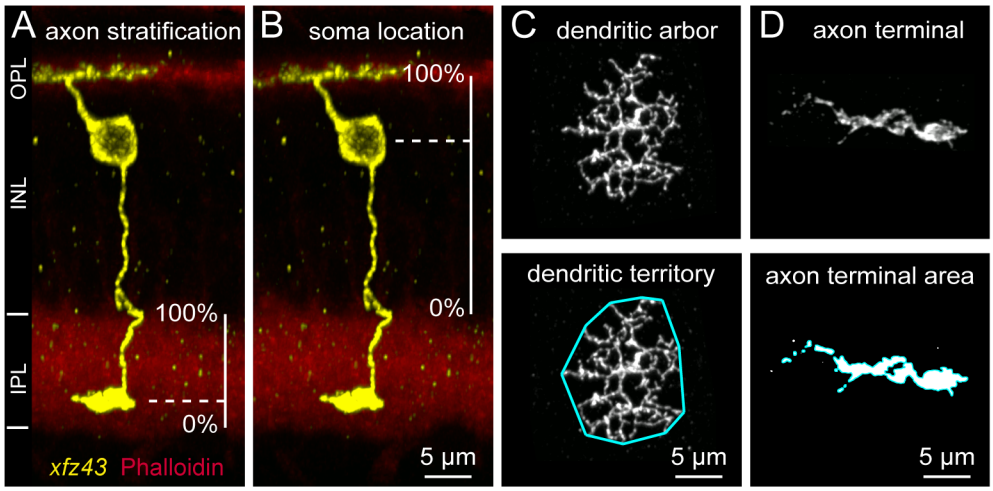

Figure 2.2 Quantitative analysis of BC morphology.

(**A**) The stratification levels of BC axons were analyzed by measuring the distance of the axon terminal from the inner (0% IPL width) to outer IPL (100% IPL width), and normalizing to the total width of the IPL. The IPL was visualized by an actin or nuclear stain. (**B**) The locations of BC somata within the INL were assessed by measuring the distance from the center of the soma to the OPL, and normalizing to the total width of the INL. The INL width was judged as the distance from the outer boundary of the IPL (0% INL width) to the OPL (100% INL width). (**C**) The sizes of BC dendritic territories were analyzed by visualizing a maximum intensity projection of the dendritic arbor en face, drawing a boundary around the outermost dendritic tips, and measuring the area within the resulting polygon (shown outlined in cyan). (**D**) BC axon terminal size was quantified as the area of the axon terminal in a thresholded maximum intensity projection. This was achieved by converting the image fluorescence into a binary mask, and measuring the masked area that corresponded to the individual axon terminal (shown outlined in cyan).

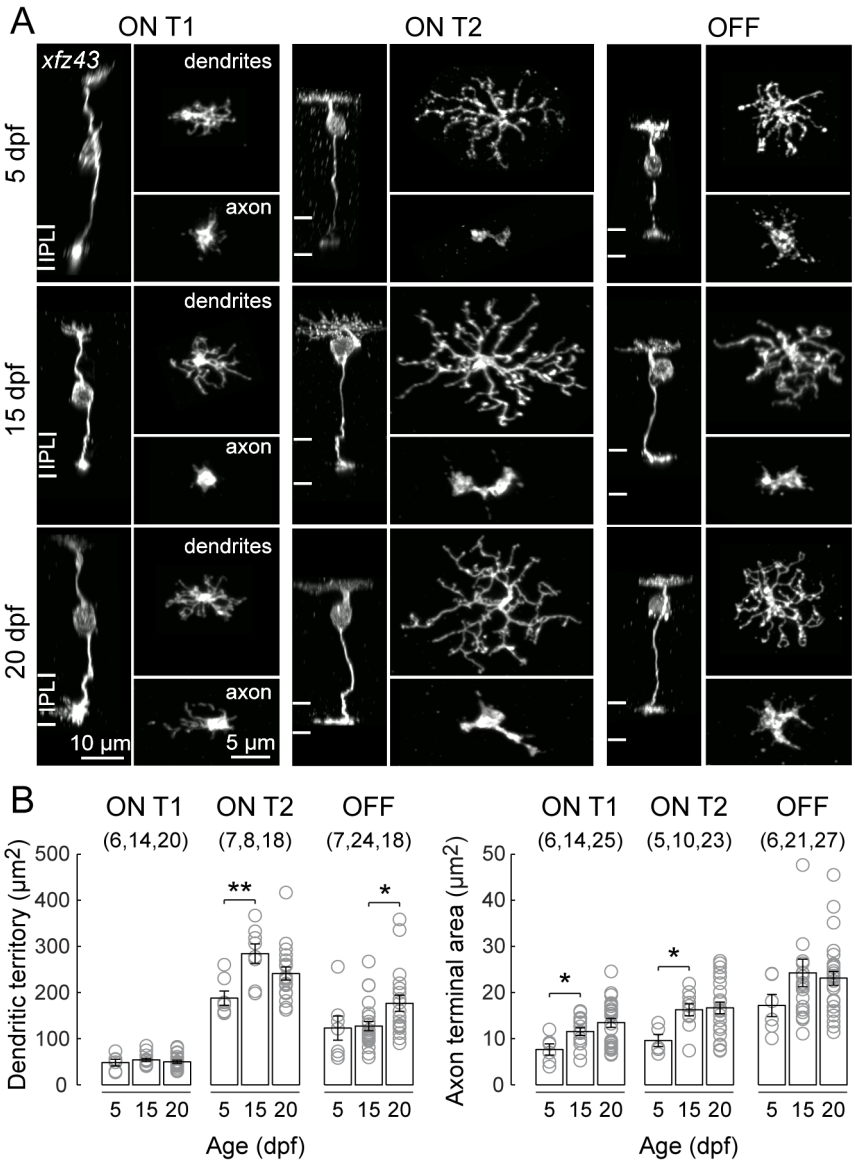

Figure 2.3 The neurites of *xfz43* BCs grow without remodeling during maturation.

(**A**) Representative ON T1, ON T2, and OFF *xfz43* BCs visualized in fixed retinal tissue at 5, 15, and 20 dpf. BCs were classified based on a combination of dendritic territory and axon stratification measures. Side views of whole BCs, *en face* views of dendritic arbors and axon terminals. (**B**) Plots across ages of the mean dendritic territory sizes and axon terminal areas for each *xfz43* BC type. Each open circle represents one cell, with the number of cells analyzed in parentheses. Error bars are ± standard error of the mean (SEM). * $P < 0.05$, ** $P < 0.01$; Wilcoxon-Mann-Whitney rank sum test.

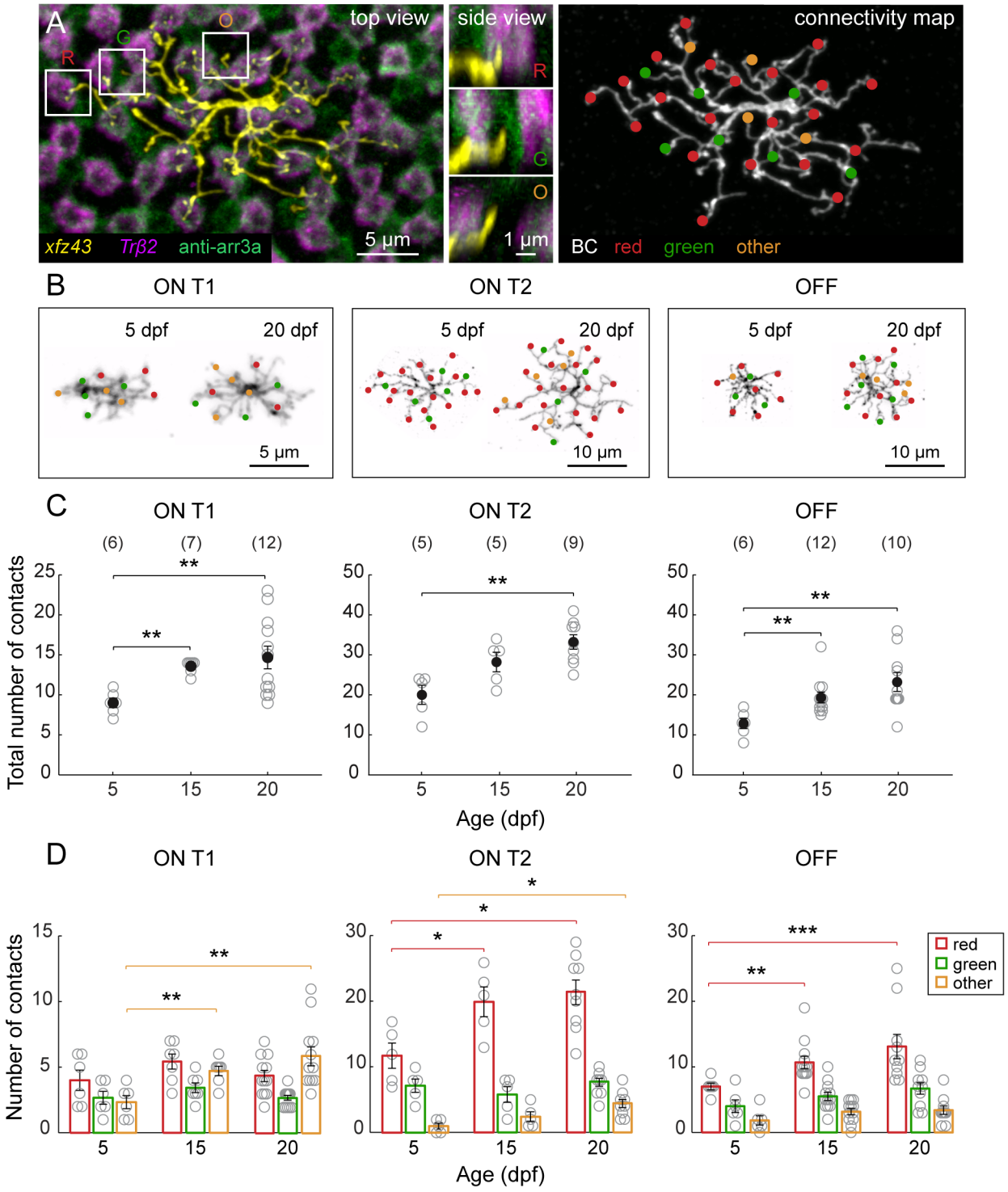

Figure 2.4 *xfz43* BCs generate type-specific connectivity patterns over time by preferential synaptogenesis.

(**A**) An individual ON T2 BC labeled by transient FP expression in a 20 dpf *xfz43* transgenic fish crossed with *Tg(trβ2:Tomato)*. *Trβ2*, red cones; anti-arr3a, red and green cones. Dendritic invaginations into red cones (R) and green cones (G), as well as dendritic tips not associated with

red or green cones, “others” (O), are evident at the level of the cone axon terminals (top view), and in vertical views of the boxed areas (side view). Filled circles map the locations of dendritic tips that contacted red or green cones, or others. (**B**) Representative connectivity maps of each *xfz43* BC type from 5 to 20 dpf. (**C**) Population data showing the mean, total number of invaginating dendritic tips per BC type from 5 to 20 dpf. (**D**) Quantification of the mean number of contacts per cone type across ages. Open circles represent values from individual cells, with the number of cells analyzed shown in parentheses. Error bars are ± SEM. * $P < 0.05$, ** $P < 0.01$, *** $P < 0.001$; Wilcoxon-Mann-Whitney rank sum test.

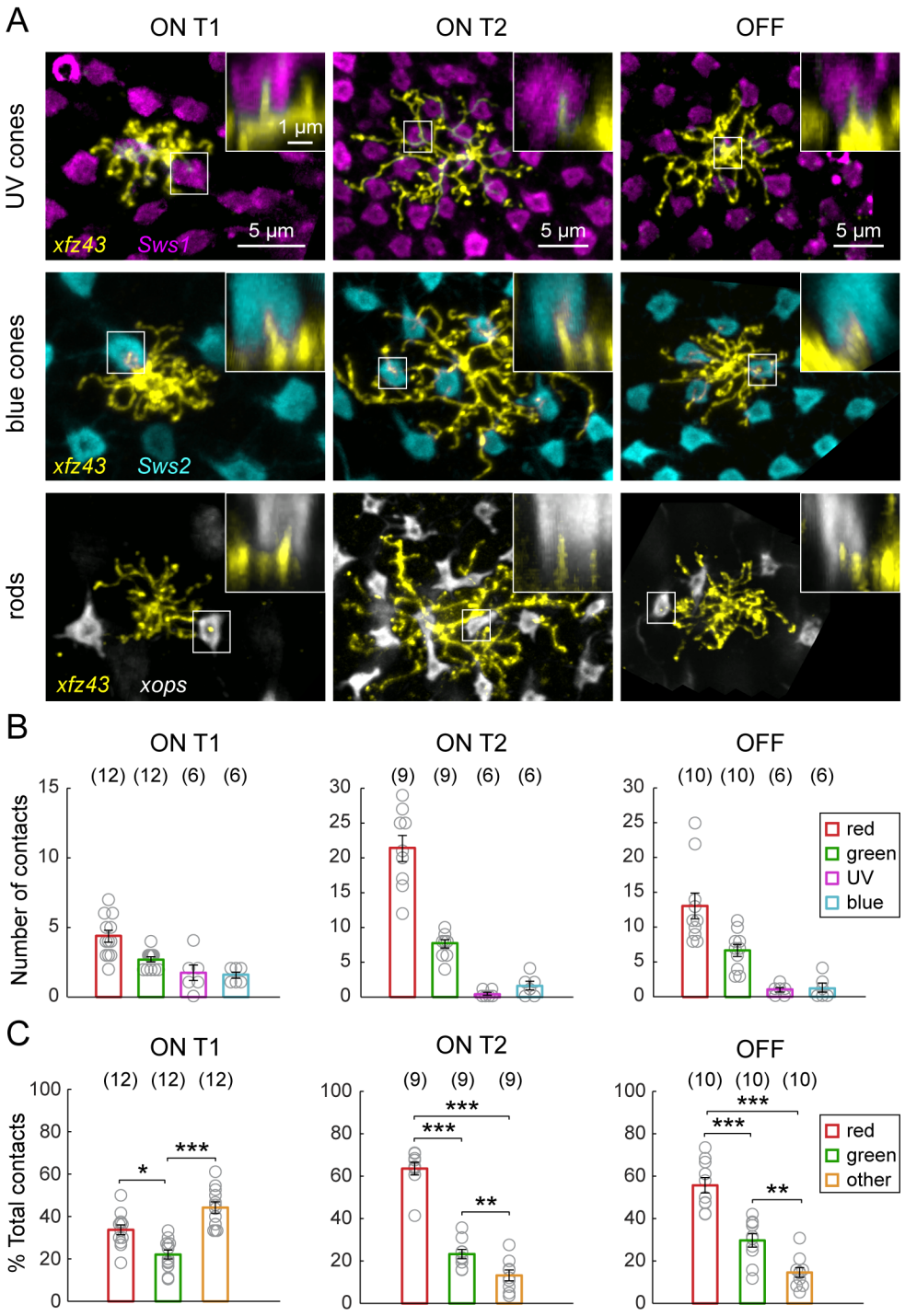

Figure 2.5 *xfz43* BC types contact non-red and green photoreceptor types to varying degrees.

(**A**) *xfz43* BCs can contact UV cones, blue cones, and rods. Images show maximum intensity projections of the dendritic arbors of individual BCs visualized in the *xfz43* fish in the background of labeled UV cones *Tg(sws1:GFP)*, blue cones *Tg(sws2:GFP)*, or rod photoreceptors *Tg(xops:GFP)* at 15 or 20 dpf. Insets are vertical views showing invaginating

dendritic tips. **(B)** Quantification of the mean number of cone photoreceptors of each type that were contacted. Data is pooled from fish in which red, green, UV and blue cones were labeled together, only UV and blue cones were labeled together, or only red and green cones were labeled. (**C**) Plots show the mean proportion of contacts made with red, green, or other cone types, relative to the total number of contacts. Each open circle represents a single cell, with the number of cells analyzed shown in parentheses. Error bars are ± SEM. * $P < 0.05$, ** $P < 0.01$, *** $P < 0.001$ Chi-square test. All measurements were made in 20 dpf *xfz43* larvae.

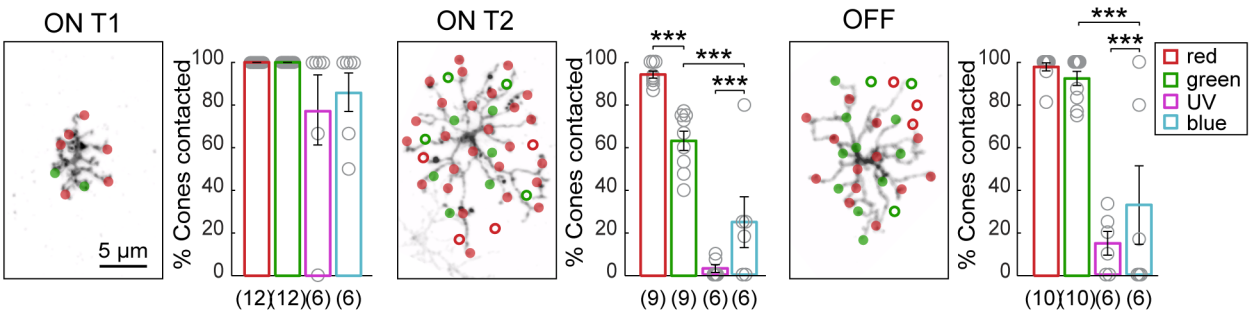

Figure 2.6 Differences in BC wiring with preferred partners to generate biased connectivity.

Plots show the percentage of cones contacted relative to the number of available cones of each type (% cones contacted). Open circles represent individual cells, with the number of cells analyzed shown in parentheses. Error bars are ± SEM. *** $P < 0.0001$, Chi-square test. Connectivity maps demonstrate the method used for quantifying the number of "available" cones of each cone type, with only red and green cones shown. In the maps, filled circles mark the locations of cone contacts, open circles denote the center of mass of cone terminals within the BC dendritic territory that were not contacted.

2.6 Tables

Table 2.1. Summary of *xfz43* BC type morphology.

	Axon stratification (% IPL)	Dendritic territory (μm^2)	Soma location (% INL)
ON T1	28.2 ± 5.0 (15)	49.8 ± 15.4 (20)	42.8 ± 11.8 (13)
ON T2	22.3 ± 6.6 * (16)	241.2 ± 60.2 *** (18)	75.4 ± 8.7 ** (16)
OFF	77.9 ± 9.9 ** (10)	176.7 ± 75.0 *** (18)	79.3 ± 7.6 ** (10)

Population data for classified *xfz43* BC types. Values are mean ± standard deviation (SD). The number of cells analyzed is shown in parentheses. Pair-wise comparisons were made with ON T1 BC measurements: * $P < 0.05$, ** $P < 10^{-4}$, *** $P < 10^{-6}$; Wilcoxon-Mann-Whitney rank sum test. All measurements were made in 20 dpf *xfz43* larvae.

Chapter 3. Mismatch of synaptic patterns between neurons produced in regeneration and during development of the vertebrate retina

3.1 Summary

Stereotypic patterns of synaptic connections between neurons underlie the ability of the central nervous system (CNS) to perform complex but circuit-specific information processing. Tremendous progress has been made toward advancing our understanding of how circuits are assembled during development, but whether the precision of this process can be recaptured after regeneration of neurons in the damaged CNS remains unclear. Here, we harnessed the regenerative capacity of the zebrafish retina to reconstruct the circuitry of neurons produced after damage. We focused on the connectivity of identified bipolar cell (BC) types that demonstrate stereotypic dendritic wiring with cone photoreceptors. After selective ablation, the targeted BC types are rapidly reproduced and largely re-establish their characteristic morphological features. The regenerated population connects with appropriate photoreceptor types and establishes the original number of synaptic contacts. However, BC types that normally bias their connectivity in favor of red cones fail to precisely recapture this synaptic partner preference upon regeneration. Furthermore, regenerated BCs succeed in forming synaptic specializations at their axon terminals, but in excess of the usual number. Altogether, we find that regenerated BCs reinstate some, but not all major features of their stereotypic wiring, suggesting that circuit patterns may be unable to regenerate with the same fidelity as in development.

Portions of Chapter 2 were published in Current Biology, which maintains copyrights for this material, and has been reprinted with permission: D'Orazi F.D., Zhao X.-F., Wong R.O., Yoshimats T. Mismatch of synaptic patterns between neurons produced in regeneration and during development of the vertebrate retina. Curr. Bio., in press.

3.2 Introduction

Most mammalian central nervous system (CNS) networks do not spontaneously replace neurons lost due to injury or disease. Techniques to restore neuronal circuitry and function by cell replacement therapy are rapidly advancing, but cell transplantation efforts are still hindered by limitations in neuronal survival and cell migration. Cell replacement therapies have thus recently focused on strategies to induce production of neurons *in situ* (Arlotta and Berninger, 2014; Becker and Becker, 2015). For example, regeneration of retinal neurons in mammals can be induced by exogenous stimulation of resident glia after retinal injury (Ueki et al., 2015). However, progress in this field has fallen short of understanding the ability of regenerated neurons to reinstate their precise synaptic wiring patterns, a fundamental requirement of CNS function.

Here, we capitalized on the regenerative ability of zebrafish (Lenkowski and Raymond, 2014) and the stereotypic organization of the retina to determine the accuracy of circuit repair after endogenous neuronal repopulation in the damaged CNS. We investigated the circuitry of identified bipolar cell (BC) types, which we previously demonstrated exhibit characteristic morphologies and stereotypic patterns of wiring with cone photoreceptors. We targeted these BCs for selective ablation in order to assess the ability of new neuronal populations to integrate into previously assembled, mature circuitry. BCs face similar challenges during retinal development as in regeneration, because they are the last neurons to differentiate during the initial assembly of retinal circuits. This led us to ask: Can regenerated BCs access developmental cues to regain their original wiring patterns? The developmental factors that guide BC integration during early retinal stages may not persist into maturity. Further, regenerated BCs are produced from a different progenitor source (Müller glia) (Ramachandran et al., 2010) than BCs generated during early development (Lenkowski and Raymond, 2014) and thus may not have access to the same intrinsic signals.

To answer this question, we reconstructed the morphology and connectivity of *xfz43* BCs (Zhao et al., 2009) after regeneration of these cell types in larval zebrafish. Selective ablation of *xfz43* BCs induced their regeneration within days, and all three BC types in general retained the capacity to acquire type-specific morphological features. Importantly, regenerated BCs form synapses at both their dendrites and axons. However, despite being reproduced *in situ*, regenerated BCs fail to precisely capture their original wiring patterns with photoreceptors.

These results suggest that developmental mechanisms that shape specific wiring patterns may not all be accessible to regenerated neuronal populations.

3.3 Methods

Selective cell ablation

xfz43 larvae were immersed in Metronidazole (Met) solution (10 mM Met in system water containing 0.2% DMSO) at 7 dpf for 20-24 hours to ablate NTR-expressing BCs. Larvae were fed regularly, and washed in clean system water at the end of treatment and raised normally.

EdU labeling

Mitotic cells were labeled in live larvae by immersion in a solution containing 0.5 mM F-ara-EdU (Yoshimatsu et al., 2016) (Sigma T511293) in system water. The duration of treatment was timed according to the experimental paradigm. Half the solution volume was replaced every other day.

For visualization of EdU labeling, fixed whole retinas were permeabilized in 0.3-0.5% TritonX-100 (Sigma T8787) in 0.1 M PBS for 30 minutes at room temperature, and then washed three times in PBS. Click reactions were carried out in PBS solution with 10 μM Cy5-azide (Lumiprobe A2020), 2 mM copper(II) sulfate (Sigma 45167), and 20 mM sodium ascorbate (Sigma A7631) for 1 hour at room temperature. Samples were processed for immunohistochemistry after three PBS washes.

In vivo imaging

Embryos were injected with pCrx:MYFP at the single cell stage, which labeled columns of retinal cells with FP to facilitate tracking of the same retinal regions across time points. Larvae were live-imaged between 7 and 8 dpf by two-photon microscopy. Fish were anesthetized with MS-222 (25-50 mg/L) in system water, immersed in melted 0.5% low-melting-point-agarose (type VII, Sigma) in system water, and mounted in 60 mm organotypic culture dishes (Falcon). After the agarose solidified, the mounted larvae were covered with system water containing 0.2 mM PTU and MS-222 (25-50 mg/L). Image stacks were acquired on a custom-built two-photon microscope with a Ti-Sapphire tunable infrared laser (Spectra-Physics) at 780-920 nm. A 1.1 NA 60x water-immersion objective lens with a refractive index correction collar (Olympus) was used. Images were acquired at an XY resolution of 0.07 μm/pixel, and 1 μm Z steps. Larvae were

released from the agarose after no longer than one hour, and returned to system water without MS-222 to recover from anesthesia.

Electron microscopy

Euthanized larvae were fixed with 4% glutaraldehyde in 0.1 M sodium cacodylate buffer, pH 7.4 and centrifuged at 13,000 rpm for 4 hours at room temperature. Samples were placed in fresh fixative overnight at room temperature, then washed three times in sodium cacodylate buffer, and placed in 1% osmium tetroxide in buffer. Tissue was dehydrated in a graded ethanol series, resin embedded, sectioned, and imaged with a transmission electron microscope.

Statistical analysis

In Figure 3.1B, the Wilcoxon-Mann-Whitney rank sum test was used to compare the densities of each cone population between control and Met-treated conditions. In Figures 3.2D, Figure 3.5B, and Figure 3.6C, the Wilcoxon-Mann-Whitney rank sum test was used to compare measurements between control and regenerated BCs. In Figure 3.3B and Figure 3.3D, the Wilcoxon-Mann-Whitney rank sum test was used to compare the densities of regenerated *xfz43* bipolar cells from different EdU treatment conditions, as well as the densities of specific cone populations between control and Met-treated conditions. In Figure 3.6D, a Chi-square test was used to compare the proportion of cones contacted between control and regeneration conditions. In Figure 3.6E, a Chi-square test was used to compare the distribution of contacts amongst partners between control and regenerated bipolar cells, as well as to compare the proportions of total contact made amongst all three partner types or in pair-wise comparisons between partner types. All statistical tests were performed using a significance level of 0.05.

All other methods are as noted in 2.2.

3.4 Results

xfz43 BCs regenerate within days of cell-specific ablation

Neuronal differentiation is complete by 74 hours post-fertilization in the zebrafish retina (Schmitt and Dowling, 1999), with the exception of the addition of rods, and visually-guided behaviors are already exhibited by 5 dpf (Easter Jr and Nicola, 1996). In order to determine the capacity of regenerated *xfz43* BCs to integrate into an established network, we selectively ablated these BCs after 5 dpf using a genetically-targeted approach (Curado et al., 2007). The bacterial enzyme, Nitroreductase (NTR; *nfsB*), converts its prodrug, Metronidazole (Met) (Lindmark and Muller, 1976) into a metabolite that is toxic to NTR-expressing cells (Curado et al., 2007). Multiphoton time-lapse imaging of *xfz43* BCs expressing NTR-mCherry FP showed that 24 hours of Met treatment caused death of the majority of *xfz43* BCs in the field of view (Figure 3.1A). Visualization of nearby non-NTR BCs expressing cerulean FP in *Tg(vsx1:MCerulean; xfz43)* double transgenic fish indicated that Met treatment did not damage non-NTR BCs (Figure 3.1A). Also, there were no obvious bystander effects on the cone photoreceptors after Met application in *xfz43* larvae; the morphology, mosaic distribution, and population densities of each cone type appeared normal at 12 dpf, 5 days post-ablation (5 dpa) (Figure 3.1B). Ultrastructural analysis further indicated that the fine structure of the cone synapses in Met-treated *xfz43* fish was intact; presynaptic ribbons localized opposite to the invaginating processes of remaining BCs despite the loss of *xfz43* BC postsynaptic partners (Figure 3.1C). Thus, *xfz43* BC ablation does not disrupt the structural arrangements of other BCs or the presynaptic cone photoreceptors in ways that would obviously interfere with the integration of new cells into the environment.

Although Met treatment was effective, ablation of the *xfz43* population was not complete. Therefore, to unequivocally identify the regenerated cohort of *xfz43* BCs, we labeled newly generated cells by exposing Met-treated animals to (2′*S*)-2′-Deoxy-2′-fluoro-5-ethynyluridine (EdU) following the ablation period. Previous studies of inner retinal regeneration suggest that cell proliferation peaks within 3-4 days of cell death (Fausett and Goldman, 2006; Fimbel et al., 2007). As such, we exposed Met-treated and control *xfz43* larvae to EdU between 9 and 12 dpf (2-5 dpa), and imaged at 20 dpf (13 dpa). The lack of EdU labeling in the inner nuclear layer (INL) of control, untreated animals confirmed that BC genesis does not occur in undamaged retinas between 9 and 12 dpf (Figure 3.2A). In contrast, EdU-positive *xfz43* BCs were evident in

Met-treated larvae, demonstrating that these cells regenerated after selective ablation (Figure 3.2A). But, at least by 13 dpa, the *xfz43* BC population density had not recovered fully (control BC density: 37.7 ± 3.3 cells per 1000 μm^2, n = 4 retinas; Met-treated BC density: 6.2 ± 0.8 cells per 1000 μm^2, n = 6 retinas; P = 0.01 Wilcoxon-Mann-Whitney Rank Sum test). Further, exposing Met-treated animals to EdU at a later stage, from 5-8 dpa, revealed that very few additional BCs are generated past 5 dpa (Figure 3.3A-B).

EdU also incorporated in the outer nuclear layer (ONL) of both control and Met-treated animals after EdU immersion from 2-5 dpa (Figure 3.2A). Transgenic labeling of the rod population in control animals confirmed that the EdU-positive cells in the ONL were late-generated rods (Figure 3.3C). Rod genesis is likely ongoing in Met-treated *xfz43* animals as well, but we also found evidence that *xfz43* ablation triggers production of new cones (Figure 3.3C). Quantification showed that the addition of new cones after BC ablation did not significantly alter the population densities of red and green cones by 13 dpa (Figure 3.3D).

Regenerated BCs largely establish type-specific morphological organization

We found that virtually all of the regenerated BCs were polarized and stratified their neurites in the appropriate plexiform layers (Figure 3.2A). Further, the axons of PKC-positive BCs ramified exclusively in the ON sublamina, as in controls (Figure 3.4A). Nonetheless, regenerated BCs occasionally showed atypical morphology. A subset of the cells made unusual axonal trajectories toward the inner plexiform layer (IPL) (<10% of 60 BCs imaged), whereas others mislocalized their somata to the outer nuclear layer (ONL) (~20% of BCs imaged) (Figure 3.2B). We also observed dendritic abnormalities, including asymmetric dendritic projections within the outer plexiform layer (OPL), as well as arbors with sparse branching (~20% of BCs imaged for each measure; Figure 3.2C, compare with Figure 2.3A). Regenerated cells with unusual morphologies thus represented the minority of the population; overall, regenerated *xfz43* BCs exhibit the basic characteristics of a BC. We then investigated whether the regenerated BCs attained type-specific characteristics. As in the original cohort, only a subset of the ON *xfz43* BCs expressed PKC (Figure 3.4B). Moreover, based on morphological features alone, regenerated BCs clustered into three groups, resembling those of ON T1, ON T2, and OFF *xfz43* BCs in controls (Figure 3.4C, compare with Figure 2.1C). Direct comparisons of age-matched control and regenerated BCs from each group demonstrated that *xfz43* BCs precisely target their axons and somata to the IPL

or INL locations appropriate for their type (Figure 3.2D). Thus, each of the three distinct *xfz43* BC types is regenerated following elimination of their original populations.

The dendritic and axonal arbors of the regenerated BCs elaborated to sizes comparable to, or in some cases greater than those of mature BCs in control animals (Figure 3.2D). The dendritic and axonal arbors of regenerated ON T1 BCs were almost twice as large as those of the cohort from age-matched controls (Figure 3.2D). The axon terminals of ON T2 BCs were slightly larger in the regenerated population, but there was no significant difference in their dendritic arbor size compared to controls. However, both the axons and dendritic arbors of OFF *xfz43* BCs were comparable in the regenerated and control populations. Thus, all three *xfz43* BC types largely attain their original morphologies upon regeneration, but show type-specific differences in whether their arbor sizes matched that of the original populations.

We wondered whether BCs that survived Met treatment similarly remodeled their synaptic territory sizes after cell loss. To address this, we first determined whether *xfz43* BCs are generated at even later stages than previously tested, i.e. from 7 dpa on. EdU treatment of ablated *xfz43* larvae from 7-13 dpa labeled, at most, two *xfz43* BCs per retina (density of EdU-positive *xfz43* BCs: 0.38 ± 0.26 cells/10,000 μm^2, $n = 7$ retinas). As such, the BCs that did not incorporate EdU between 1-7 dpa likely survived Met treatment. We subsequently labeled individual *xfz43* BCs with MYFP via plasmid injection in *xfz43* embryos, and treated these fish with Met, followed by EdU from 1-7 dpa. Analysis of EdU-negative *xfz43* BCs at 13 dpa revealed that, in contrast to their regenerated counterparts, surviving ON T1 and OFFS did not alter their dendritic and axonal territory sizes (Figure 3.2D). However, surviving ON T2 BCs did expand their axonal arbors, and even more so than the regenerated population ($P = 0.02$, Wilcoxon-Mann-Whitney rank sum test) (Figure 3.2D). Thus, the plasticity of a given BC type may vary under different conditions, whether in response to the loss of neighboring cells, or while re-integrating into a mature circuit after regenerating.

Regenerated BCs capture most but not all features of their synaptic wiring patterns

We next determined whether or not regenerated BCs made synapses and were able to re-establish their original stereotypic patterns of connectivity. BCs form specialized ribbon synapses in the IPL, which can be visualized by immunolabeling for Ribeye A (Figure 3.5A), a major component protein of these presynaptic structures (Wan, 2005). Ribeye A was present in the

axon terminals of regenerated *xfz43* BCs of all three types, as in age-matched controls (Figure 3.5A). But, the terminals of each BC type contained on average a higher total number of ribbons upon regeneration (Figure 3.5B). Further, ribbon density increased for regenerated OFF BCs when compared to cells from age-matched controls (Figure 3.5B). As such, regenerated BCs develop presynaptic specializations upon regeneration, but there may be an over-abundance of contact with their postsynaptic partners.

Assessing the precision of regenerated *xfz43* BC rewiring was more tractable for their dendritic connections with cones. We focused on ON T2 and OFF BCs to determine whether cells showing biased connectivity with specific cone types maintain these preferences upon regeneration. We found that regenerated cells of both types formed invaginating dendritic tips into cone axons and made approximately the same total number and density of cone contacts as their counterparts in age-matched controls (Figure 3.6B). Compared to controls, ON T2 BCs increased connectivity with all partner types except for red cones, and OFF BCs increased contact with the least-preferred ("other") photoreceptors types (Figure 3.6C). Furthermore, ON T2 and OFF cells failed to contact all of the available red cones during regeneration (Figure 3.6D). These outcomes resulted in an altered distribution of contacts amongst partner types (Figure 3.6C, E). Regenerated ON T2 BCs maintained a preference for red cones (Figure 3.6E), but the extent of their bias towards red cones was reduced upon regeneration, as they contacted only ~1.5 red cones: 1 green cone instead of about 3:1 (P = 0.003, Wilcoxon-Mann-Whitney rank sum test) (Figure 3.6D). The proportion of connections that regenerated OFF cells made with red cones, green cones, and others were approximately equal (Figure 3.6E), suggesting that their bias for red cones was highly diminished.

3.5 Discussion

Differentiation of regenerated BCs

The morphologies of regenerated *xfz43* BCs largely matched those of the original populations, however, not all regenerating BCs were normal in appearance. Some cells had larger neurite arbors, which may be due to a decrease in homotypic repulsion between BCs of the same type (Grueber and Sagasti, 2010). Indeed, *xfz43* BC types do not fully recover their population densities after regeneration. However, the majority of *xfz43* BCs that survived did not remodel their arbors upon loss of homotypic neighbors. These observations together suggest that in general, regenerating BCs may be more plastic than BCs that have already established their territories during development. Alternatively, because BCs regenerate within days of their ablation, survivors may not have sufficient time to respond to the loss of homotypic neighbors.

Regenerated BCs appear to re-adopt their appropriate molecular identities, despite being produced from a different progenitor source than that in early development. Regenerated cells in the zebrafish telencephalon (Kroehne et al., 2011; Skaggs et al., 2014) and spinal cord (Kuscha et al., 2012a, 2012b; Reimer et al., 2008) similarly can acquire type-specific molecular characteristics, but are sometimes derived from radial glia that also participate in initial neurogenesis (Becker and Becker, 2015; Kim et al., 2008). The ability of regenerated BCs to target and elaborate within the appropriate synaptic layers with sublaminar precision further suggests that environmental cues directing neurite outgrowth are maintained in the mature CNS. Additional support for this hypothesis comes from studies in other brain regions of mice and zebrafish, in which the long-range axons of transplanted or regenerated neurons target correct areas (Skaggs et al., 2014; Michelsen et al., 2015; Magavi and Lois, 2008; Gaillard et al., 2007). Mistargeting has also been observed (Grimaldi et al., 2005; Magavi and Lois, 2008), however, suggesting that although developmental guidance cues likely persist, they may be variably accessible to newborn neurons in mature environments. Future experiments comparing the molecular profiles of early and late-born cells of the same type would be highly informative for distinguishing between key changes in extrinsic cues and differences in intrinsic properties.

Recapturing specific synaptic patterns in regeneration

Our current study shows that replacement neurons are able to form synapses with mature circuitry, an observation previously made in other CNS systems after damage (Barber et al., 2013; Gaillard et al., 2007; Grimaldi et al., 2005; Kroehne et al., 2011; MacLaren et al., 2006; Michelsen et al., 2015; Pearson et al., 2012; Reimer et al., 2008; Singh et al., 2013; Skaggs et al., 2014; Yoshimatsu et al., 2016). Further, we found that although regenerated *xfz43* BCs establish their original numbers of input synapses, the axons of all three BC types doubled their number of ribbons. For the ON BCs, increased ribbon formation may simply correspond to the larger axonal territories of the regenerated population, which likely bring the axonal processes in proximity to additional postsynaptic partners. Indeed, in mice the loss of homotypic neighbors causes BC axons to take over the synaptic territory of ablated BCs that share the same postsynaptic partner (Okawa et al., 2014). Regenerated BCs may be able to form connections with appropriate partners because their axons stratify within the sublamina characteristic of their type. But, this does not exclude the possibility that regenerated BCs also contact novel partners that intermingle in the same sublamina. The increase in ribbons may alternatively be due to an alteration in BC transmission. It was previously demonstrated that hyperactive BCs form an excess of excitatory synapses with RGCs in mice (Soto et al., 2012). If the activity of regenerated BCs is modified, it would further suggest that regenerated synapses with intact cones may be dysfunctional, or that the physiology of regenerated BC circuitry overall is disrupted, despite physical reconnection.

Visualizing ON T2 and OFF BCs together with their preferred presynaptic partners enabled us to resolve whether mechanisms that guide input partner preference and synapse allocation persist in regeneration. Regenerated ON T2 and OFF BCs alike still contact red and green cones, suggesting that signals to facilitate synaptogenesis with these partner types are accessible. Overall, regenerated BCs regained the stereotypic numbers of synapses with photoreceptors that are characteristic of their original populations. Similar observations were made of transplanted Purkinje cells after grafting cerebellar primordia in the damaged adult CNS. It was further revealed that the donor cells were contacted by the appropriate number of afferents after a period of synaptic refinement, as observed during normal development (Gardette et al., 1990; Sotelo et al., 1990). In contrast, ON T2 and OFF *xfz43* BC types do not preferentially increase synaptogenesis with red cones over other cone types during regeneration. Thus, the regenerating BCs do not appear to re-deploy the developmental strategy that they

would normally undertake to attain their unequal distribution of synapses amongst their contact partners. It is unlikely that regenerated BC wiring is altered simply because the BCs had not yet fully matured at the time of analysis, because the distributions of contacts amongst photoreceptor types do not resemble those of immature *xfz43* BCs, and regenerated BCs are otherwise morphologically mature. Thus, there may be separate mechanisms that regulate the total number of synapses made between BCs and photoreceptors, and that govern the distribution of these synapses across photoreceptor types.

We observed that both regenerated ON T2 and OFF BCs increased their number of minor (non-red cone, non-green cone) contacts, and ON T2 BCs also synapsed with more green cones compared to controls. In the H3 horizontal cell circuit, suppression of synaptogenesis with the secondary partner depends upon the activity of the primary input. If red cones similarly influence *xfz43* BC contacts with other input types, it could imply that transmission from red cones onto regenerated BCs may be dysfunctional, or that mature red cones do not induce the same suppressive effect as at immature ages. Another consideration is that production of rods increases with maturation (Stenkamp, 2011), giving the regenerating BCs greater opportunity to contact this minor partner type than during development. The consequences of rewiring into a different pool of potential inputs in the mature CNS may introduce an additional hurdle for regenerating neurons to precisely recapture their original connectivity patterns.

In conclusion, the fact that regenerated BCs can synaptically “plug in” at both their dendrites and axons suggests that these cells likely achieve functional integration in the retina. However, because stereotypic synaptic distributions do not appear to be re-established, regenerated BCs may exhibit visual response properties that do not resemble those of the original population. Moreover, our observations suggest that developmental strategies are not perfectly re-engaged in retinal regeneration. Our findings underscore that replacement neurons, although generated endogenously, do not necessarily have access to developmental cues that would readily facilitate completion of the final steps in circuit repair.

3.6 Figures

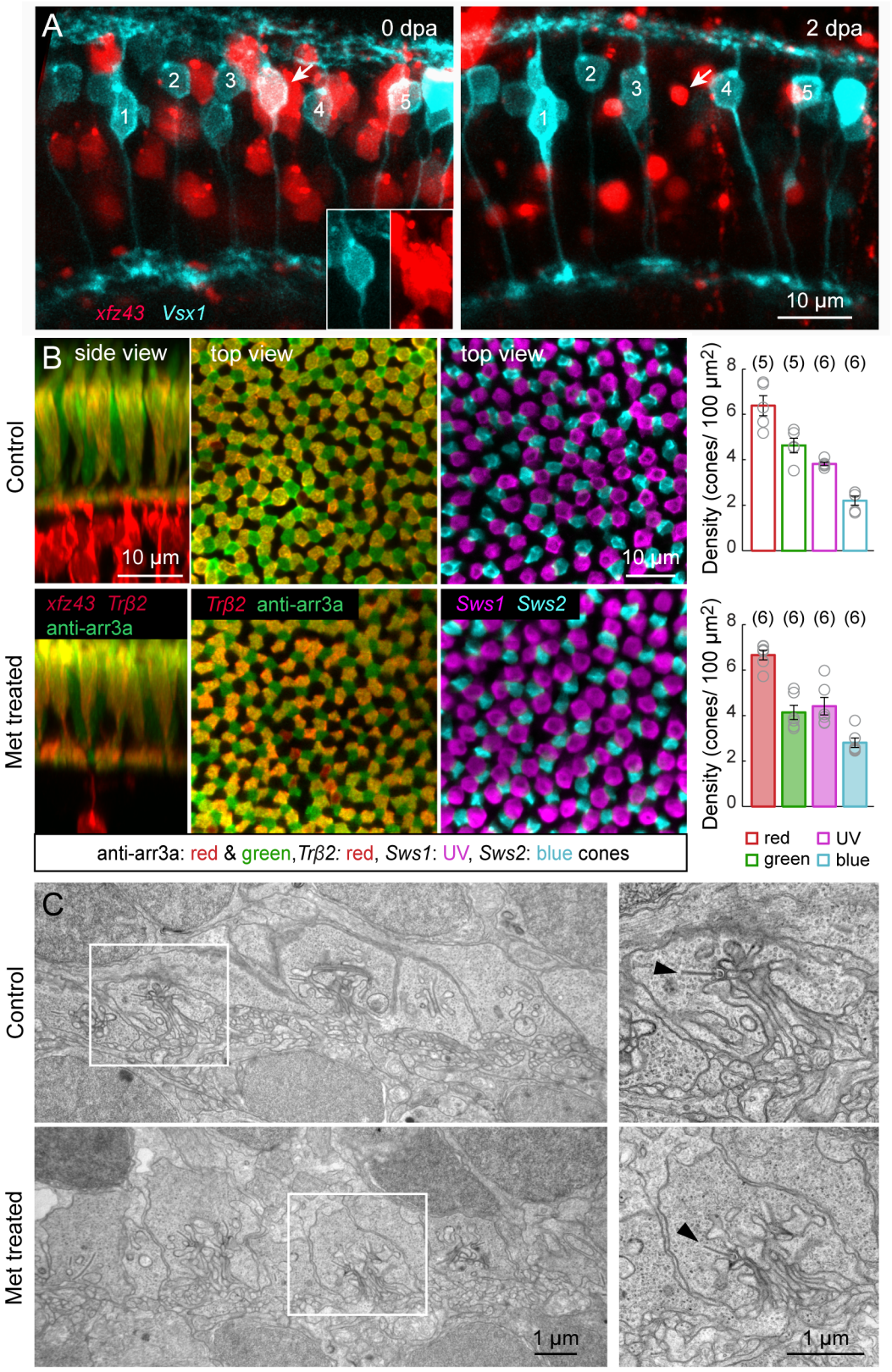
A
0 dpa
2 dpa
1
2
3
4
5
xfz43 Vsx1
10 μm
B
side view
top view
top view
Control
Met treated
10 μm
xfz43 Trβ2
anti-arr3a
Trβ2 anti-arr3a
Sws1 Sws2
anti-arr3a: red & green, Trβ2: red, Sws1: UV, Sws2: blue cones
Density (cones/ 100 μm2)
(5) (5) (6) (6)
(6) (6) (6) (6)
red
green
UV
blue
C
Control
Met treated
1 μm

Figure 3.1 Nitroreductase-induced ablation of *xfz43* BCs does not damage neighboring cells.

(**A**) Multiphoton time lapse imaging of *xfz43* BCs in the background of *Tg(Vsx1:MCerulean)* before and after cell ablation at 7 dpf. Larvae were imaged immediately prior to Met immersion, at 0 days post ablation (dpa), and after treatment, at 2 dpa. *Vsx1* labels a population of BCs that includes a subset of *xfz43* OFF BCs (arrow, inset). The somata of one of the *Vsx1* BCs translocated between imaging sessions (arrowhead). (**B**) Ablation of *xfz43* BCs in the background of transgenically or immunostained cones. Red and green cones were visualized in *xfz43* fish crossed with *Tg(trβ2:Tomato)* larvae together with anti-arrestin3a immunostaining. UV and blue cones were visualized in *xfz43* larvae crossed with *Tg(sws1:GFP; sws2:mCherry)*. Maximum intensity projections of confocal image stacks from 12 dpf (5 dpa) control or Met-treated retinas. Plots show the mean cell density of each cone type from Met-treated larvae at 5 dpa, and from age-matched control animals. Each open circle represents a single retina, with the number of retinas analyzed shown in parentheses. Error bars are ± SEM. Pair-wise comparisons of the densities of each cone population between conditions showed no significant differences ($P > 0.05$, Wilcoxon-Mann-Whitney rank sum test). (**C**) Electron micrograph of the OPL in control and Met-treated retinas from 12 dpf *xfz43* larvae. Insets show the ribbon synapses of single cone axon terminals. Arrowheads mark presynaptic ribbons.

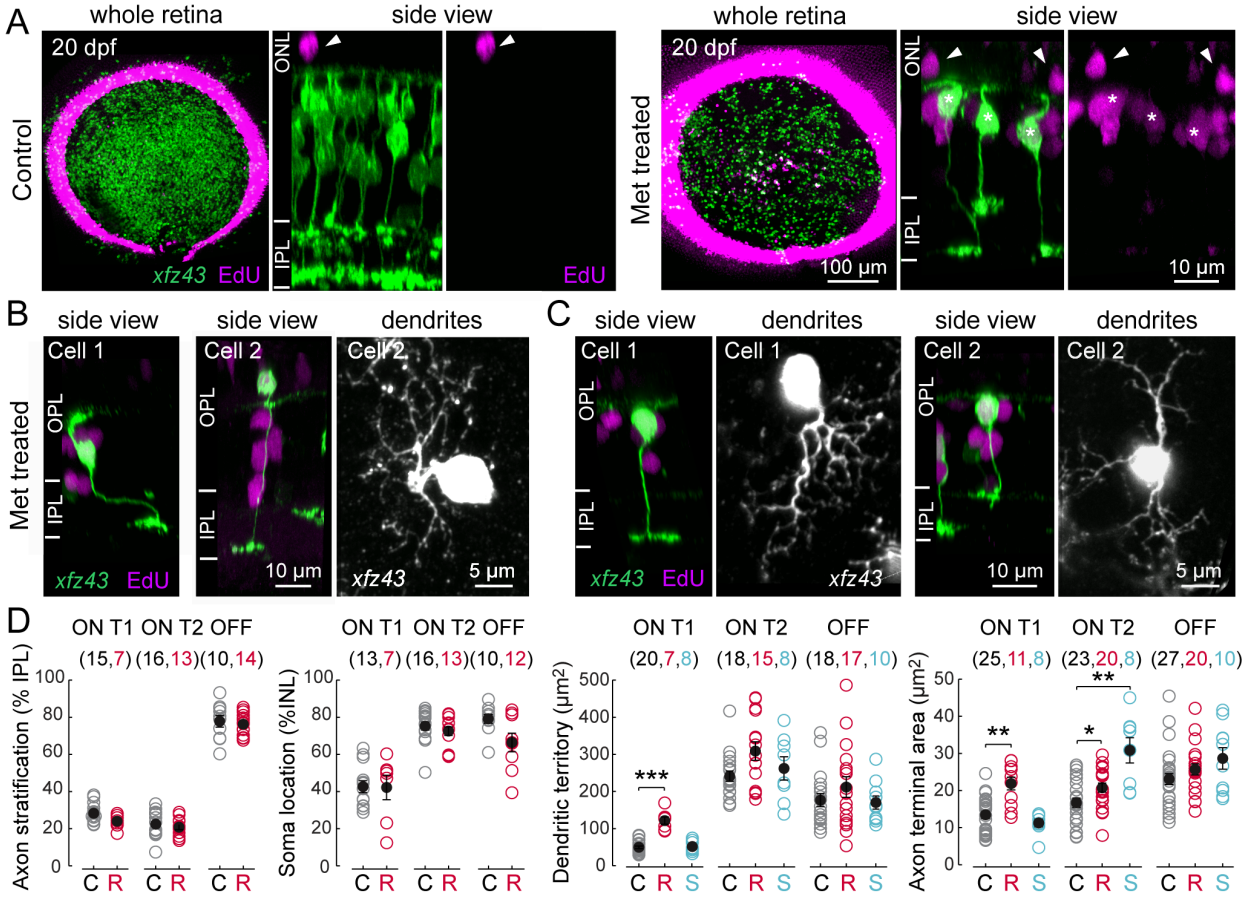

Figure 3.2 Regenerated *xfz43* BCs resemble age-matched BCs from intact tissue.

(**A**) Maximum intensity projections of wholemount retinas from 20 dpf (13 dpa) control and Met-treated *xfz43* fish in which mitotic cells were labeled by EdU application from 9-12 dpf (2-5 dpa). The dense ring of EdU-positive cells at the peripheral retina demarcates cells generated in the ciliary marginal zone, a region of ongoing proliferation (Lenkowski and Raymond, 2014). Asterisks in side views mark *xfz43* BCs that incorporated EdU, arrowheads mark EdU-positive cells in the outer nuclear layer (ONL). (**B**) Examples of regenerated *xfz43* BCs with abnormal axon trajectories (cell 1), or mislocalized somata (cell 2). (**C**) Examples of regenerated *xfz43* BCs with abnormal dendritic phenotypes; cell 1 has an asymmetric arbor relative to the cell body, cell 2 shows an unusually sparse dendritic arbor. In (B) and (C), side views are orthogonal rotations of the image stack acquired from the wholemount retina. Top views are the maximum intensity projections of the cell somata and their dendrites tilted slightly relative to the z-axis of the image stack, in order to illustrate the dendritic arbor, the primary dendrite, and the cell body, where possible. (**D**) Quantification of regenerated (R, red) and survivor (S, cyan) *xfz43* BC morphology. Cell types were classified using a combination of at least two morphological features: whether the BC stratified in ON or OFF IPL layers, dendritic territory size, and/or PKC expression. Plots show the population mean compared with control (C, gray) data. Open circles represent individual cells, with the number of cells analyzed shown in parentheses. Error bars are ± SEM. * $P < 0.05$, ** $P < 0.01$, *** $P < 0.001$; Wilcoxon-Mann-Whitney rank sum test. All measurements were made in 20 dpf (13 dpa) larvae.

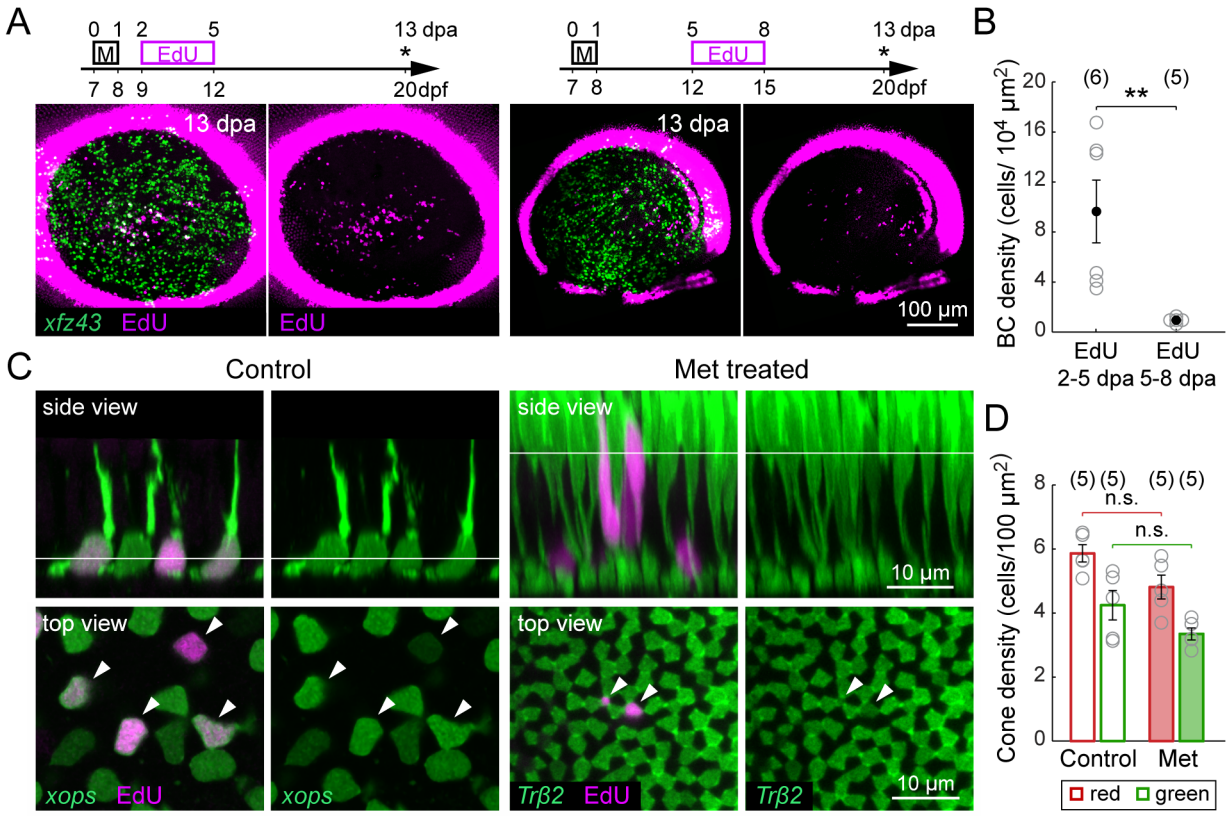

Figure 3.3 Proliferation of retinal neurons after targeted ablation of BCs.

(**A**) Peak proliferation occurs within 2-5 dpa. Timelines demonstrate the timing of EdU immersion after Met (M) application in two different groups: 2-5 or 5-8 dpa. Asterisks denote age at which larvae were fixed for imaging. Maximum intensity projections of wholemount retinas from 13 dpa Met-treated *xfz43* fish that were immersed in EdU. (**B**) Comparison of the mean density of EdU-positive *xfz43* BCs between larvae treated with EdU from 2-5 or 5-8 dpa. ** $P < 0.01$, Wilcoxon-Mann-Whitney rank sum test. (**C**) Photoreceptor genesis in the ONL of control and Met-treated *xfz43* larvae. (Side view) Orthogonal views of confocal image stacks from control and Met-treated *xfz43* animals, with co-labeling for EdU together with rods *Tg(xops:GFP)* or red cones *Tg(trβ2:Tomato)*. (Top view) En face view of the photoreceptors and EdU-labeled nuclei at the levels indicated in the side views. Arrowheads mark EdU-positive nuclei. (**D**) Quantification of the mean cell density of red or green cones in retinas from Met-treated and age-matched control *xfz43* fish crossed with *Tg(trβ2:Tomato)* and immunostained with anti-arrestin3a. Pair-wise comparisons showed that cone densities did not differ between control and Met-treated retinas (red cone density: $P > 0.05$, green cone density: $P > 0.05$, Wilcoxon-Mann-Whitney rank sum test). Each open circle represents a single retina, with the number of retinas analyzed shown in parentheses. Error bars are ± SEM. All measurements were made in 20 dpf (13 dpa) *xfz43* larvae.

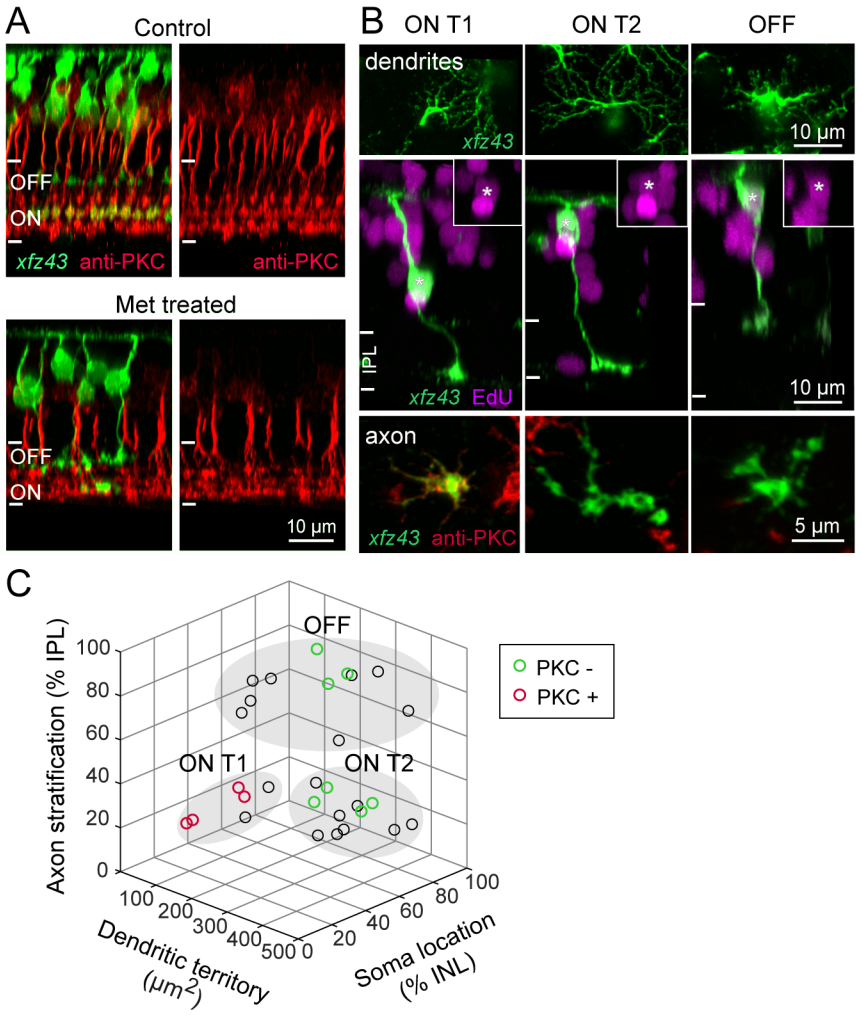

Figure 3.4 Regenerated BCs recover characteristic molecular expression and morphology.

(**A**) PKC-positive BCs stratify in ON layers of IPL in the retinas of control and Met-treated *xfz43* fish. Orthogonal views from maximum intensity projections of *xfz43* BCs together with anti-PKC labeling in 20 dpf control or Met-treated *xfz43* larvae. (**B**) Regenerated *xfz43* BCs show type-specific PKC expression. Maximum intensity projections from confocal image stacks of regenerated *xfz43* BCs from 20 dpf tissue. Asterisks mark EdU-positive BC nuclei, also shown in insets. En face views show dendritic arbors, or axonal arbors together with PKC immunolabeling. (**C**) Regenerated *xfz43* BCs cluster in characteristic groups by morphological measurements. 3D scatter plot of population data for regenerated *xfz43* BCs from 20 dpf Met-treated retinas. Each circle represents a single cell, $n = 29$ cells. Cells that were analyzed for PKC expression are green (PKC-negative) or red (PKC-positive). Filled, gray ovals depict the groups by which cells were classified as ON T1, ON T2, or OFF types using the K-means clustering algorithm.

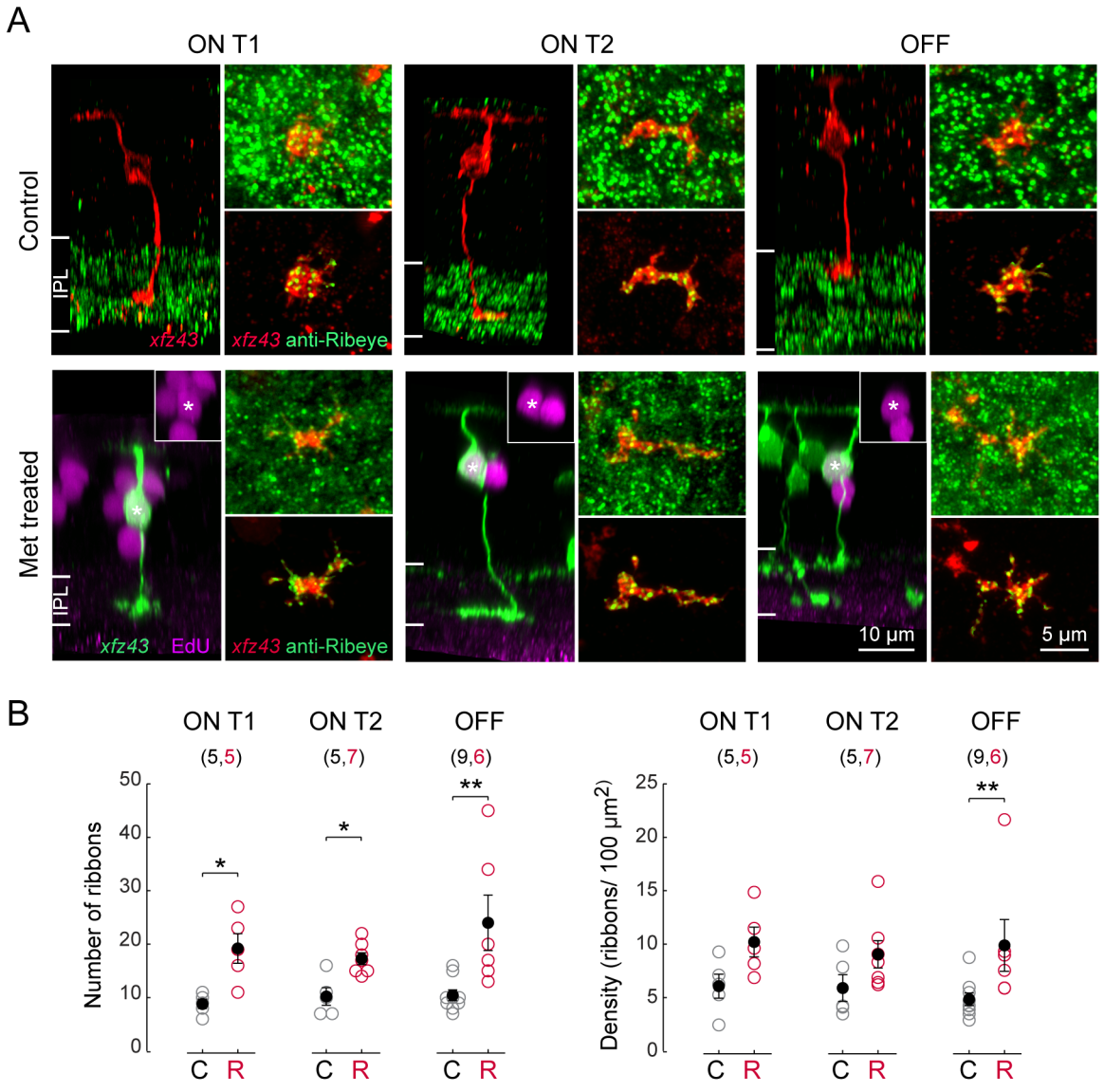

Figure 3.5 Regenerated BCs form excess ribbon synapses in the IPL.

(**A**) Examples of individual ON T1, ON T2, and OFF BCs visualized together with Ribeye A immunolabeling in fixed tissue from control or Met-treated larvae at 20 dpf (13 dpa). The Ribeye A antibody produced the expected staining pattern, showing punctate labeling within the IPL. Individual BCs in control tissue were visualized by DNA plasmid injection. Regenerated BCs in Met-treated tissue were identified by NTR-mCherry expression and EdU incorporation. *En face* views of axon terminal synapses labeled with anti-Ribeye A. A volumetric mask of the mCherry signal (*xfz43*) was used for visualization of ribbon synapses within an BC individual terminal (bottom panel). (**B**) Comparisons of the mean number and density of Ribeye A puncta on *xfz43* BC axon terminals of regenerated (R, red) BCs with counts from BCs in control (C, gray) tissue. Open circles represent individual cells, with the number of cells analyzed shown in parentheses. Error bars are ± SEM. * $P < 0.05$, ** $P < 0.01$; Wilcoxon-Mann-Whitney rank sum test. All measurements were made in 20 dpf (13 dpa) larvae.

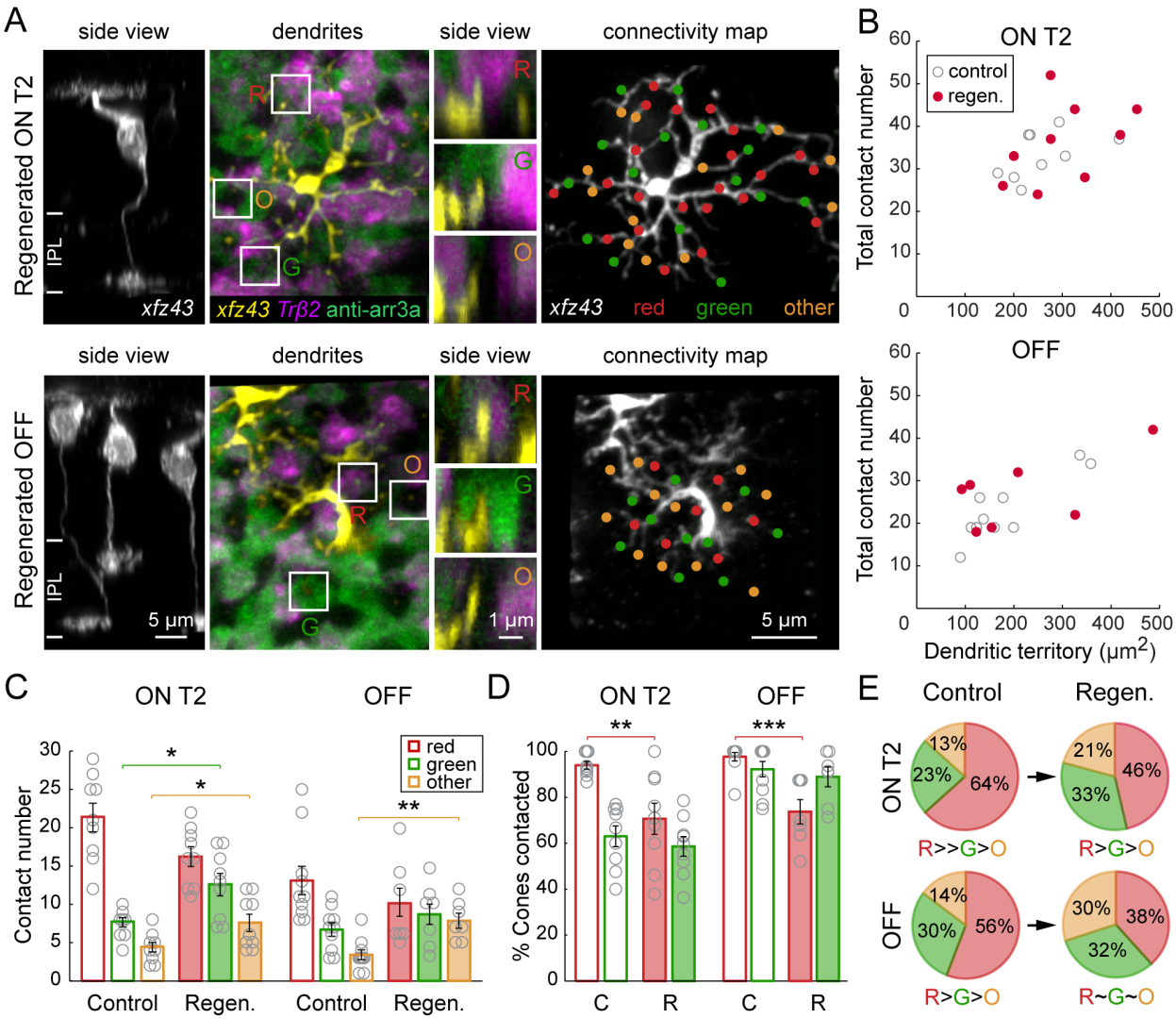

Figure 3.6 Regenerated ON T2 and OFF *xfz43* BCs do not maintain their stereotypic synapse distributions amongst preferred partners.

(**A**) Regenerated ON T2 and OFF *xfz43* BCs, as identified by EdU incorporation, together with red and green cones in *xfz43* fish crossed with *Tg(trβ2:MA-YFP)*. Vertical views of the boxed areas show dendritic invaginations into red cones (R) and green cones (G), as well as dendritic tips not associated with red or green cones, "others" (O). (**B**) Total contact number versus dendritic territory size of regenerated (regen., red) or age-matched control (gray) ON T2 or OFF cells. The total contact densities of regenerated cells did not differ from those of control populations (ON T2: $P > 0.05$; regenerated OFF: $P > 0.05$; Wilcoxon-Mann-Whitney rank sum test). (**C**) Comparisons of the mean number of contacts made per cone type between regenerated and control *xfz43* BCs of the same type. * $P < 0.05$, ** $P < 0.01$; Wilcoxon-Mann-Whitney rank sum test. (**D**) Quantification of the proportion of available cones of each type that ON T2 and OFF BCs contacted in control (C) and regenerated retinas (R). ** $P < 0.01$, *** $P < 0.001$; Chi-square test.(**E**) Pie charts show the mean proportion of the total contact number that was made with red cones, green cones, or other photoreceptors for control and regenerated BC populations.

The contact distributions of regenerated cells of both types differed from those of control populations (ON T2: $P < 0.0001$; OFF: $P = 0.0002$, Chi-square test). Regenerated ON T2 BCs still made a higher proportion of contacts with red cones compared to green cones ($P = 0.02$, Chi-square test), and a higher proportion of contacts with green cones compared to others ($P = 0.002$, Chi-square test). The distribution of contacts amongst distinct partner types did not significantly differ for regenerated OFF BCs ($P > 0.05$, Chi-square test). Open circles represent individual cells, with the number of cells analyzed shown in parentheses. Error bars are ± SEM. All measurements were made in 20 dpf (13 dpa) larvae.

Chapter 4. Retinal regeneration is non-specific but biased after loss of select neuronal cell types

4.1 Introduction

The loss of neurons in mammalian retinal degenerative diseases can result in visual impairment or blindness, and these outcomes are largely irreversible because lost neurons are not spontaneously replaced. In striking contrast, some non-mammalian vertebrates are able to restore diverse neuron populations after retinal injury via regeneration. The retinas of teleost fish and mammals share a common anatomical plan, and both possess Müller glia, cells that are activated to support neuronal regeneration after injury in teleosts (Karl and Reh, 2010). As such, many studies have sought to understand the cellular and molecular mechanisms that underlie native retinal regeneration (Goldman, 2014; Gorsuch and Hyde, 2014; Lenkowski and Raymond, 2014), in order to develop strategies to stimulate the same process in mammals (Karl and Reh, 2010). Such techniques necessitate methods to accurately match neuronal replacement to the injury, especially because many retinal degenerative diseases primarily impact specific neuronal cell types (Hoon et al., 2014). Indeed, retinal circuitry comprises numerous specialized neuronal cell types, and regulation of their relative proportions is fundamental to proper visual processing. However, recent evidence suggests that retinal regeneration can result in genesis of inappropriate types of neurons that were not lost in the original injury (Powell et al., 2016; Yoshimatsu et al., 2016). Thus, it remains unclear whether regeneration can be harnessed to recover neuronal populations of the appropriate cell type(s) after damage in the vertebrate retina.

Here, we investigated the regeneration of cone photoreceptor populations after their ablation in larval zebrafish to directly assess the specificity of regeneration. Cone photoreceptors convey daytime color information, and appear in morphologically and functionally distinct types (Ebrey and Koutalos, 2001). Like in humans, disparate cone types in zebrafish express distinct opsins, with maximal sensitivity to specific light wavelengths. Zebrafish possess four cone types, including red, green, ultraviolet (UV), or blue cones (Fadool and Dowling, 2008). These cone populations are arranged in an organized mosaic across the retina, and are present in stable abundances relative to one another: red > green ~ UV > blue cone density (Allison et al., 2010). We took advantage of the uniquely stereotypic organization of the zebrafish cone populations to 1) determine whether regeneration is conditional, i.e. whether regeneration is only stimulated

after the death of specific neuron types, and 2) investigate the accuracy of endogenous neuronal replacement.

To achieve these aims, we fate-mapped the regenerated cone population after ablating either the entire cone population or select cone types in larval zebrafish. The loss of all cones, red cones, or UV cones resulted in cone regeneration. In contrast, ablation of blue cones failed to trigger cone genesis, indicating that regeneration responds to specific cell death conditions. Analysis of the composition of regenerated populations after red or UV cone ablation demonstrated that although cone regeneration is non-selective, it is biased toward the cone type that was ablated. Global cone ablation induced generation of all cone types, and regenerated cones were present in relative densities that approximate the hierarchy observed in intact larvae. However, across cone ablation paradigms, the ablated cone types failed to repopulate the retina completely, demonstrating that regenerative neurogenesis may be limited. Collectively, these results suggest that regeneration does not completely recapitulate the steps that lead to the generation of the appropriate numbers and proportions of neuronal cell types during early retinal development.

4.2 Methods

Transgenic zebrafish

All procedures were conducted in accordance with University of Washington Institutional Animal Care and Use Committee guidelines. Embryonic and larval fish were raised at 28°C in a room with a normal light cycle, lights on from 9:00 to 23:00. Embryos were maintained in system water until 12-24 hours post fertilization (hpf), at which point embryos were placed in system water containing 0.2 mM N-Phenylthiorurea (PTU) (Sigma P7629) to prevent pigmentation. Transgenic larvae were screened for FP expression after hatching. Screened larvae were removed from PTU-containing system water, and transferred to a University of Washington zebrafish facility where they were fed regularly. Zebrafish larvae were euthanized by MS-222 (Sigma A5040) overdose (200-500 mg/L). See table below for a list of all the transgenic lines used.

Table. List of transgenic lines.

Transgenic	Source	Retinal Cells	Shorthand
Tg(gnat2:nfsBmCherry)	*	all cone types	*gnat2*
Tg(thrb:G4VP16; UAS:nfsBmCherry)	*Q31* (Yoshimatsu et al., 2016)6); *c264* (Davison et al., 2007)7)	red cones	*trβ2*
Tg(thrb:Tomato)	*Q22* (Suzuki et al., 2013)3)	red cones	*trβ2*
Tg(thrb:MA-YFP)	*Q23* (Suzuki et al., 2013)3)	red cones	*trβ2*
Tg(opn1sw1:nfsBmCherry)	*Q28* (Yoshimatsu et al., 2016)6)	blue cones	*sws1*
Tg(-5.5opn1sw1:EGFP)	*kj9* (Takechi et al., 2003)3)	UV cones	*sws1*
Tg(opn1sw2:nfsBmCherry)	*Q30* (Yoshimatsu et al., 2016)6)	blue cones	*sws2*
Tg(-3.5opn1sw2:EGFP	*kj11* (Takechi et al., 2008)8)	blue cones	*sws2*
Tg(gfap:GFP)	*mi2001* (Bernardos and Raymond,	Müller glia	*gfap*

*The *Tg(gnat2:nfsBmCherry)* transgenic line was generated by injecting pTol2pA-gnat2-nfsBmCherry plasmid into fertilized eggs at the one-cell stage, and progeny were screened by mCherry expression. The pTol2pA-gnat2-nfsBmCherry plasmid was generated in a Gateway

recombination reaction: p5E:gnat2 (Suzuki et al., 2013), pME:nfsBmCherry (Yoshimatsu et al., 2016), p3EpA, and pDestTol2pA (Kwan et al., 2007).

Selective cell ablation

To ablate specific cone populations, NTR-expressing larvae were immersed in Metronidazole (Met) solution (10 mM Met in system water) at 7 dpf for 1 or 6 hours, according to the experimental paradigm. Larvae were fed regularly, washed in clean system water at the end of treatment, and raised normally.

EdU labeling

Mitotic cells were labeled in live larvae by immersion in a solution containing 0.5 mM F-ara-EdU (Yoshimatsu et al., 2016) (Sigma T511293) in system water. The duration of treatment was timed according to the experimental paradigm. Half the solution volume was replaced every other day.

For visualization of EdU labeling, fixed whole retinas were permeabilized in 0.3-0.5% TritonX-100 (Sigma T8787) in 0.1 M PBS for 30 minutes at room temperature, and then washed three times in PBS. Click reactions were carried out in PBS solution with 10 μM Cy5-azide (Lumiprobe A2020), 2 mM copper(II) sulfate (Sigma 45167), and 20 mM sodium ascorbate (Sigma A7631) for 1 hour at room temperature. Samples were processed for immunohistochemistry after three PBS washes.

Immunohistochemistry

After euthanasia, larvae were fixed in a solution of 4% paraformaldehyde and 3% sucrose in 0.1 M phosphate-buffered saline (PBS), pH 7.4 at room temperature, and retinas were dissected out within 1-3 days. Fixed, whole retinas were blocked in PBS containing 5% normal donkey serum and 0.5% TritonX-100 for 1-4 hours at room temperature. Tissue was incubated in primary antibody in blocking solution for 1-5 days at 4°C. After three washes in 0.5% TritonX-100 in PBS, samples were incubated in secondary antibody solution for 1 day at 4°C. Samples were washed three times in PBS, mounted in 0.7% agarose, and coverslipped in Vectashield (Vector Labs). See tables below for lists of all primary and secondary antibodies used.

Table. List of primary antibodies.

Antibody	Host	Concentration	Source
anti-arrestin3a	mouse	1:100	ZIRC
anti-DsRed	rabbit	1:500	Clontech 632496
anti-GFP	chicken	1:500	Abcam ab13970
anti-GFP	mouse	1:200	Neuromab 72-132
anti-GFP	rabbit	1:500	Abcam ab13970
anti-UV opsin	rabbit	1:1000	Gift of Jeremy Nathans

Table. List of secondary antibodies.

Antibody	Host	Concentration	Source
anti-chicken IgY DyLight488	goat	1:500	Jackson ImmunoResearch
anti-mouse IgG DyLight405	goat	1:500	Jackson ImmunoResearch
anti-mouse IgG DyLight488	donkey	1:500	Jackson ImmunoResearch
anti-mouse IgG DyLight649	goat	1:500	Jackson ImmunoResearch
anti-rabbit IgG DyLight488	donkey	1:500	Jackson ImmunoResearch
anti-rabbit IgG Alexa Fluor 568	donkey	1:500	Life Technologies
anti-rabbit IgG Alexa Fluor 647	donkey	1:500	Jackson ImmunoResearch

Confocal image acquisition

Image stacks were acquired on a confocal microscope (Olympus FV1000 or Leica TCS SP8) using a 1.35 numerical aperture (NA) 60x oil (Olympus), 63x oil (1.4 NA) (Leica), 20x oil (0.85 NA) (Olympus), or a 20x oil (0.75 NA) (Leica) objective lens. Images were acquired at the following resolutions: high magnification images for orthogonal rotations, 0.18 μm per pixel XY and 0.3 μm Z step; identifying regenerated cone cell types, 0.18 μm per pixel XY and 0.5 μm Z step; whole retinas, between 0.1 and 0.4 μm per pixel XY, and 1 μm Z steps.

Image analysis

Image stacks were median filtered in Fiji (NIH) (Schindelin et al., 2012). Maximum intensity projections were generated in Amira (FEI). Three-dimensional (3D) image reconstructions were digitally sliced using the Amira slice functions. All measurements were made in Fiji. Image brightness, contrast, and hue were further adjusted in Photoshop (Adobe) or GIMP.

Cell densities across the retina were assessed by counting the number of labeled cells within an area in central, dorsal retina. In 10 dpf larvae, cones were counted within the area of a rectangle, ~ 5000 μm^2. In 15 dpf larvae, cones were counted within the area of an oval, ~ 15,000 μm^2.

Statistical analysis

In Figure 4.2B, a one-way ANOVA was used to test for differences in cone densities across cone ablation conditions. Pair-wise comparisons between cone ablation conditions were made using the Wilcoxon-Mann-Whitney rank sum test. In Figure 4.7, a one-way ANOVA was used to test for differences in cone densities across cone types in each ablation condition. Pair-wise comparisons between cone types were made using the Wilcoxon-Mann-Whitney rank sum test. In Table 4.1, pair-wise comparisons between cone types in control populations and regenerated populations were made using the Wilcoxon-Mann-Whitney rank sum test. All statistical tests were performed using a significance level of 0.05.

4.3 Results

Selective and pan ablation of cone photoreceptors in larval zebrafish retina

To gain a deeper understanding of the limits of progenitor fate specification during regeneration, we targeted specific photoreceptor populations for cell death using the Nitroreductase/Metrondazole technique. Expression of Nitroreductase (NTR; *nfsB*) can be genetically targeted to specific cell types, such that application of its prodrug Metronidazole (Met) only induces cytotoxicity in NTR-expressing cells (Curado et al., 2007). We investigated the efficacy of this approach to ablate the three cone photoreceptor populations for which transgenic tools are currently available: *Tg(trβ2:G4VP16; UAS:nfsBmCherry)* (red cones), *Tg(sws1:nfsBmCherry)* (UV cones), or *Tg(sws2:nfsBmCherry)* (blue cones) (Yoshimatsu et al., 2016). We treated red, UV, and blue cone ablation larvae with 10 mM Met for 1 hour at 7 days post-fertilization (dpf) (Figure 4.1A), a stage by which retinal circuitry is functionally mature(Easter Jr and Nicola, 1996). The fusion of mCherry fluorescent protein (FP) to NTR facilitated visualization of each of the targeted populations. Examination of whole retinas from Met-treated larvae at 10 dpf, or 3 days post-ablation (dpa) (Figure 4.1A) revealed that only sparse, punctate mCherry signal remained in central regions (Figure 4.1B). The remaining FP-expressing cones in the retinal peripheral margin are likely cells that were generated after Met treatment, as the periphery hosts a stem cells niche that supports ongoing cell genesis (Lenkowski and Raymond, 2014). To confirm the specificity of NTR-induced ablation, we visualized neighboring cone populations in fixed tissue at 3 dpa (Figure 4.2A). The mosaic arrangement of non-targeted cone types was preserved after the ablation of red, UV, or blue cones (Figure 4.2A). Whereas the population densities of targeted cone types were almost completely diminished, the densities of each non-targeted cone population remained unchanged at 3 dpa (Figure 4.2B). Thus, brief Met treatment was effective in eliminating the majority of cells of each cone type, without killing neighboring cones via bystander effects.

To gain further insight into the specificity and robustness of cone regeneration, we targeted the entire cone population for ablation. We generated the *Tg(gnat2:nfsBmCherry)* line, in which the *guanine nucleotide binding protein, alpha transducing activity polypeptide 2* (*gnat2*) promoter drives *nfsB-mCherry* expression in all cone types, and treated these fish with Met for 1 hour at 7 dpf as before (Figure 4.2A). Examination of whole retinas from Met-treated

fish at 3 dpa revealed that brief Met treatment was insufficient to induce death of cone photoreceptors (Figure 4.3A). We therefore extended Met treatments to 6 or 24 hours. Whereas cone ablation was primarily restricted to dorsal retinal regions in fish treated with Met for 6 hours at 3 dpa, ablation spanned almost the entire retina in fish treated for 24 hours (Figure 4.3A). Moreover, analysis at a later stage (8 dpa) revealed that the ablation persisted in *gnat2* fish that had been treated with Met for 24 hours. Cones repopulated dorsal regions of the retina by 8 dpa in fish treated for 6 hours, but in 24 hour-treated fish, large regions still completely lacked cones (Figure 4.3B). We hypothesized that the lack of cone repopulation may have resulted from damage to the cells that produce regenerative progenitors, Müller glia. Indeed, visualization of Müller cells at 3 dpa in 6 or 24 hour-treated larvae demonstrated that the Müller glia became disorganized after extended Met treatment (Figure 4.3C). There were apparent breaks in the outer limiting membrane, indicating that Müller glia had retracted their apical processes. This may be a consequence of the fact that Müller glia respond to photoreceptor death by phagocytosing the dead or dying cells (Bailey et al., 2010; Morris et al., 2008), which would potentially render Müller cells vulnerable to cytotoxic agents, and especially so when prodrug treatment is long-lasting. Thus, in order to ablate cone photoreceptors without inducing secondary damage that might inhibit cone repopulation, we proceeded with a 6-hour Met treatment paradigm in *gnat2* fish.

Selective cone ablation triggers non-specific cone genesis

We next evaluated whether selective cone ablation only induced repopulation of the lost cone types. To unequivocally identify newly proliferated cones, we exposed control and cone-ablated larvae to the thymidine analog (2′*S*)-2′-Deoxy-2′-fluoro-5-ethynyluridine (EdU). Previous studies investigating regeneration after widespread photoreceptor loss in zebrafish reported that progenitor proliferation peaks between 1 and 4 dpa (Bernardos et al., 2007; Vihtelic and Hyde, 2000; Yoshimatsu et al., 2016). Further, a recent study examining cone regeneration after selective loss of UV cones in larvae demonstrated that repopulation plateaus between 7 and 10 dpa (Yoshimatsu et al., 2016). As such, we treated cone ablation fish with EdU from 1-4 dpa, before analysis of fixed, whole retinas at 8 dpa (Figure 4.4A). We observed that EdU sparsely labeled nuclei in the outer nuclear layer (ONL) of control larvae (Figure 4.4B); however, EdU never incorporated into cones, demonstrating that cone genesis is not ongoing in control fish

(Figure 4.4B). Instead, the EdU-positive nuclei likely mark newborn rod progenitors or rods, as these photoreceptors are seeded into central retinal regions from late larval stages through adulthood (Stenkamp, 2011). In contrast to controls, EdU incorporation was robust in the ONL of cone-ablated fish, indicating that new photoreceptors were generated between 1-4 dpa in response to the death of all or select types of cone photoreceptors (Figure 4.4C-D). The level of EdU incorporation in the ONL appeared to occur to different extents, depending on the cone type that was ablated (Figure 4.4C-D). However, it was apparent that regenerated cone populations did not fully compensate for neuron loss, as they did not reach their original population densities (Figure 4.4D) (Table 4.1). Regenerated cones often appeared in patches of clusters, such that they did not appear to localize in their typical mosaic organization in the ONL (compare Figure 4D with Figure 2A). We also observed mitotic label in the inner nuclear layer (INL) of cone ablation retinas, but not in control retinas (Figure 4.4C). The EdU-positive nuclei in undamaged layers may mark newly-generated inner retinal neurons, as observed after photoablation of all photoreceptors in adult zebrafish (Powell et al., 2016).

In addition to inducing the regeneration of lost cell type(s), the ablation of specific neurons can provoke the genesis of ectopic neuron types (Powell et al., 2016; Yoshimatsu et al., 2016). Indeed, EdU appeared to incorporate into non-targeted photoreceptors in the ONL, in addition to the ablated cone types (Figure 4.4D). To address this, we visualized non-targeted cones in retinas in which a specific cone type was eliminated. EdU labeling demonstrated that, in each case in which one cone type was ablated, other cone types were generated together with the ablated type (data not shown). In Figure 4.5, images from UV cone-ablated retinas are shown in order to demonstrate the technique used for identifying regenerated cones of each type, as determined by EdU incorporation. In brief, to visualize non-targeted cone types, NTR-expressing transgenic fish were crossed with other transgenic lines in which specific cone types (red, UV, or blue) express FP (Figure 4.5A-B), and immunostained for arrestin 3a to label red and green cones (Figure 4.5A) (see Methods).

We also evaluated the composition of regenerated populations after ablation of all cone photoreceptor types, as shown in Figure 4.6. We visualized red cones by crossing *Tg(gnat2:nfsBmCherry)* fish with the *Tg(trβ2:MYFP)* line, and distinguished green and UV cones by immunostaining for arrestin 3a and UV-opsin, respectively (Figure 4.6A-B). Blue cones were identified by the process of elimination; after identifying *gnat2*-positive cells that

colabeled with *trβ2*, arrestin 3a, or UV-opsin, any remaining *gnat2*-positive photoreceptors were classified as blue cones (Figure 4.6B). Thus, in a single larva, we could distinguish which of the EdU-positive nuclei were associated with red, green, UV, or blue cones after cone photoreceptor death and regeneration (Figure 4.6C).

Cone type-specific proliferative advantages and biases in cone regeneration

Quantitation of the composition of the regenerated population revealed that specific cone types appear to hold a proliferative advantage, depending on the identity of the population ablated. The robustness of cone regeneration roughly correlated with the density of the population ablated; all > red > UV > blue cone types (Figure 4.7). Global cone death induced regeneration of all cone types, and the relative abundance of regenerated cells of each type approximates the normal hierarchy: R>G>UV~B (Figure 4.7). However, the stereotypic relationship between the densities of each cone type was not preserved in regeneration; whereas cones in control retinas are present in a ratio of 1.8 red: 1.3 green: 1.3 UV: 1 blue cone, regenerated cones in retinas with general cone death appear in a ratio of 3.9 red: 2 green: 1.2 UV: 1 blue cone on average. Thus, genesis was especially skewed toward red and green cones after ablation of all cones. Like retinas in which all cones were ablated, ablation of red cones induced genesis of all cone types (Figure 4.7). However, regenerated red cones appeared in the highest density, demonstrating that regeneration was biased toward red cones after their selective ablation. Likewise, UV cone ablation biased regeneration toward UV cones. Other cone types were also generated after UV cone ablation; new red and blue cones were consistently produced, but green cones were only sometimes generated, and in extremely low numbers. Finally, as reported previously, ablation of the blue cone population induced a very weak regenerative response (Yoshimatsu et al., 2016). Ablating blue cones only stimulated cone genesis in half the retinas analyzed (4/8 retinas). No UV cones incorporated EdU, and EdU-positive blue, red, or green cones were present in approximately equal numbers (EdU-positive blue cone density = 0.01 ± 0.03 cells per 1000 μm^2, n = 8 retinas; EdU-positive red cone density = 0.02 ± 0.02 cells per 1000 μm^2, n = 8 retinas; EdU-positive green cone density = 0.02 ± 0.02 cells per 1000 μm^2, n = 7 retinas) (Figure 4.7). Thus, it appears that unlike fish in which red or UV cones were ablated, photoreceptor regeneration was not skewed toward the targeted cone type in blue cone-ablated larvae.

Müller glia proliferate in response to global and selective cone death

Several studies in fish retinal regeneration have suggested that a minimum number of cells must die in order to stimulate Müller glia-mediated regeneration (Braisted and Raymond, 1992; Montgomery et al., 2010). In a recent investigation, UV cones were selectively ablated by light lesioning in adult zebrafish, and although Müller glia upregulated markers of dedifferentiation, they did not incorporate mitotic markers (Nagashima et al., 2013). We thus wondered whether the loss of blue cones, the least abundant cone type in the larval retina, was insufficient to induce proliferation of Müller glia. To test this hypothesis, we treated control and cone-ablated larvae with EdU from 1-3 dpa, and fixed at 3 dpa in order to detect any EdU-positive Müller glia before the end of the proliferation period (Figure 4.8A). Visualizing EdU labeling across the whole retina in control larvae showed that as expected, there was little to no EdU incorporation in the inner retina (Figure 4.8B). In contrast, there was robust EdU incorporation in the inner nuclear layer of retinas from larvae in which all cones, or only red, UV, or blue cones were ablated. Across ablation paradigms, EdU-positive nuclei appeared in columns, reminiscent of the neurogenic columns commonly observed during Müller glia-mediated regeneration (Lenkowski and Raymond, 2014)(Figure 4.8B). To confirm that these columns were associated with proliferating Müller glia, we visualized Müller glia by crossing cone ablation fish with the *Tg(gfap:GFP)* line. Indeed, EdU colabeled the nuclei of *gfap*-positive nuclei after ablation of all or only red, UV, or blue cones (Figure 4.8C). We therefore conclude that the loss of any cone type population in larval zebrafish is sufficient to provoke Müller glia proliferation, but the death of a single cone population is not always sufficient to induce reproduction of cones.

4.4 Discussion

Determinants of the composition of regenerated neuronal populations

It is clear that even in a system with the native capacity to regenerate diverse neuronal cell types, regeneration is not selective. After ablating single cone types, we found that in addition to the ablated cohort, other cone types were also regenerated. In corroboration of this observation, experiments in which specific neuron types (Yoshimatsu et al., 2016), or select retinal layers (Powell et al., 2016; Raymond et al., 2006) were ablated resulted in genesis of inappropriate (non-ablated) neuron types. Moreover, analysis at late time points revealed that ectopic neuronal types can persist until at least 30 days post-ablation (Powell et al., 2016), suggesting that excess neurons are not later culled back. As such, neuron replacement is imprecise, and may even introduce a negative impact on retinal function and organization. These unexpected outcomes underscore the necessity of advancing our understanding of the determinants of cell fate and proliferation in regeneration, in order to tailor repair to specific retinal injuries.

Although retinal regeneration is non-selective, our quantitative analysis of cone regeneration after eliminating a single cone type suggests that cell replacement is biased toward the ablated neuron type. Similar observations were made in adult zebrafish and larval frogs. Ablation of select retinal layers in adult zebrafish biased regenerative proliferation toward the affected layer(s) (Powell et al., 2016). Also, ablation of specific amacrine cells or inner retinal neuronal subsets in the developing frog retina biased progenitors toward producing the ablated neuronal cell type over others (Reh, 1987; Reh and Tully, 1986). Thus, observations to date suggest that neuronal progenitors can "sense" which cell type is lost after retinal injury. Although the mechanisms by which regeneration is biased toward the lost neuronal population in mature CNS systems are still under investigation, clues come from studies of neurogenesis and cell fate specification during retinal development (Agathocleous and Harris, 2009; Bassett and Wallace, 2012; Brzezinski and Reh, 2015; Cayouette et al., 2006). Altogether, these studies suggest that there are at least three potential mechanisms by which biased regeneration may occur, which directly or indirectly influence cell fate specification and neuronal number.

First, cell fate specification of neuronal progenitors may be biased toward the ablated neuronal population. This could occur via inductive signaling from dying neurons. During vertebrate retinal development, cell fate specification is largely controlled by a hierarchy of cell-

intrinsic transcription factors (Boije et al., 2014). Extrinsic cues impinge upon intrinsic programs, often by regulating the timing of cell cycle exit and differentiation in neuroepithelial-derived progenitors. Several of these signaling pathways are activated during regeneration (Gorsuch and Hyde, 2014; Lenkowski and Raymond, 2014). Like in development, Notch signaling appears to play a role in balancing progenitor proliferation and neuronal differentiation during regeneration (Lenkowski and Raymond, 2014). Further, there are several examples of extrinsic signals that specify cell fate more directly during vertebrate retinal development; retinoic acid and thyroid hormone bind ligand-regulated transcription factors to promote the differentiation of rods and cones, respectively (Sernagor et al., 2006; Swaroop et al., 2010). However, the potential roles of these known inductive signals in cell fate specification during neuronal regeneration in the retina remain largely unexplored. In addition to re-deploying developmental cues, the response to cell loss involves upregulation of cell death signaling pathways (Gorsuch and Hyde, 2014; Lenkowski and Raymond, 2014). These are often sufficient to initiate regeneration, but all so far appear to be "general" death signals that are unlikely to convey signals to specify select cell fates. For example, the inflammatory cytokine TNFα is necessary for Müller glia proliferation, but its expression is increased in both dying photoreceptors and dying inner retinal neurons after the selective elimination of either of these populations (Nelson et al., 2013). Lastly, it has been proposed that differential expression of Fgf signaling components in disparate retinal layers in larval and adult zebrafish retinas may provide a framework for layer-specific death signaling (Gorsuch and Hyde, 2014). This hypothesis has yet to be tested, although similar apical-basal gradients of extracellular cues modulate cell type specification during retinal development (Del Bene et al., 2008). Further, how such gradients could mediate the specification of cells intermingling within a single layer, like cones, is unclear. Overall, there is ample evidence that the upregulation of developmental signaling pathways generates an environment that is permissive for neurogenesis during regeneration in the mature retina. But, there are no apparent candidate cues to instruct progenitors to differentiate into specific neuronal cell types.

A second potential mechanism that could bias neuronal regeneration toward specific cell types is the selective proliferation of fate-restricted progenitors or precursors. Indeed, differentiated neurons in the developing retina can limit their population size via negative feedback signaling, which inhibits the proliferation of particular fate-restricted progenitors

(Cayouette et al., 2006). For example, RGCs secrete SHH to inhibit the proliferation of progenitor cells during the early retinal stages when RGCs are typically produced in mice (Wang et al., 2005). Depletion of RGCs from the developing mouse retina results in an increased proportion of the progenitor pool expressing transcription factors necessary for RGC fate, indicating that negative feedback is cell type-specific (Mu et al., 2005). It has been hypothesized that a similar mechanism maintains homeostasis in the mature zebrafish retina, such that ablation of particular populations disinhibits the proliferation of specific progenitors (Powell et al., 2016). Surviving neurons from non-targeted populations may continue to provide negative feedback, and thus act to reduce the generation of ectopic cell types during regeneration. Direct evidence for the proliferation of select progenitor types during regeneration comes from investigations of the influence of neurotransmitter signaling in salamander midbrain (Berg et al., 2013). Dopaminergic neuron populations are normally fully restored after selective chemical ablation, but their regeneration is blocked when pharmacological agents are applied to compensate for the loss of dopaminergic signaling after neuronal cell death (Berg et al., 2011). Berg et al. showed that this blockade is selective; dopaminergic signaling inhibited production of dopaminergic neurons, but not of other midbrain neuron types during their regeneration. Intriguingly, recent evidence shows that there are dedicated precursors for each cone type during zebrafish retinal development (Suzuki et al., 2013), providing a potential foundation for the selective regulation of progenitor proliferation during cone regeneration. However, unlike salamander dopaminergic neurons, it is unlikely that each cone type regulates proliferation of its specific precursor via neurotransmitter signaling because all cone types release the same neurotransmitter, glutamate.

Finally, it is possible that selective cell death plays a role in sculpting the composition of the regenerated cone population. Our observations do not exclude the potential scenario in which all cone types are generated after ablation of any cone population, but only a subset of regenerated neuronal types survive. Indeed, programmed cell death can play a role in limiting neuron population size and regulating cell spacing during retinal development (Hoon et al., 2014; Sernagor et al., 2006). In the developing chick retina, differentiated, stratified RGCs secrete the neurotrophin NGF, which induces the death of RGCs still migrating into the ganglion cell layer via activation of the $p75^{NTR}$ receptor and downstream pro-apoptotic pathways (Frade et al., 1996; González-Hoyuela et al., 2001). NGF-mediated cell death is specific to migrating RGCs, likely because the already-laminated RGCs co-express TrkA along with $p75^{NTR}$, which renders p75

^{NTR}-mediated NGF signaling neurotrophic rather than apoptotic (González-Hoyuela et al., 2001). Thus, in addition to inhibiting progenitor proliferation, neuronal populations can regulate their numbers via targeted death of homotypic, post-mitotic cells. Further, suppression of apoptosis during retinal development in mice disrupts the normally organized spacing of cells in the dopaminergic amacrine cell population (Raven et al., 2003). It has been proposed that cell death could play a similar role in regulating the highly regular mosaic arrangement of cone types during growth in the adult zebrafish retina (Allison et al., 2010). This regulation may further extend to the elimination of ectopic cones during regeneration in larvae. In the future, assessing whether or not cell death is elevated after regeneration is complete, and whether ectopic cones persist, will provide insight into the extent to which cell death dictates the ultimate composition of regenerated neuronal populations.

The mechanisms proposed above are not mutually exclusive; retinal regeneration likely involves to some extent the orchestrated regulation of progenitor proliferation, fate specification, and neuron survival. However, it is clear that the spatially and temporally coordinated mechanisms that generate retinal neurons in the correct numbers and proportions during development are not perfectly recapitulated after selective ablation in mature circuits. The hierarchy of relative cone type abundances is approximately recaptured after pan cone ablation and regeneration. However, none of the cone types recover their original population densities, as previously observed in adult zebrafish (Raymond and Barthel, 2004; Stenkamp and Cameron, 2002). Likewise, the targeted cone populations do not fully repopulate after single cone population elimination, and as a result, the regenerated cone populations fail to organize into their typical mosaic arrangements. Understanding the relative contributions of the dying versus intact neuron populations in dictating neuron fate and number during regeneration in mature circuits will be critical to tailoring regeneration for retinal repair.

Activation of Müller glia-mediated cone regeneration

Our observations after selectively ablating specific cone types present the possibility that retinal regeneration is conditional. Whereas elimination of the red or UV cone populations alone induces robust to moderate cone regeneration, the death of blue cones only sometimes induces cone regeneration, and only to an extremely weak degree. It is unlikely that these differences arise from a limitation in the competency of Müller glia-derived progenitors. A body of work on

zebrafish retinal regeneration has indisputably demonstrated that Müller glia-derived progenitors are multipotent, i.e. capable of differentiating into each of the major retinal neuron classes (Fausett and Goldman, 2006; Goldman, 2014; Ramachandran et al., 2010). Similarly, these progenitors appear to be competent to produce blue cones specifically; we observed that new blue cones are produced after the ablation of all cones, or of red or UV cones (Yoshimatsu et al., 2016).The lack of cone regeneration after ablation of blue cone types raises the question: what factors dictate whether or not Müller glia-mediated regeneration is initiated?

Some of the earliest investigators of teleost retinal regeneration posited that substantial cell death is a fundamental factor in triggering a robust regeneration response from Müller glia (Braisted and Raymond, 1992). A study directly tested this hypothesis by analyzing regeneration after the elimination of different proportions of the same neuronal cell type (Montgomery et al., 2010). Whereas loss of the entire rod population induced proliferation of Müller glia, death of only a subset of rods did not stimulate Müller glial division, suggesting that Müller glia are sensitive to the extent of cell death. Further, it was recently shown that the robustness of the regeneration response roughly correlates with the extent of death. Comparisons of retinas in which the cone and rod photoreceptor populations were ablated to different degrees by light lesioning revealed that the proportion of Müller glial cells that undergo cell division, as well as the extent of progenitor proliferation, corresponds with the magnitude of photoreceptor death (Thomas et al., 2012). In support of this observation, we found that the level of cone regeneration roughly correlated with the density of the ablated population: all cone types > red cones > UV cones > blue cones. The ability of Müller glia to sense the extent of cell death could be mediated by the cumulative levels of cell death signals (discussed in the previous section), which presumably would be proportional to the density of dying neurons. However, the densities of UV versus blue cones only differ slightly: 1.3 UV cones: 1 blue cone. The disparity in whether regeneration is triggered after the ablation of these populations further raises the possibility that there is a threshold for the extent of cell death, above which regeneration is initiated.

Recent work has suggested that substantial cell loss is specifically required for cell division amongst Müller glia, which results in the production of neuronal progenitors. The loss of a subset of UV cones in adult zebrafish stimulated dedifferentiation of Müller glia, one of the initial steps in regeneration, but did not induce subsequent asymmetric cell division (Nagashima et al., 2013). We were thus surprised to find that Müller glia undergo mitosis in response to the

death of blue cones, similar to our observations after ablating more abundant cone types. What cell types are produced from this cell division, if not cone photoreceptors? Müller glia act as stem cells under two different circumstances; in addition to producing neuronal progenitors in response to cell loss, they support ongoing rod genesis in intact circuits by undergoing slow asymmetric divisions that generate new rod precursors (Bernardos et al., 2007). Thus, Müller glia-derived progenitors must undergo a fate switch in order to support cone regeneration. Evidence for such a tradeoff between cone regeneration and basal rod genesis comes from work showing that cones regenerate at the expense of rod production after loss of UV cones in larval zebrafish (Fraser et al., 2013). As such, blue cone death may be insufficient to drive the rod-to-cone competency change in Müller glia-derived progenitors. Given that Müller glia appear to increase their rate of division after blue cone loss, it is possible that blue cone death increases the normal production of rods at the expense of cone regeneration. Alternatively, neuronal progenitors may instead be biased toward non-photoreceptor fates.

Here, we demonstrate that Müller glia are sensitive to the death of blue cones, as they undergo division after selective blue cone ablation. This result eliminates the possibility that blue cones cannot activate the injury-related pathways necessary for Müller glia division and progenitor production (Gorsuch and Hyde, 2014; Lenkowski and Raymond, 2014). We therefore hypothesize that the failure to regenerate blue cones may be because blue cone death does not trigger a change in progenitor competency to support cone genesis. Future work can address this hypothesis by fate-mapping all of the neuronal progeny after blue cone ablation, which would reveal whether rods or other retinal neuron types are produced in lieu of cone photoreceptors. Our comparison of the regeneration response across cone ablation paradigms further suggests that activation of the fate switch in progenitors may require extensive cell death. However, it remains possible that cone regeneration only occurs after the death of non-blue cone types because of differences in the origin, not density, of cell death. We can begin to tease apart these possibilities by manipulating the densities of each cone population prior to selective ablation.

Conclusion

In conclusion, retinal regeneration appears to be inherently limited after the loss of select neuronal populations. These limitations are especially pertinent to retinal diseases that affect specific retinal neuron types, such as retinitis pigmentosa, an inherited retinal degeneration

disorder that primarily affects photoreceptors (Hamel, 2006). For future applications in mammals, the focus of the neuronal regeneration field should not only be on understanding the differences between mammalian and teleost systems that dictate whether regeneration is initiated, but also on how to control the extent and specificity of neuronal regeneration. Our ability to manipulate regeneration for the best restorative outcomes will depend upon a more advanced knowledge of the molecular and cellular mechanisms involved in dictating cell proliferation, fate specification, neuronal survival, and patterning in both retinal development and regeneration. Of particular interest are the potential intrinsic differences between the neuroepithelial-derived progenitors that support retinal development and the Müller glia-derived progenitors produced in regeneration. Challenges may also arise in recapitulating retinal neurogenesis based on differences in the retinal environment at different stages of maturation.

4.5 Figures

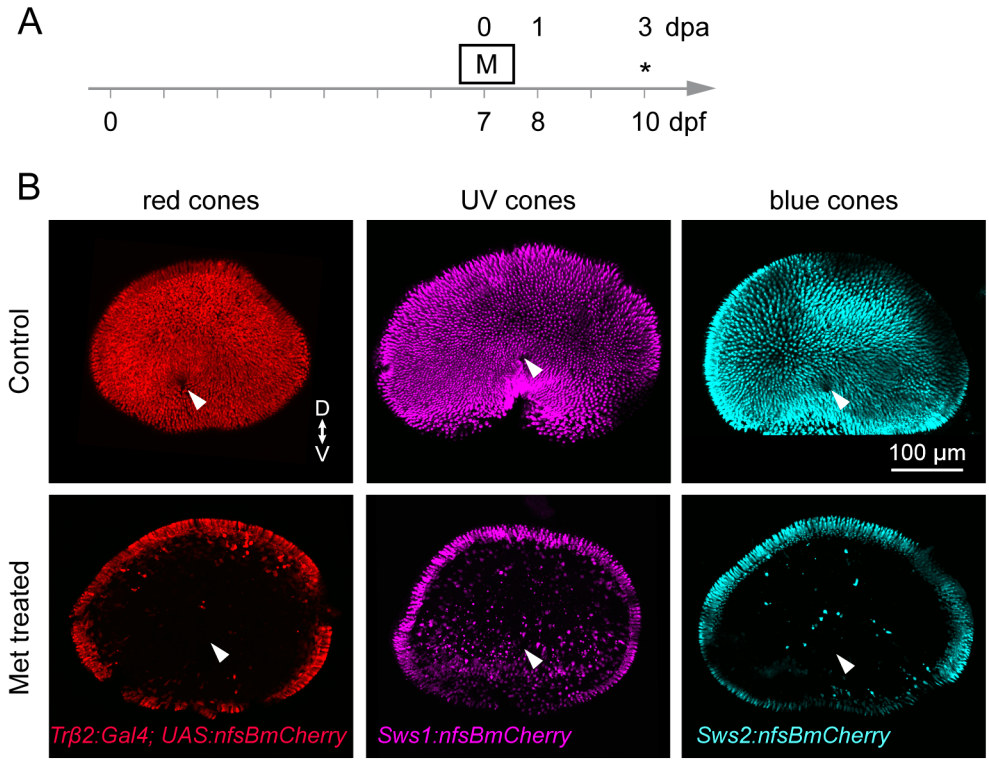

Figure 4.1 Selective ablation of specific cone populations in larval zebrafish.

(**A**) Timeline demonstrates timing of Met (M) treatment. Asterisks denotes the age at which larvae were fixed for analysis. (**B**) *En face* views of wholemount, fixed retinas from 10 dpf Met-treated and control fish. Specific cone populations were targeted for ablation by selective expression of *nfsB*. *Tg(trβ2:G4VP16; UAS:nfsBmCherry)* fish were used to ablate red cones, *Tg(sws1:nfsBmCherry)* fish were used to ablate UV cones, and the *Tg(sws2:nfsBmCherry*) line was used to ablate blue cones. Arrowheads denote the optic nerve head. ("D" dorsal, "V" ventral.)

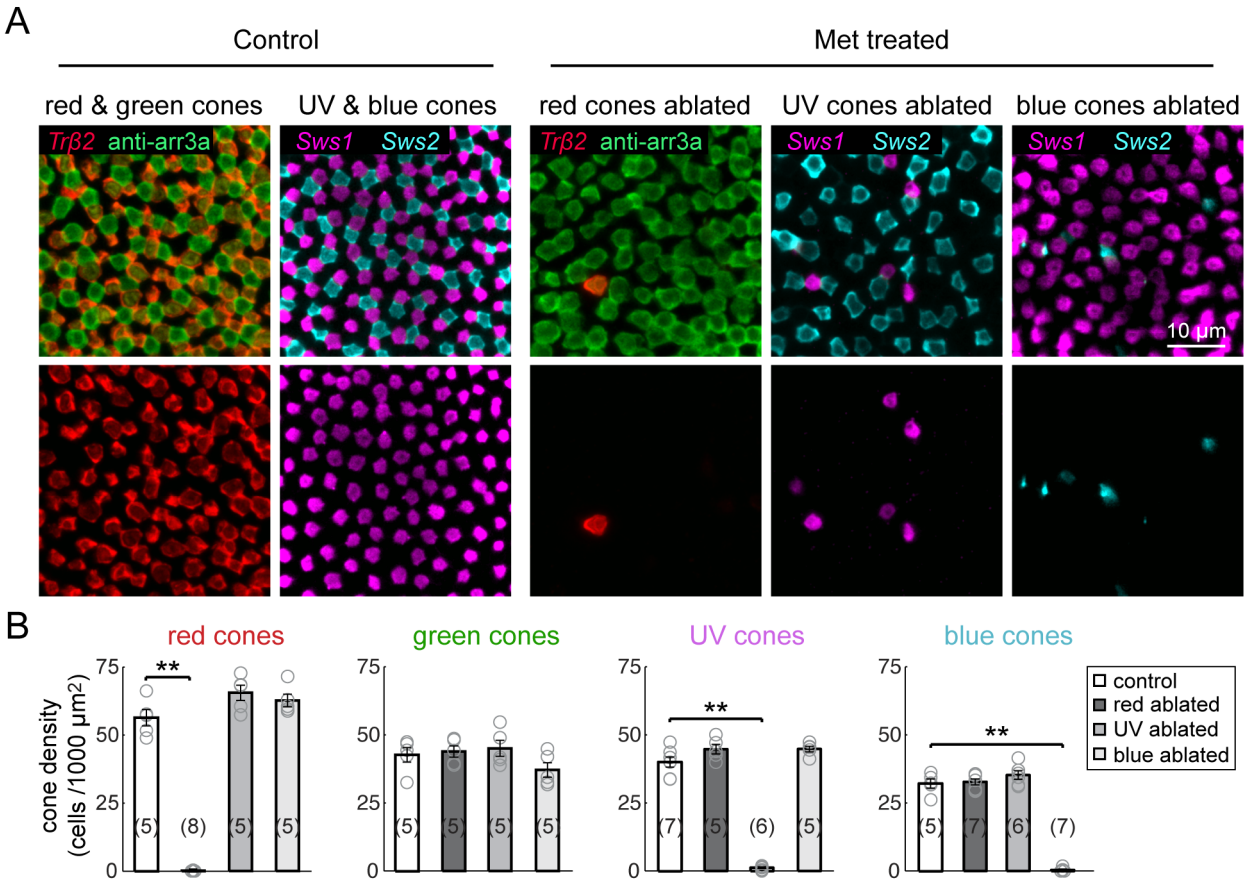

Figure 4.2 Selective cone ablation does not damage neighboring cones.

Ablation of red, UV, or blue cone populations in the background of transgenically-labeled or immunostained cones. *nfsB*-expressing fish were crossed with the *Tg(trβ2:tdTomato)* line to visualize non-targeted red cones, with *Tg(sws1:GFP)* fish to visualize non-targeted UV cones, or with *Tg(sws2:GFP)* to visualize non-targeted blue cones. Anti-arrrestin3a immunostaining labels both red and green cones. (**A**) Maximum intensity projections of confocal image stacks from 10 dpf (3 dpa) control or Met-treated retinas. (**B**) Plots show the mean cell density of each cone type from Met-treated larvae at 3 dpa, and from age-matched control fish. Each open circle represents a single retina, with the numbers of retinas analyzed shown in parentheses. Error bars are ± SEM. ** $P < 0.01$; Wilcoxon-Mann-Whitney rank sum test

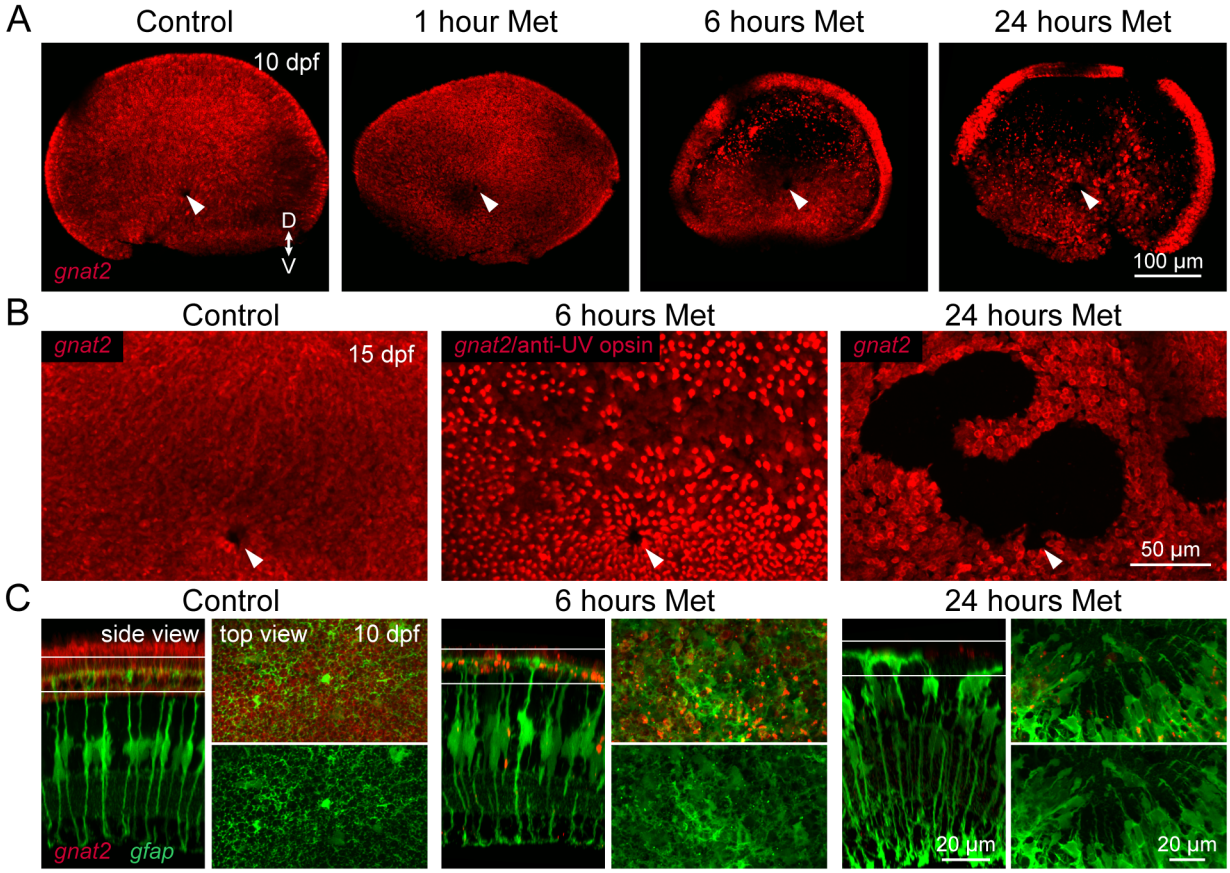

Figure 4.3 Optimizing Met treatment to ablate all cones without damaging Müller glia. (**A**) *En face* views of wholemount, fixed retinas from 10 dpf Met-treated and control fish from the *Tg(gnat2:nfsBmCherry)* line. Fish were treated with Met for 1 hour, 6 hours, or 24 hours at 7 dpf. Arrowheads denote the optic nerve head. ("D" dorsal, "V" ventral.) (**B**) High-magnification, *en face* views of dorsal retinal regions in 15 dpf control and Met-treated *gnat2* larvae. In fish treated with Met for 6 hours, UV opsin immunolabeling was visualized in the same channel as *gnat2* transgenic labeling. Arrowheads denote the optic nerve head. (**C**) Visualization of Müller glia in 10 dpf larvae after different durations of Met treatment of *Tg(gnat2:nfsBmCherry; gfap:GFP)* double transgenic fish. (Side view) Orthogonal views of central retinal regions. Shown are images from control animals and from fish treated with Met for 6 or 24 hours. (Top view) *En face* views of the outer nuclear layer (ONL) together with Müller glia end feet, at the level indicated in the side views.

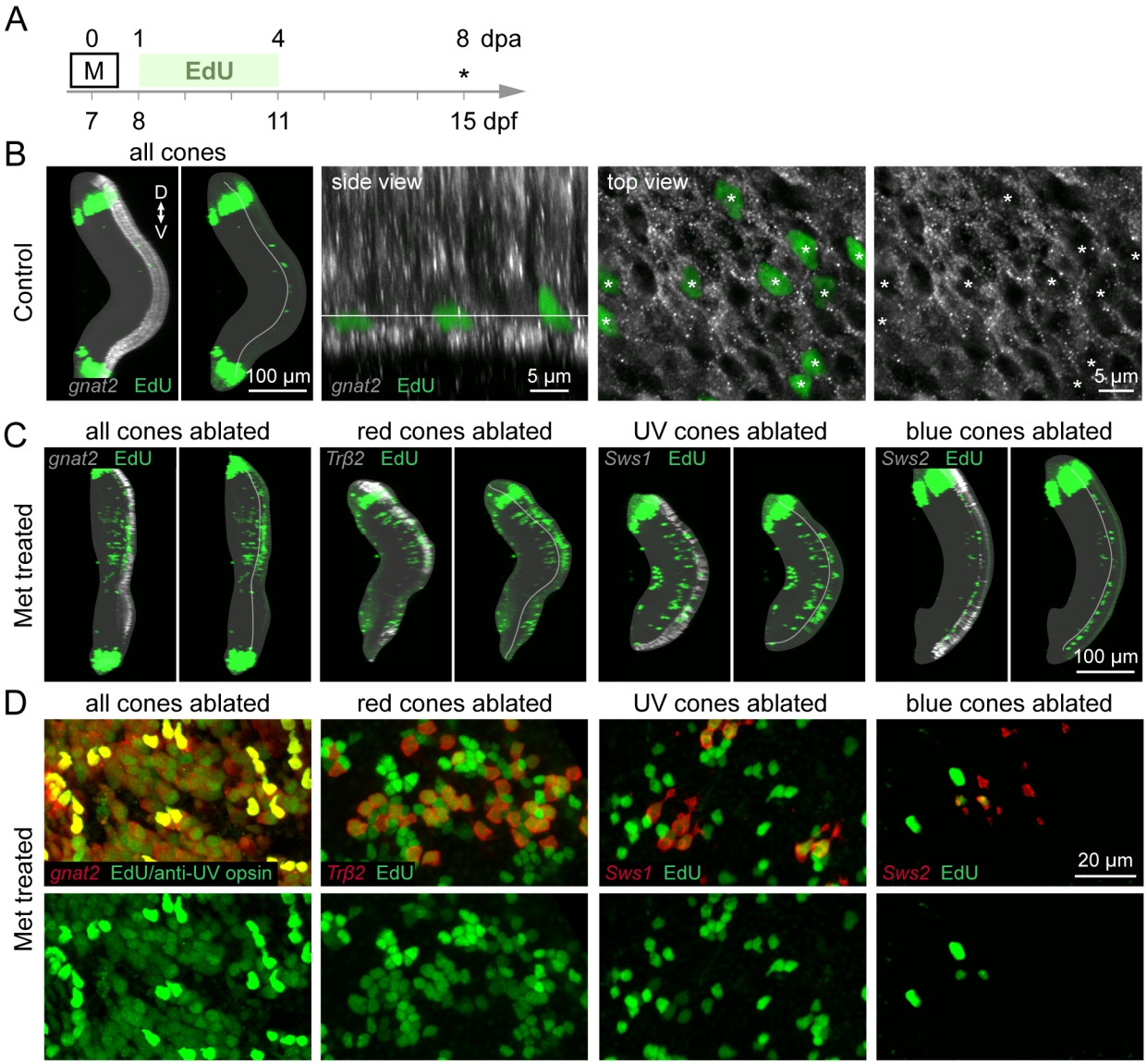

Figure 4.4 Cone ablation induces proliferation of photoreceptors within days of cell death.

(**A**) Timeline demonstrates the timing of Met and EdU treatment in cone ablation and control fish. Asterisk denotes age at which larvae were fixed for analysis. (**B**) Maximum intensity projections of confocal image stacks from 15 dpf control *Tg(gnat2:nfsBmCherry)* larvae that were treated with EdU. In the orthogonal view of the whole retina, the boundary between the ONL and inner nuclear layer (INL) is outlined in the panel showing EdU labeling alone. The dense bands of EdU-positive cells at the peripheral retina demarcate cells generated in the ciliary marginal zone at the time of EdU treatment. (Side view) Orthogonal rotation showing the photoreceptor layer. (Top view) *En face* views of photoreceptors together with EdU labeling, at the level indicated in the side view. Arrowheads point to EdU-positive nuclei. (**C**) Orthogonal views of whole eyes from 15 dpf (8 dpa) fish in which specific cone populations or all cone photoreceptors were ablated. The targeted cone population is visualized by *nfsB-mCherry* expression (gray scale), and shown together with EdU labeling (green). The boundary between the ONL and INL is outlined in the panels showing EdU labeling alone. (**D**) *En face*, high-magnification views showing EdU colabeling in the ONL of 15 dpf cone-ablated fish.

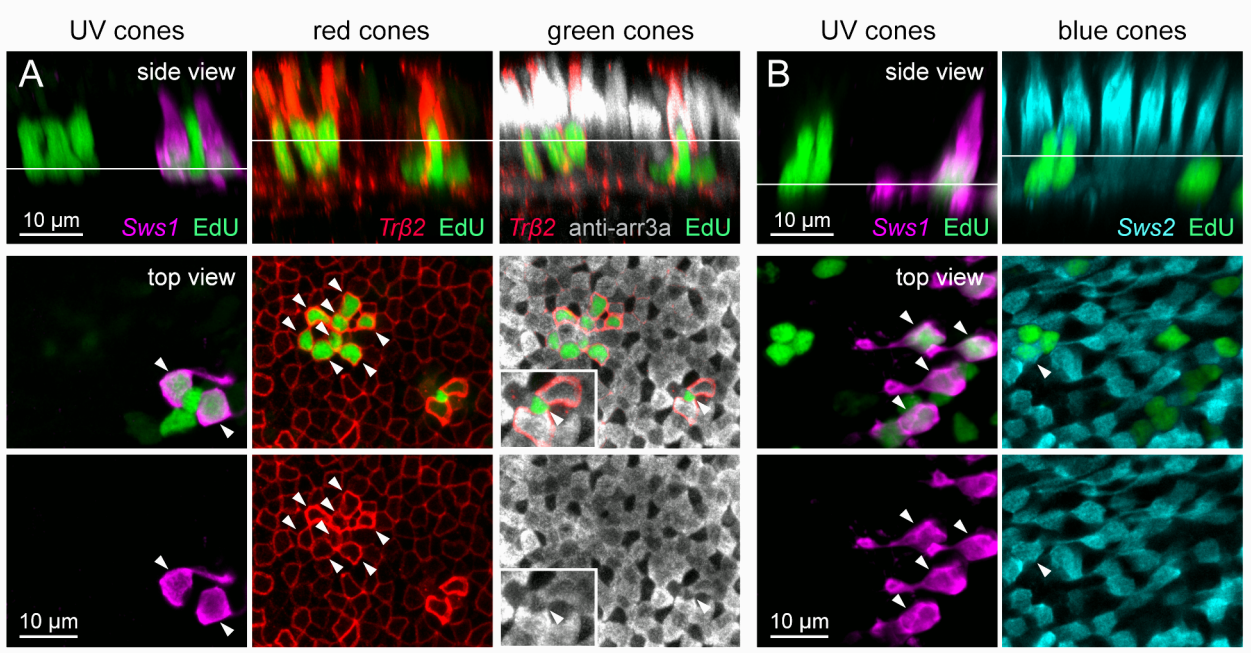

Figure 4.5 Identification of regenerated cone types after ablation of select cone populations.

Demonstration of how different cone types were distinguished in the population of regenerated photoreceptors after UV cone ablation. (**A**) Identification of regenerated UV, red, and green cones after UV cone ablation in *Tg(sws1:nfsBmCherry; trβ2:MYFP)* double transgenic fish, with arrestin3a immunostaining and EdU labeling. (**B**) Identification of regenerated UV and blue cones after UV cone ablation in *Tg(sws1:nfsBmCherry; sws2:GFP)* double transgenic fish with EdU labeling. In (A) and (B), side views are orthogonal rotations of the ONL from UV cone-ablated retinas. Top views show the nuclei located at the level of the line indicated in the side view. Arrowheads point to EdU-positive nuclei.

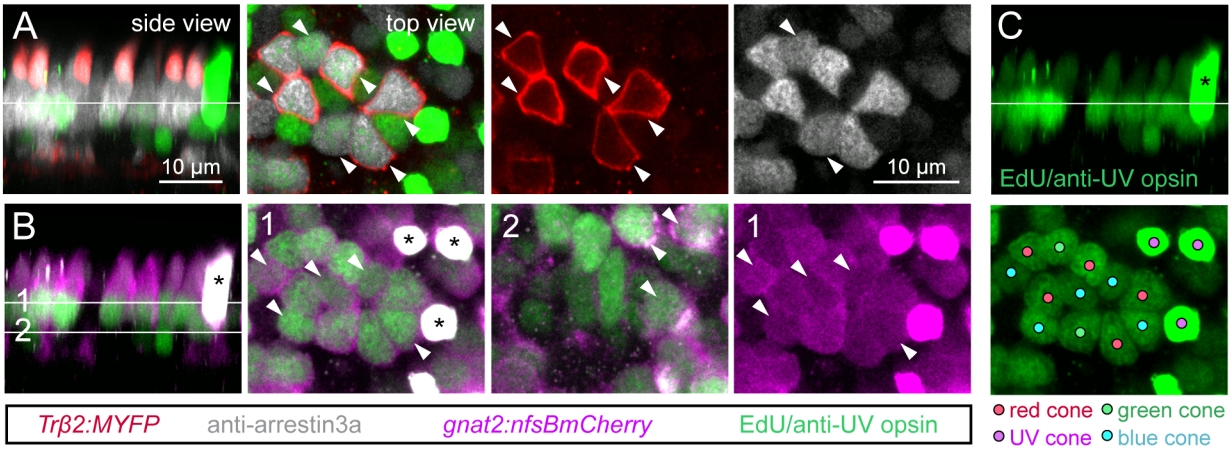

Figure 4.6 Identification of regenerated cone types after ablation of all cones.

Demonstration of how each cone type was distinguished in retinas from 15 dpf, Met-treated *Tg(gnat2:nfsBmCherry; trβ2:MYFP)* double transgenic larvae. (**A**) Identification of regenerated red and green cones. *Trβ2* labels red cones alone, and anti-arrestin3a labels both red and green cones (gray). EdU and anti-UV opsin were visualized in the same channel (green). (**B**) Identification of regenerated UV and blue cones. *gnat2* labels all cone types (magenta), anti-UV opsin labels UV cones (green). Line 1 in the side view marks the level at which blue cone nuclei were visualized for top views, line 2 marks the level at which UV cone nuclei were visualized for top views. (**C**) Representative map of different cone types in the regenerated population. Filled circles denote the identity of each EdU-positive nucleus. In A-C, side views are orthogonal rotations of the ONL; top views show the nuclei located at the level of the line indicated in the side view. Arrowheads point to EdU-positive cones, asterisks mark UV opsin-positive cones.

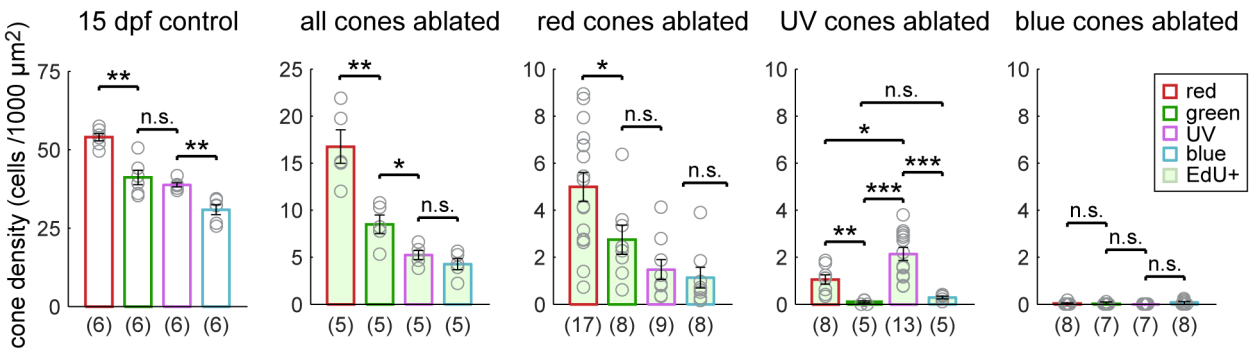

Figure 4.7 Selective cone ablation induces biased and incomplete regeneration of specific cone types.

Quantification of the densities of each cone type in control retinas, and of each cone type in the regenerated population (EdU-positive) after selective cone ablation. Plots show the mean population density across control and cone ablation conditions in 15 dpf fish. Each open circle represents one cell, with the numbers of cells analyzed in parentheses. Error bars are ± SEM. * $P < 0.05$, ** $P < 0.01$, *** $P < 0.001$; Wilcoxon-Mann-Whitney rank sum test

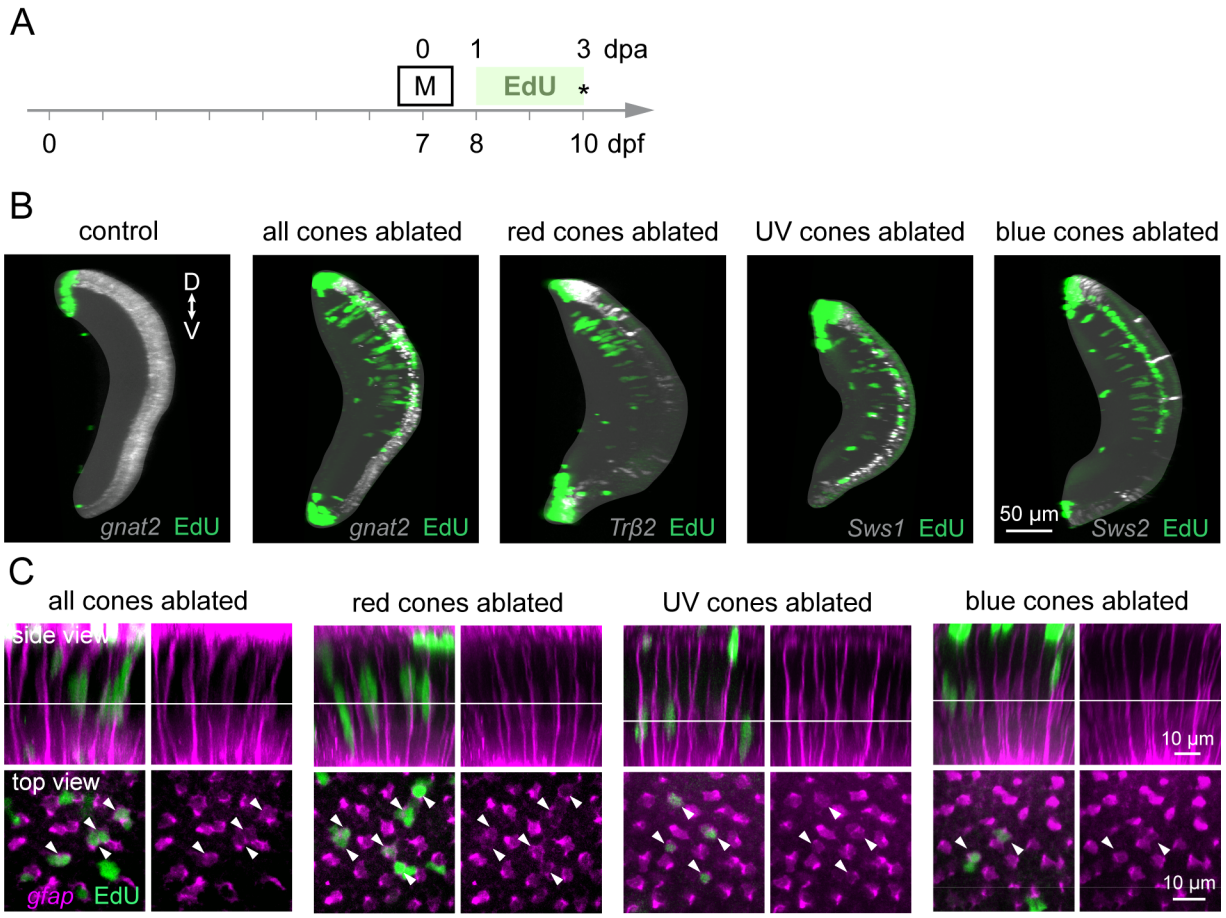

Figure 4.8 Müller glia undergo cell division in response to death of cone populations, regardless of type.

(**A**) Timeline demonstrates the timing of EdU application after Met treatment in cone-ablated fish. Asterisk denotes the age at which larvae were fixed for analysis. (**B**) Orthogonal rotations of whole retinas from 10 dpf control and cone-ablated fish treated with EdU: *Tg(gnat2:nfsBmCherry)* (all cones), *Tg(trβ2:G4VP16; UAS:nfsBmCherry)* (red cones), *Tg(sws1:nfsBmCherry)* (UV cones), and *Tg(sws2:nfsBmCherry)* (blue cones). ("D" dorsal, "V" ventral). (**C**) Cone-ablated fish were crossed with *Tg(gfap:GFP)* to visualize Müller glia for EdU colabeling. (Side view) Orthogonal rotations showing Müller glia together with EdU labeling. (Top view) *En face* views of EdU-positive nuclei, taken at the level indicated in the side views. Arrowheads mark EdU-positive nuclei.

4.6 Tables

Table 4.1. Comparison of cone population densities in control fish and fish with cone regeneration.

		all ablated				R ablated	UV ablated	B ablated
		regen. R	regen. G	regen. UV	regen. B	regen. R	regen. UV	regen. B
Control	R	0.004				0.004		
	G		0.004					
	UV			0.004			0.00007	
	B				0.004			0.0007

P-values from pair-wise comparisons of cone densities in 15 dpf unablated, control fish versus regenerated (EdU-positive) cone densities in Met-treated fish, Wilcoxon-Mann-Whitney rank sum test. ("Regen." regenerated, "R" red cones, "G" green cones, "UV" UV cones, and "B" blue cones).

Chapter 5. Conclusions and future directions

Summary and conclusions

In this thesis, I explored the fidelity with which neuronal circuits are reconstructed after regeneration in the retina. I first tracked the acquisition of type-specific morphological features and stereotypic wiring patterns in a population of identified bipolar cells during retinal development. This provided insight into the cellular strategies that different neurons deploy to acquire their specific morphological characteristics, and furthermore established a framework for investigating the maturation and synaptic integration of regenerated cells of the same type. Confocal reconstruction of regenerated bipolar cell circuits demonstrated that regenerated cells in general retained the capacity to acquire type-specific features, and to form synapses at their dendritic and axonal compartments. However, quantitative analysis revealed that regenerated bipolar cells failed to precisely pattern their dendritic and axonal connections. In the second portion of this thesis, I investigated the specificity of retinal regeneration in replacing lost neuron populations. I ablated the entire population of a single cone type, or all four cone types together, in larval zebrafish. Fate-mapping the regenerated cone populations across these experimental conditions suggested that regenerative neurogenesis is non-specific, but biased toward the cognate cone type. Collectively, these results suggest that regenerating circuits may be restricted in their capacity to engage developmental mechanisms that precisely pattern neuronal cell composition and connectivity in the retina.

Several questions remain to be addressed to fully explore the restorative potential and intrinsic limitations of retinal regeneration. I discuss these topics below, and propose experiments that may provide groundwork for future progress.

Control of neuronal cell fate and number in regeneration

The observation that regeneration is biased toward replacing the specific cell types that were lost after damage indicates that cell fate choice during regeneration is not random. However, whether the regulation of progenitor cell fate choice during regeneration involves developmental mechanisms is unclear. Neurogenesis and cell fate specification are sequential processes during initial retinal development, which involve both progressive changes in progenitor competence, as

well as a changing molecular environment over time. The significance of the timing and sequence of changes in progenitor competence and extracellular signaling during development is still under investigation. It remains possible that regenerating circuits can exert control over the composition of newborn cells, whether or not this process involves the same sequential mechanisms as in development.

How is regeneration biased toward particular cell fates? A tempting hypothesis is that dying neurons activate a signal that biases retinal progenitor cells toward their cell fate. This signal could be a positive, instructive cue. Alternatively, neuron loss may cease the production of a signal that normally inhibits progenitors from adopting specific cell fates. In either case, single-cell sequencing of retinal progenitor cells in the regenerating retina may provide candidate cues. The extent to which cell death plays an instructive role in modulating cell fate can be further addressed by analyzing the progeny and molecular profiles of retinal progenitor cells that are produced in the absence of retinal injury. This could be achieved by stimulating Müller glia in intact retinas; for example, Wan et al. induced the dedifferentiation of Müller glia and the production of progenitor cells by applying HB-EGF in undamaged zebrafish retinas (Wan et al., 2012). Further, isolation of retinal progenitor cells for single-cell analysis can be achieved by utilizing transgenic lines that temporarily or indelibly label Müller glia-derived cells (Bernardos and Raymond, 2006; Bernardos et al., 2007; Fausett et al., 2008; Fimbel et al., 2007; Ramachandran et al., 2010).

Instead, the observed cell fate biases may simply be an effect of differences in neuronal survival across cone ablation conditions. Death of regenerated cells may also contribute to the failure of both ablated cone and bipolar cell types to completely recover their population densities. These possibilities can begin to be addressed by assessing the identity of regenerated cells at even earlier stages, and assaying for cone apoptosis during and after cone regeneration. If death of a substantial number of regenerated cones indeed occurs, it would be of interest to gain further understanding of why regenerated cones of specific types are more prone to death than others under certain cone ablation conditions. Assessing the level of apoptosis and the identity of dying cells after ablating specific cone populations in combination (e.g., ablating red and UV cones, red and blue, or UV and blue cones together) may provide insight to that end.

Regulation of biased connectivity during development and in regeneration

Previous work has provided mechanistic insight into how biased photoreceptor connectivity is regulated during zebrafish retinal development. Yoshimatsu et al. (2014) demonstrated that contact with the primary cone partner inhibited synaptogenesis with the secondary partner during assembly of the H3 HC circuit. Manipulation of neurotransmission from each partner type suggested that this heterosynaptic regulation is dependent upon the activity of the primary input, but not of the secondary input (Yoshimatsu et al., 2014). Whether red cones play a similar role in regulating ON T2 bipolar cell synaptogenesis with green cones is an open possibility. I could approach this question as done previously, by manipulating the relative abundances of the primary and secondary cone partner types, and by selectively silencing each cone type. For example, if a reduction in the availability of red cones resulted in ON T2 bipolar cells contacting more green cones than usual, this observation would indicate that contact with red cones influences synaptogenesis with green cones. Subsequent experiments to reduce or increase neurotransmission from red cones would reveal whether the influence of red cone-bipolar cell contact is mediated by transmission from red cones.

Exploration of the role of activity-dependent factors that mediate synaptic organization during development may help explain why regenerated circuits in mature systems recover some, but not all elements of stereotypic connectivity. For example, if manipulation of red cone neurotransmission during retinal development results in decreased synaptogenesis with *xfz43* bipolar cells, this observation may help explain why regenerated *xfz43* bipolar cells show reduced red cone contact. This would indicate that red cones undergo physiological changes that affect their neurotransmission after loss of *xfz43* postsynaptic partners. However, it was also previously demonstrated that in the zebrafish H3 HC circuit, altered neurotransmission from the primary cone partner did not affect H3 HC synaptogenesis with this partner type (Yoshimatsu et al., 2014). Moving forward, the role of neurotransmission from red and other cone type partners in regulating bipolar cell synaptogenesis during regeneration could be addressed by experiments comparing the electrophysiological responses of cones in developing, mature, and bipolar cell-ablated retinas. To that end, tethering genetically-encoded calcium indicators to presynaptic proteins can serve as a reporter of synaptic activity *in vivo*. SyGCaMP is a fluorescent calcium sensor that is targeted to presynaptic domains via fusion with synaptophysin (Dreosti et al., 2009). Calcium influx is required for neurotransmitter release; as such, increased fluorescence

over baseline levels is indicative of increased neurotransmission in cells expressing SyGCaMP. I could thus gauge photoreceptor transmission by measuring changes in the frequency and duration of calcium influx (as indicated by changes in fluorescence over time) in response to physiologically appropriate light stimuli. For example, I could target SyGCaMP expression to red cones alone using the *trβ2* promoter, and in these animals I would use red light stimuli to illicit neurotransmission from red cones. For a given stimulus condition, differences in the average frequency, duration, or amplitude of calcium influx in red cones from bipolar cell-ablated retinas compared to those from intact retinas may suggest alterations in cone neurotransmission in regenerating bipolar cell circuits.

Identifying the specific molecular factors that mediate the assembly of cone connectivity in the bipolar cell circuit during zebrafish development will provide important mechanistic insight. In the future, this could be achieved by performing molecular profiling of each cone partner type and bipolar cells. Techniques for single-cell sequencing are rapidly advancing (Yang et al., 2015), and retinal neurons in the zebrafish are especially amenable to isolation due to the availability of transgenic tools in this system. In point of fact, two transgenic lines were recently developed in the Wong lab, *vsx1* and *vsx2*, each of which labels a single bipolar cell type and drives FP expression in all cells of that type (data not published). In contrast with *xfz43*, the specificity of the *vsx1* and *vsx2* lines will be advantageous in discerning cell type-specific transcriptional programs. Ultimately, identification of molecular mediators of synaptic connectivity during development will provide candidates for investigation in regenerating circuits. My observations of regenerated connectivity already provide some guidance as to what kinds of signaling mechanisms are likely to be disrupted during *xfz43* bipolar cell regeneration. I observed that regenerated cells maintain, if not expand their dendritic arbors compared to control cells. This indicates that a lack of dendritic growth is unlikely to explain the inability of regenerated ON T2 and OFF bipolar cells to bias their connectivity toward red cones. Similarly, regenerated cells of each type formed approximately the appropriate total number of dendritic tips, suggesting that regenerated bipolar cells maintain the ability to form synapses in general. Together, these observations lead me to hypothesize that regenerated cells show disrupted cone biases as a result of alterations in molecular signaling that regulates synaptogenesis with specific partner types.

Other important elements of stereotypic synaptic connectivity

The experiments presented here are amongst the first to investigate the specificity and quantitative accuracy of neuronal wiring in regenerated circuits. These are important insights because specialized neuronal functions depend upon stereotypic features of wiring such as partner selection, synaptic number, and synaptic allocation amongst partner types.

However, my characterization of *xfz43* bipolar cell axonal connectivity was incomplete due to a lack of tools to visualize individual cells of specific retinal ganglion cell and amacrine cell types. This problem can be remedied in the future by the development of additional immunohistochemical markers or transgenic lines. Realizing a more complete analysis of bipolar cell output connectivity will also pave the way for work to examine the potential interdependence between dendritic and axonal connectivity in developing and regenerating bipolar cell circuits. Research is already underway to this end in adult zebrafish. Using the *vsx1* and *vsx2* transgenic lines, which label disparate ON bipolar cell types, we are investigating the influence of altered dendritic connectivity on the output connectivity of identified bipolar cells. Preliminary results suggest that prolonged loss of photoreceptor partners results in an increase in ribbon number, similar to my observations of regenerated bipolar cells that have reconnected with intact photoreceptors.

In addition to the identity and number of its presynaptic partners, several other wiring features shape an individual neuron's response to afferent input, including its expression of specific neurotransmitter receptors. For example, the dendrites of ON bipolar cells express "sign-inverting" glutamate receptors that cause bipolar cell hyperpolarization upon glutamate binding; these receptors include excitatory amino acid transporters that couple to a chloride current, or metabotropic glutamate receptors (Connaughton and Nelson, 2000; Wong et al., 2005). *xfz43* bipolar cells thus may demonstrate an additional level of synaptic organization by expressing specific glutamate receptors or transporters at their dendritic synapses with particular cone types. Future work can address this possibility by combining immunohistochemistry to label specific glutamate receptor subsets together with super-resolution microscopy to visualize their localization at specific contact sites on bipolar cell dendrites. Indeed, preliminary examinations of *vsx1* and *vsx2* bipolar cells in adult zebrafish show that these bipolar cell types express different glutamate receptors and transporters at their dendritic tips, depending on whether the tip contacts a rod or a cone.

Further, as mentioned previously, the dendrites of bipolar cells form either invaginating or basal contacts with cones. The structure of the dendritic ending as well as its relative distance from the ribbon release site likely influences neuronal encoding (DeVries et al., 2006). For this work, I only assessed invaginating dendritic contacts because they were more amenable to resolution by light microscopy. Nonetheless, basal contacts can be unambiguously identified in the future using electron microscopy. These experiments will also necessitate a technique for distinguishing *xfz43* bipolar cells from surrounding bipolar cell types in order to target electron microscopy analysis to the appropriate area. This could include the near-infrared-branding method used in correlative light and electron microscopy (Bishop et al., 2011; Bleckert et al., 2013). Together, analyses of glutamate receptor expression and dendritic structural specializations will lend greater insight into the specialized functions of individual bipolar cells, in both intact and regenerated circuits.

Recovery of function at the level of individual neurons and higher visual processing

The ultimate goal of neuronal circuit repair is to recover functionality. I found that regenerated populations failed to fully repopulate the retina, after ablating a subset of bipolar cells or specific cone types. The failure of regenerated cones to repopulate the retina is likely to have considerable functional consequences. Each cone type is fundamental to the generation of different chromatic channels in the visual pathway, and color vision directly contributes to specific visual behaviors in zebrafish. For example, the optomotor response, whereby zebrafish visually track a whole-field moving stimulus in order to swim in the direction of the perceived motion, appears to depend upon red and green color vision, but not UV or blue color perception (Orger and Baier, 2005). The impacts of incomplete cone regeneration will thus likely manifest at the level of higher visual processing and behavior, as well as at the level of downstream neurons in the retina. By contrast, it is more difficult to predict the functional consequences of incomplete bipolar cell regeneration. Unlike cones, distinct bipolar cell types have yet to be linked to specific visually-guided behaviors in zebrafish. It is possible that the reduction in *xfz43* bipolar cell density after regeneration may not have significant effects on global visual function. Nonetheless, recent work has provided evidence that secondary (non-photoreceptor) retinal neurons can have a measurable effect on distinct behaviors. Barker and Baier (2015) laser-ablated a subset of retinal ganglion cells that project to the AF7 area of the tectum (Barker and

Baier, 2015), which has been shown to mediate prey capture behavior in larval zebrafish (Semmelhack et al., 2014). Using calcium imaging, they observed that retinal ganglion cell ablation altered the size tuning of the postsynaptic tectal neurons, a response feature that underlies accurate detection of prey size. Incomplete repopulation of *xfz43* bipolar cells could similarly alter the response properties of their postsynaptic partners, potentially as a consequence of decreased synaptic drive. However, my ability to investigate this possibility is impeded by the paucity of tools to target individual cells of specific retinal ganglion cell and amacrine cell types for electrophysiological recording or functional imaging in the zebrafish retina.

My observation that regenerated bipolar cells form both dendritic and axonal presynaptic specializations suggest, but do not conclusively demonstrate, that regenerated bipolar cells are capable of functional integration with surrounding circuitry. Functional recovery has been shown at the level of visually-guided behavior (Sherpa et al., 2008) and neuronal population responses in regenerated zebrafish retinas (Lindsey and Powers, 2007; Mensinger and Powers, 1999), but the relationship between the connectivity and physiology of individual cells in regenerated circuits remains unexplored. Dissecting this relationship is fundamental to determining whether regenerated neurons directly contribute to functional recovery, or whether recovery is largely due to adaptation in the surviving circuitry.

The bipolar cell circuit in particular is poised for functional analysis. The photoreceptor-bipolar cell synapse is the first synapse in the pathway of visual sensation, and light input can be easily manipulated under physiological conditions. While single-cell recordings have been performed previously in retinal slices from adult zebrafish (Connaughton and Nelson, 2000), it will likely be challenging to record from individual cells in the retinas of larval zebrafish, which are far smaller. Indeed, current work in the Wong lab is utilizing the *vsx1* and *vsx2* transgenic lines mentioned previously to perform electrophysiological analysis of bipolar cells after cone regeneration in adults. Functional assessment is still possible in larvae, however, as the Lagnado group has optimized the use of genetically-encoded calcium indicators to assess bipolar cell synaptic activity in larval zebrafish *in vivo* (Dreosti et al., 2009; Rosa et al., 2016). In the future, crossing calcium indicator transgenic lines with the *xfz43* or other bipolar cell-labeling lines will facilitate characterization of bipolar cell activity in intact and regenerated retinas in larval fish. Post-hoc analysis of the cone connectivity of bipolar cells targeted for functional analysis will

provide insight into the relative impact of different stereotypic wiring features on bipolar cell response properties.

SUPPLEMENTAL MOVIES

Movie S1. Identification of invaginating contacts from BC dendrites in red or green cone axon terminals.

The movie shows a reconstruction of an entire *xfz43* ON T2 BC (yellow) together with the axons of red (magenta and green) and green cones (green only), as visualized in the background of *Tg(trβ2:Tomato)* together with immunostaining at 20 dpf. The BC dendrite arbor and cone axons are visualized in a thin plane by digitally slicing away the rest of the image. As the image of the BC rotates from a side to top view, the red and green cone channels are flashed on.

BIBLIOGRAPHY

Agathocleous, M., and Harris, W.A. (2009). From progenitors to differentiated cells in the vertebrate retina. Annu. Rev. Cell Dev. Biol. *25*, 45–69.

Allison, W.T., Barthel, L.K., Skebo, K.M., Takechi, M., Kawamura, S., and Raymond, P.A. (2010). Ontogeny of cone photoreceptor mosaics in zebrafish. J. Comp. Neurol. *518*, 4182–4195.

Altshuler, D., Lo Turco, J.J., Rush, J., and Cepko, C. (1993). Taurine promotes the differentiation of a vertebrate retinal cell type in vitro. Dev. Camb. Engl. *119*, 1317–1328.

Arlotta, P., and Berninger, B. (2014). Brains in metamorphosis: reprogramming cell identity within the central nervous system. Curr. Opin. Neurobiol. *27*, 208–214.

Arshavsky, V.Y., and Burns, M.E. (2012). Photoreceptor signaling: supporting vision across a wide range of light intensities. J. Biol. Chem. *287*, 1620–1626.

Austin, C.P., Feldman, D.E., Ida, J.A., and Cepko, C.L. (1995). Vertebrate retinal ganglion cells are selected from competent progenitors by the action of Notch. Dev. Camb. Engl. *121*, 3637–3650.

Baier, H. (2013). Synaptic laminae in the visual system: molecular mechanisms forming layers of perception. Annu. Rev. Cell Dev. Biol. *29*, 385–416.

Bailey, T.J., Fossum, S.L., Fimbel, S.M., Montgomery, J.E., and Hyde, D.R. (2010). The inhibitor of phagocytosis, O-phospho-L-serine, suppresses Müller glia proliferation and cone cell regeneration in the light-damaged zebrafish retina. Exp. Eye Res. *91*, 601–612.

Barber, A.C., Hippert, C., Duran, Y., West, E.L., Bainbridge, J.W.B., Warre-Cornish, K., Luhmann, U.F.O., Lakowski, J., Sowden, J.C., Ali, R.R., et al. (2013). Repair of the degenerate retina by photoreceptor transplantation. Proc. Natl. Acad. Sci. *110*, 354–359.

Barker, A.J., and Baier, H. (2015). Sensorimotor decision making in the zebrafish tectum. Curr. Biol. CB *25*, 2804–2814.

Bassett, E.A., and Wallace, V.A. (2012). Cell fate determination in the vertebrate retina. Trends Neurosci. *35*, 565–573.

Battista, A.G., Ricatti, M.J., Pafundo, D.E., Gautier, M.A., and Faillace, M.P. (2009). Extracellular ADP regulates lesion-induced in vivo cell proliferation and death in the zebrafish retina. J. Neurochem. *111*, 600–613.

Becker, C.G., and Becker, T. (2015). Neuronal Regeneration from Ependymo-Radial Glial Cells: Cook, Little Pot, Cook! Dev. Cell *32*, 516–527.

Belliveau, M.J., Young, T.L., and Cepko, C.L. (2000). Late retinal progenitor cells show intrinsic limitations in the production of cell types and the kinetics of opsin synthesis. J. Neurosci. Off. J. Soc. Neurosci. *20*, 2247–2254.

Berg, D.A., Kirkham, M., Beljajeva, A., Knapp, D., Habermann, B., Ryge, J., Tanaka, E.M., and Simon, A. (2011). Efficient regeneration by activation of neurogenesis in homeostatically quiescent regions of the adult vertebrate brain. Development *138*, 180–180.

Berg, D.A., Belnoue, L., Song, H., and Simon, A. (2013). Neurotransmitter-mediated control of neurogenesis in the adult vertebrate brain. Dev. Camb. Engl. *140*, 2548–2561.

Bernardos, R.L., and Raymond, P.A. (2006). GFAP transgenic zebrafish. Gene Expr. Patterns GEP *6*, 1007–1013.

Bernardos, R.L., Barthel, L.K., Meyers, J.R., and Raymond, P.A. (2007). Late-stage neuronal progenitors in the retina are radial Müller glia that function as retinal stem cells. J. Neurosci. Off. J. Soc. Neurosci. *27*, 7028–7040.

Bishop, D., Nikić, I., Brinkoetter, M., Knecht, S., Potz, S., Kerschensteiner, M., and Misgeld, T. (2011). Near-infrared branding efficiently correlates light and electron microscopy. Nat. Methods *8*, 568–570.

Blackshaw, S., Harpavat, S., Trimarchi, J., Cai, L., Huang, H., Kuo, W.P., Weber, G., Lee, K., Fraioli, R.E., Cho, S.-H., et al. (2004). Genomic Analysis of Mouse Retinal Development. PLOS Biol *2*, e247.

Bleckert, A., and Wong, R.O.L. (2011). Identifying roles for neurotransmission in circuit assembly: insights gained from multiple model systems and experimental approaches. BioEssays News Rev. Mol. Cell. Dev. Biol. *33*, 61–72.

Bleckert, A., Parker, E.D., Kang, Y., Pancaroglu, R., Soto, F., Lewis, R., Craig, A.M., and Wong, R.O.L. (2013). Spatial relationships between GABAergic and glutamatergic synapses on the dendrites of distinct types of mouse retinal ganglion cells across development. PloS One *8*, e69612.

Bodnarenko, S.R., and Chalupa, L.M. (1993). Stratification of ON and OFF ganglion cell dendrites depends on glutamate-mediated afferent activity in the developing retina. Nature *364*, 144–146.

Bodnarenko, S.R., Jeyarasasingam, G., and Chalupa, L.M. (1995). Development and regulation of dendritic stratification in retinal ganglion cells by glutamate-mediated afferent activity. J. Neurosci. Off. J. Soc. Neurosci. *15*, 7037–7045.

Boije, H., MacDonald, R.B., and Harris, W.A. (2014). Reconciling competence and transcriptional hierarchies with stochasticity in retinal lineages. Curr. Opin. Neurobiol. *27*, 68–74.

Boye, S.E., Boye, S.L., Lewin, A.S., and Hauswirth, W.W. (2013). A Comprehensive Review of Retinal Gene Therapy. Mol. Ther. *21*, 509–519.

Braisted, J.E., and Raymond, P.A. (1992). Regeneration of dopaminergic neurons in goldfish retina. Dev. Camb. Engl. *114*, 913–919.

Bringmann, A., and Wiedemann, P. (2012). Müller glial cells in retinal disease. Ophthalmol. J. Int. Ophtalmol. Int. J. Ophthalmol. Z. Für Augenheilkd. *227*, 1–19.

Bringmann, A., Pannicke, T., Grosche, J., Francke, M., Wiedemann, P., Skatchkov, S.N., Osborne, N.N., and Reichenbach, A. (2006). Müller cells in the healthy and diseased retina. Prog. Retin. Eye Res. *25*, 397–424.

Bringmann, A., Iandiev, I., Pannicke, T., Wurm, A., Hollborn, M., Wiedemann, P., Osborne, N.N., and Reichenbach, A. (2009). Cellular signaling and factors involved in Müller cell gliosis: neuroprotective and detrimental effects. Prog. Retin. Eye Res. *28*, 423–451.

Brzezinski, J.A., and Reh, T.A. (2015). Photoreceptor cell fate specification in vertebrates. Dev. Camb. Engl. *142*, 3263–3273.

Cayouette, M., Barres, B.A., and Raff, M. (2003). Importance of intrinsic mechanisms in cell fate decisions in the developing rat retina. Neuron *40*, 897–904.

Cayouette, M., Poggi, L., and Harris, W.A. (2006). Lineage in the vertebrate retina. Trends Neurosci. *29*, 563–570.

Connaughton, V.P., and Nelson, R. (2000). Axonal stratification patterns and glutamate-gated conductance mechanisms in zebrafish retinal bipolar cells. J. Physiol. *524 Pt 1*, 135–146.

Cuenca, N., Pinilla, I., Sauvé, Y., Lu, B., Wang, S., and Lund, R.D. (2004). Regressive and reactive changes in the connectivity patterns of rod and cone pathways of P23H transgenic rat retina. Neuroscience *127*, 301–317.

Curado, S., Anderson, R.M., Jungblut, B., Mumm, J., Schroeter, E., and Stainier, D.Y.R. (2007). Conditional targeted cell ablation in zebrafish: A new tool for regeneration studies. Dev. Dyn. *236*, 1025–1035.

Davison, J.M., Akitake, C.M., Goll, M.G., Rhee, J.M., Gosse, N., Baier, H., Halpern, M.E., Leach, S.D., and Parsons, M.J. (2007). Transactivation from Gal4-VP16 transgenic insertions for tissue-specific cell labeling and ablation in zebrafish. Dev. Biol. *304*, 811–824.

Del Bene, F., Wehman, A.M., Link, B.A., and Baier, H. (2008). Regulation of neurogenesis by interkinetic nuclear migration through an apical-basal notch gradient. Cell *134*, 1055–1065.

DeVries, S.H., Li, W., and Saszik, S. (2006). Parallel Processing in Two Transmitter Microenvironments at the Cone Photoreceptor Synapse. Neuron *50*, 735–748.

D'Orazi, F.D., Suzuki, S.C., and Wong, R.O. (2014). Neuronal remodeling in retinal circuit assembly, disassembly, and reassembly. Trends Neurosci. *37*, 594–603.

Dowling, J.E. (1970). Organization of vertebrate retinas. Invest. Ophthalmol. *9*, 655–680.

Dowling, J.E. (2012). The Retina: An Approachable Part of the Brain, Revised Edition (Cambridge, Mass: Belknap Press).

Dreosti, E., Odermatt, B., Dorostkar, M.M., and Lagnado, L. (2009). A genetically encoded reporter of synaptic activity in vivo. Nat. Methods *6*, 883–889.

Duan, X., Krishnaswamy, A., De la Huerta, I., and Sanes, J.R. (2014). Type II Cadherins Guide Assembly of a Direction-Selective Retinal Circuit. Cell *158*, 793–807.

Dunn, F.A., and Wong, R.O.L. (2012). Diverse Strategies Engaged in Establishing Stereotypic Wiring Patterns among Neurons Sharing a Common Input at the Visual System's First Synapse. J. Neurosci. *32*, 10306–10317.

Easter Jr, S.S., and Nicola, G.N. (1996). The development of vision in the zebrafish (Danio rerio). Dev. Biol. *180*, 646–663.

Ebrey, T., and Koutalos, Y. (2001). Vertebrate photoreceptors. Prog. Retin. Eye Res. *20*, 49–94.

Euler, T., Haverkamp, S., Schubert, T., and Baden, T. (2014). Retinal bipolar cells: elementary building blocks of vision. Nat. Rev. Neurosci. *15*, 507–519.

Fadool, J.M. (2003). Development of a rod photoreceptor mosaic revealed in transgenic zebrafish. Dev. Biol. *258*, 277–290.

Fadool, J., and Dowling, J. (2008). Zebrafish: A model system for the study of eye genetics. Prog. Retin. Eye Res. *27*, 89–110.

Fausett, B.V., and Goldman, D. (2006). A role for alpha1 tubulin-expressing Müller glia in regeneration of the injured zebrafish retina. J. Neurosci. *26*, 6303–6313.

Fausett, B.V., Gumerson, J.D., and Goldman, D. (2008). The proneural basic helix-loop-helix gene ascl1a is required for retina regeneration. J. Neurosci. Off. J. Soc. Neurosci. *28*, 1109–1117.

Fimbel, S.M., Montgomery, J.E., Burket, C.T., and Hyde, D.R. (2007). Regeneration of Inner Retinal Neurons after Intravitreal Injection of Ouabain in Zebrafish. J. Neurosci. *27*, 1712–1724.

Fischer, A.J., and Reh, T.A. (2001). Müller glia are a potential source of neural regeneration in the postnatal chicken retina. Nat. Neurosci. *4*, 247–252.

Frade, J.M., Rodríguez-Tébar, A., and Barde, Y.A. (1996). Induction of cell death by endogenous nerve growth factor through its p75 receptor. Nature *383*, 166–168.

Fraser, B., DuVal, M.G., Wang, H., and Allison, W.T. (2013). Regeneration of cone photoreceptors when cell ablation is primarily restricted to a particular cone subtype. PloS One *8*, e55410.

Freund, C.L., Gregory-Evans, C.Y., Furukawa, T., Papaioannou, M., Looser, J., Ploder, L., Bellingham, J., Ng, D., Herbrick, J.A., Duncan, A., et al. (1997). Cone-rod dystrophy due to mutations in a novel photoreceptor-specific homeobox gene (CRX) essential for maintenance of the photoreceptor. Cell *91*, 543–553.

Furukawa, T., Morrow, E.M., and Cepko, C.L. (1997). Crx, a novel otx-like homeobox gene, shows photoreceptor-specific expression and regulates photoreceptor differentiation. Cell *91*, 531–541.

Gaillard, A., Prestoz, L., Dumartin, B., Cantereau, A., Morel, F., Roger, M., and Jaber, M. (2007). Reestablishment of damaged adult motor pathways by grafted embryonic cortical neurons. Nat. Neurosci. *10*, 1294–1299.

Gardette, R., Crepel, F., Alvarado-Mallart, R.M., and Sotelo, C. (1990). Fate of grafted embryonic Purkinje cells in the cerebellum of the adult "Purkinje cell degeneration" mutant mouse. II. Development of synaptic responses: an in vitro study. J. Comp. Neurol. *295*, 188–196.

Godinho, L., Williams, P.R., Claassen, Y., Provost, E., Leach, S.D., Kamermans, M., and Wong, R.O.L. (2007). Nonapical Symmetric Divisions Underlie Horizontal Cell Layer Formation in the Developing Retina In Vivo. Neuron *56*, 597–603.

Goldman, D. (2014). Müller glial cell reprogramming and retina regeneration. Nat. Rev. Neurosci. *15*, 431–442.

Gomes, F.L.A.F., Zhang, G., Carbonell, F., Correa, J.A., Harris, W.A., Simons, B.D., and Cayouette, M. (2011). Reconstruction of rat retinal progenitor cell lineages in vitro reveals a surprising degree of stochasticity in cell fate decisions. Development *138*, 227–235.

González-Hoyuela, M., Barbas, J.A., and Rodríguez-Tébar, A. (2001). The autoregulation of retinal ganglion cell number. Dev. Camb. Engl. *128*, 117–124.

Gorsuch, R.A., and Hyde, D.R. (2014). Regulation of Müller glial dependent neuronal regeneration in the damaged adult zebrafish retina. Exp. Eye Res. *123*, 131–140.

Grimaldi, P., Carletti, B., and Rossi, F. (2005). Neuronal replacement and integration in the rewiring of cerebellar circuits. Brain Res. Brain Res. Rev. *49*, 330–342.

Grueber, W.B., and Sagasti, A. (2010). Self-avoidance and Tiling: Mechanisms of Dendrite and Axon Spacing. Cold Spring Harb. Perspect. Biol. *2*, a001750.

Hamel, C. (2006). Retinitis pigmentosa. Orphanet J. Rare Dis. *1*, 40.

Hashimoto, K., and Kano, M. (2013). Synapse elimination in the developing cerebellum. Cell. Mol. Life Sci. *70*, 4667–4680.

Hatakeyama, J., Tomita, K., Inoue, T., and Kageyama, R. (2001). Roles of homeobox and bHLH genes in specification of a retinal cell type. Development *128*, 1313–1322.

Haverkamp, S., Grünert, U., and Wässle, H. (2000). The cone pedicle, a complex synapse in the retina. Neuron *27*, 85–95.

Haverkamp, S., Michalakis, S., Claes, E., Seeliger, M.W., Humphries, P., Biel, M., and Feigenspan, A. (2006). Synaptic plasticity in CNGA3(-/-) mice: cone bipolar cells react on the missing cone input and form ectopic synapses with rods. J. Neurosci. Off. J. Soc. Neurosci. *26*, 5248–5255.

Haverkamp, S., Specht, D., Majumdar, S., Zaidi, N.F., Brandstätter, J.H., Wasco, W., Wässle, H., and Tom Dieck, S. (2008). Type 4 OFF cone bipolar cells of the mouse retina express calsenilin and contact cones as well as rods. J. Comp. Neurol. *507*, 1087–1101.

He, J., Zhang, G., Almeida, A.D., Cayouette, M., Simons, B.D., and Harris, W.A. (2012). How variable clones build an invariant retina. Neuron *75*, 786–798.

Hertz, J., Qu, B., Hu, Y., Patel, R.D., Valenzuela, D.A., and Goldberg, J.L. (2014). Survival and Integration of Developing and Progenitor-Derived Retinal Ganglion Cells Following Transplantation. Cell Transplant. *23*, 855–872.

Hitchcock, P.F., Lindsey Myhr, K.J., Easter, S.S., Mangione-Smith, R., and Jones, D.D. (1992). Local regeneration in the retina of the goldfish. J. Neurobiol. *23*, 187–203.

Holt, C.E., Bertsch, T.W., Ellis, H.M., and Harris, W.A. (1988). Cellular determination in the Xenopus retina is independent of lineage and birth date. Neuron *1*, 15–26.

Hoon, M., Okawa, H., Della Santina, L., and Wong, R.O.L. (2014). Functional architecture of the retina: Development and disease. Prog. Retin. Eye Res. *42*, 44–84.

Hu, M., and Easter Jr., S.S. (1999). Retinal Neurogenesis: The Formation of the Initial Central Patch of Postmitotic Cells. Dev. Biol. *207*, 309–321.

Inoue, T., Hojo, M., Bessho, Y., Tano, Y., Lee, J.E., and Kageyama, R. (2002). Math3 and NeuroD regulate amacrine cell fate specification in the retina. Dev. Camb. Engl. *129*, 831–842.

Isshiki, T., Pearson, B., Holbrook, S., and Doe, C.Q. (2001). Drosophila neuroblasts sequentially express transcription factors which specify the temporal identity of their neuronal progeny. Cell *106*, 511–521.

Johnson, R.E., and Kerschensteiner, D. (2014). Retrograde Plasticity and Differential Competition of Bipolar Cell Dendrites and Axons in the Developing Retina. Curr. Biol. *24*, 2301–2306.

Karl, M.O., and Reh, T.A. (2010). Regenerative medicine for retinal diseases: activating endogenous repair mechanisms. Trends Mol. Med. *16*, 193–202.

Karl, M.O., Hayes, S., Nelson, B.R., Tan, K., Buckingham, B., and Reh, T.A. (2008). Stimulation of neural regeneration in the mouse retina. Proc. Natl. Acad. Sci. U. S. A. *105*, 19508–19513.

Kassen, S.C., Thummel, R., Campochiaro, L.A., Harding, M.J., Bennett, N.A., and Hyde, D.R. (2009). CNTF induces photoreceptor neuroprotection and Müller glial cell proliferation through two different signaling pathways in the adult zebrafish retina. Exp. Eye Res. *88*, 1051–1064.

Keeley, P.W., and Reese, B.E. (2010). Role of afferents in the differentiation of bipolar cells in the mouse retina. J. Neurosci. Off. J. Soc. Neurosci. *30*, 1677–1685.

Kerschensteiner, D., Morgan, J.L., Parker, E.D., Lewis, R.M., and Wong, R.O.L. (2009). Neurotransmission selectively regulates synapse formation in parallel circuits in vivo. Nature *460*, 1016–1020.

Kim, H., Shin, J., Kim, S., Poling, J., Park, H.-C., and Appel, B. (2008). Notch-regulated oligodendrocyte specification from radial glia in the spinal cord of zebrafish embryos. Dev. Dyn. Off. Publ. Am. Assoc. Anat. *237*, 2081–2089.

Kim, I.-J., Zhang, Y., Meister, M., and Sanes, J.R. (2010). Laminar restriction of retinal ganglion cell dendrites and axons: subtype-specific developmental patterns revealed with transgenic markers. J. Neurosci. Off. J. Soc. Neurosci. *30*, 1452–1462.

Kim, J., Wu, H.-H., Lander, A.D., Lyons, K.M., Matzuk, M.M., and Calof, A.L. (2005). GDF11 controls the timing of progenitor cell competence in developing retina. Science *308*, 1927–1930.

Kroehne, V., Freudenreich, D., Hans, S., Kaslin, J., and Brand, M. (2011). Regeneration of the adult zebrafish brain from neurogenic radial glia-type progenitors. Development *138*, 4831–4841.

Kuscha, V., Barreiro-Iglesias, A., Becker, C.G., and Becker, T. (2012a). Plasticity of tyrosine hydroxylase and serotonergic systems in the regenerating spinal cord of adult zebrafish. J. Comp. Neurol. *520*, 933–951.

Kuscha, V., Frazer, S.L., Dias, T.B., Hibi, M., Becker, T., and Becker, C.G. (2012b). Lesion-induced generation of interneuron cell types in specific dorsoventral domains in the spinal cord of adult zebrafish. J. Comp. Neurol. *520*, 3604–3616.

Kwan, K.M., Fujimoto, E., Grabher, C., Mangum, B.D., Hardy, M.E., Campbell, D.S., Parant, J.M., Yost, H.J., Kanki, J.P., and Chien, C.-B. (2007). The Tol2kit: a multisite gateway-based construction kit for Tol2 transposon transgenesis constructs. Dev. Dyn. Off. Publ. Am. Assoc. Anat. *236*, 3088–3099.

Lenkowski, J.R., and Raymond, P.A. (2014). Müller glia: Stem cells for generation and regeneration of retinal neurons in teleost fish. Prog. Retin. Eye Res. *40*, 94–123.

Li, Y.N., Matsui, J.I., and Dowling, J.E. (2009). Specificity of the horizontal cell-photoreceptor connections in the zebrafish (*Danio rerio*) retina. J. Comp. Neurol. *516*, 442–453.

Li, Y.N., Tsujimura, T., Kawamura, S., and Dowling, J.E. (2012). Bipolar cell-photoreceptor connectivity in the zebrafish (Danio rerio) retina. J. Comp. Neurol. *520*, 3786–3802.

Lindmark, D.G., and Muller, M. (1976). Antitrichomonad Action, Mutagenicity, and Reduction of Metronidazole and Other Nitroimidazoles. Antimicrob. Agents Chemother. *10*, 476–482.

Lindsey, A.E., and Powers, M.K. (2007). Visual behavior of adult goldfish with regenerating retina. Vis. Neurosci. *24*, 247–255.

MacLaren, R.E., Pearson, R.A., MacNeil, A., Douglas, R.H., Salt, T.E., Akimoto, M., Swaroop, A., Sowden, J.C., and Ali, R.R. (2006). Retinal repair by transplantation of photoreceptor precursors. Nature *444*, 203–207.

Magavi, S.S.P., and Lois, C. (2008). Transplanted neurons form both normal and ectopic projections in the adult brain. Dev. Neurobiol. *68*, 1527–1537.

Maier, W., and Wolburg, H. (1979). Regeneration of the goldfish retina after exposure to different doses of ouabain. Cell Tissue Res. *202*, 99–118.

Marquardt, T. (2003). Transcriptional control of neuronal diversification in the retina. Prog. Retin. Eye Res. *22*, 567–577.

Masland, R.H. (2012). The Neuronal Organization of the Retina. Neuron *76*, 266–280.

Maslim, J., and Stone, J. (1986). Synaptogenesis in the retina of the cat. Brain Res. *373*, 35–48.

Mataruga, A., Kremmer, E., and Müller, F. (2007). Type 3a and type 3b OFF cone bipolar cells provide for the alternative rod pathway in the mouse retina. J. Comp. Neurol. *502*, 1123–1137.

Mears, A.J., Kondo, M., Swain, P.K., Takada, Y., Bush, R.A., Saunders, T.L., Sieving, P.A., and Swaroop, A. (2001). Nrl is required for rod photoreceptor development. Nat. Genet. *29*, 447–452.

Mensinger, A.F., and Powers, M.K. (1999). Visual function in regenerating teleost retina following cytotoxic lesioning. Vis. Neurosci. *16*, 241–251.

Michelsen, K.A., Acosta-Verdugo, S., Benoit-Marand, M., Espuny-Camacho, I., Gaspard, N., Saha, B., Gaillard, A., and Vanderhaeghen, P. (2015). Area-Specific Reestablishment of Damaged Circuits in the Adult Cerebral Cortex by Cortical Neurons Derived from Mouse Embryonic Stem Cells. Neuron *85*, 982–997.

Montgomery, J.E., Parsons, M.J., and Hyde, D.R. (2010). A novel model of retinal ablation demonstrates that the extent of rod cell death regulates the origin of the regenerated zebrafish rod photoreceptors. J. Comp. Neurol. *518*, 800–814.

Morgan, J.L., Soto, F., Wong, R.O.L., and Kerschensteiner, D. (2011). Development of Cell Type-Specific Connectivity Patterns of Converging Excitatory Axons in the Retina. Neuron *71*, 1014–1021.

Morris, A.C., Scholz, T.L., Brockerhoff, S.E., and Fadool, J.M. (2008). Genetic dissection reveals two separate pathways for rod and cone regeneration in the teleost retina. Dev. Neurobiol. *68*, 605–619.

Mu, X., Fu, X., Sun, H., Liang, S., Maeda, H., Frishman, L.J., and Klein, W.H. (2005). Ganglion cells are required for normal progenitor- cell proliferation but not cell-fate determination or patterning in the developing mouse retina. Curr. Biol. CB *15*, 525–530.

Mumm, J.S., Williams, P.R., Godinho, L., Koerber, A., Pittman, A.J., Roeser, T., Chien, C.-B., Baier, H., and Wong, R.O.L. (2006). In vivo imaging reveals dendritic targeting of laminated afferents by zebrafish retinal ganglion cells. Neuron *52*, 609–621.

Nagashima, M., Barthel, L.K., and Raymond, P.A. (2013). A self-renewing division of zebrafish Müller glial cells generates neuronal progenitors that require N-cadherin to regenerate retinal neurons. Dev. Camb. Engl. *140*, 4510–4521.

Negishi, K., Sugawara, K., Shinagawa, S., Teranishi, T., Kuo, C.H., and Takasaki, Y. (1991a). Induction of immunoreactive proliferating cell nuclear antigen (PCNA) in goldfish retina following intravitreal injection with tunicamycin. Brain Res. Dev. Brain Res. *63*, 71–83.

Negishi, K., Stell, W.K., Teranishi, T., Karkhanis, A., Owusu-Yaw, V., and Takasaki, Y. (1991b). Induction of proliferating cell nuclear antigen (PCNA)-immunoreactive cells in goldfish retina following intravitreal injection with 6-hydroxydopamine. Cell. Mol. Neurobiol. *11*, 639–659.

Nelson, B.R., Ueki, Y., Reardon, S., Karl, M.O., Georgi, S., Hartman, B.H., Lamba, D.A., and Reh, T.A. (2011). Genome-wide analysis of Müller glial differentiation reveals a requirement for Notch signaling in postmitotic cells to maintain the glial fate. PloS One *6*, e22817.

Nelson, C.M., Ackerman, K.M., O'Hayer, P., Bailey, T.J., Gorsuch, R.A., and Hyde, D.R. (2013). Tumor necrosis factor-alpha is produced by dying retinal neurons and is required for Muller glia proliferation during zebrafish retinal regeneration. J. Neurosci. Off. J. Soc. Neurosci. *33*, 6524–6539.

Oh, E.C.T., Khan, N., Novelli, E., Khanna, H., Strettoi, E., and Swaroop, A. (2007). Transformation of cone precursors to functional rod photoreceptors by bZIP transcription factor NRL. Proc. Natl. Acad. Sci. U. S. A. *104*, 1679–1684.

Ohsawa, R., and Kageyama, R. (2008). Regulation of retinal cell fate specification by multiple transcription factors. Brain Res. *1192*, 90–98.

Okawa, H., Della Santina, L., Schwartz, G.W., Rieke, F., and Wong, R.O.L. (2014). Interplay of cell-autonomous and nonautonomous mechanisms tailors synaptic connectivity of converging axons in vivo. Neuron *82*, 125–137.

Ooto, S., Akagi, T., Kageyama, R., Akita, J., Mandai, M., Honda, Y., and Takahashi, M. (2004). Potential for neural regeneration after neurotoxic injury in the adult mammalian retina. Proc. Natl. Acad. Sci. U. S. A. *101*, 13654–13659.

Orger, M.B., and Baier, H. (2005). Channeling of red and green cone inputs to the zebrafish optomotor response. Vis. Neurosci. *22*, 275–281.

Pearson, B.J., and Doe, C.Q. (2003). Regulation of neuroblast competence in Drosophila. Nature *425*, 624–628.

Pearson, R.A., Barber, A.C., Rizzi, M., Hippert, C., Xue, T., West, E.L., Duran, Y., Smith, A.J., Chuang, J.Z., Azam, S.A., et al. (2012). Restoration of vision after transplantation of photoreceptors. Nature *485*, 99–103.

Peng, Y.W., Hao, Y., Petters, R.M., and Wong, F. (2000). Ectopic synaptogenesis in the mammalian retina caused by rod photoreceptor-specific mutations. Nat. Neurosci. *3*, 1121–1127.

Peterson, R.E., Fadool, J.M., Mcclintock, J., and Linser, P.J. (2001). Müller cell differentiation in the zebrafish neural retina: Evidence of distinct early and late stages in cell maturation. J. Comp. Neurol. *429*, 530–540.

Poché, R.A., Raven, M.A., Kwan, K.M., Furuta, Y., Behringer, R.R., and Reese, B.E. (2008). Somal positioning and dendritic growth of horizontal cells are regulated by interactions with homotypic neighbors. Eur. J. Neurosci. *27*, 1607–1614.

Pollak, J., Wilken, M.S., Ueki, Y., Cox, K.E., Sullivan, J.M., Taylor, R.J., Levine, E.M., and Reh, T.A. (2013). ASCL1 reprograms mouse Muller glia into neurogenic retinal progenitors. Dev. Camb. Engl. *140*, 2619–2631.

Powell, C., Grant, A.R., Cornblath, E., and Goldman, D. (2013). Analysis of DNA methylation reveals a partial reprogramming of the Müller glia genome during retina regeneration. Proc. Natl. Acad. Sci. *110*, 19814–19819.

Powell, C., Cornblath, E., Elsaeidi, F., Wan, J., and Goldman, D. (2016). Zebrafish Müller glia-derived progenitors are multipotent, exhibit proliferative biases and regenerate excess neurons. Sci. Rep. *6*, 24851.

Qin, Z., Kidd, A.R., Thomas, J.L., Poss, K.D., Hyde, D.R., Raymond, P.A., and Thummel, R. (2011). FGF signaling regulates rod photoreceptor cell maintenance and regeneration in zebrafish. Exp. Eye Res. *93*, 726–734.

Qiu, F., Jiang, H., and Xiang, M. (2008). A comprehensive negative regulatory program controlled by Brn3b to ensure ganglion cell specification from multipotential retinal precursors. J. Neurosci. Off. J. Soc. Neurosci. *28*, 3392–3403.

Ramachandran, R., Reifler, A., Parent, J.M., and Goldman, D. (2010). Conditional gene expression and lineage tracing of tuba1a expressing cells during zebrafish development and retina regeneration. J. Comp. Neurol. *518*, 4196–4212.

Ramachandran, R., Zhao, X.-F., and Goldman, D. (2011). Ascl1a/Dkk/beta-catenin signaling pathway is necessary and glycogen synthase kinase-3beta inhibition is sufficient for zebrafish retina regeneration. Proc. Natl. Acad. Sci. U. S. A. *108*, 15858–15863.

Ramachandran, R., Zhao, X.-F., and Goldman, D. (2012). Insm1a-mediated gene repression is essential for the formation and differentiation of Müller glia-derived progenitors in the injured retina. Nat. Cell Biol. *14*, 1013–1023.

Randlett, O., MacDonald, R.B., Yoshimatsu, T., Almeida, A.D., Suzuki, S.C., Wong, R.O., and Harris, W.A. (2013). Cellular Requirements for Building a Retinal Neuropil. Cell Rep. *3*, 282–290.

Rao, R.C., Hennig, A.K., Malik, M.T.A., Chen, D.F., and Chen, S. (2011). Epigenetic regulation of retinal development and disease. J. Ocul. Biol. Dis. Infor. *4*, 121–136.

Rapaport, D.H., Patheal, S.L., and Harris, W.A. (2001). Cellular competence plays a role in photoreceptor differentiation in the developing Xenopus retina. J. Neurobiol. *49*, 129–141.

Raven, M.A., Eglen, S.J., Ohab, J.J., and Reese, B.E. (2003). Determinants of the exclusion zone in dopaminergic amacrine cell mosaics. J. Comp. Neurol. *461*, 123–136.

Raven, M.A., Oh, E.C.T., Swaroop, A., and Reese, B.E. (2007). Afferent control of horizontal cell morphology revealed by genetic respecification of rods and cones. J. Neurosci. Off. J. Soc. Neurosci. *27*, 3540–3547.

Raymond, P.A., and Barthel, L.K. (2004). A moving wave patterns the cone photoreceptor mosaic array in the zebrafish retina. Int. J. Dev. Biol. *48*, 935–945.

Raymond, P.A., Reifler, M.J., and Rivlin, P.K. (1988). Regeneration of goldfish retina: rod precursors are a likely source of regenerated cells. J. Neurobiol. *19*, 431–463.

Raymond, P.A., Barthel, L.K., Bernardos, R.L., and Perkowski, J.J. (2006). Molecular characterization of retinal stem cells and their niches in adult zebrafish. BMC Dev. Biol. *6*, 36.

Reese, B.E., Raven, M.A., and Stagg, S.B. (2005). Afferents and homotypic neighbors regulate horizontal cell morphology, connectivity, and retinal coverage. J. Neurosci. Off. J. Soc. Neurosci. *25*, 2167–2175.

Reh, T.A. (1987). Cell-specific regulation of neuronal production in the larval frog retina. J. Neurosci. Off. J. Soc. Neurosci. *7*, 3317–3324.

Reh, T.A., and Kljavin, I.J. (1989). Age of differentiation determines rat retinal germinal cell phenotype: induction of differentiation by dissociation. J. Neurosci. Off. J. Soc. Neurosci. *9*, 4179–4189.

Reh, T.A., and Tully, T. (1986). Regulation of tyrosine hydroxylase-containing amacrine cell number in larval frog retina. Dev. Biol. *114*, 463–469.

Reimer, M.M., Sorensen, I., Kuscha, V., Frank, R.E., Liu, C., Becker, C.G., and Becker, T. (2008). Motor Neuron Regeneration in Adult Zebrafish. J. Neurosci. *28*, 8510–8516.

Roesch, K., Jadhav, A.P., Trimarchi, J.M., Stadler, M.B., Roska, B., Sun, B.B., and Cepko, C.L. (2008). The transcriptome of retinal Müller glial cells. J. Comp. Neurol. *509*, 225–238.

Rosa, J.M., Ruehle, S., Ding, H., and Lagnado, L. (2016). Crossover Inhibition Generates Sustained Visual Responses in the Inner Retina. Neuron *90*, 308–319.

Salbreux, G., Barthel, L.K., Raymond, P.A., and Lubensky, D.K. (2012). Coupling Mechanical Deformations and Planar Cell Polarity to Create Regular Patterns in the Zebrafish Retina. PLOS Comput Biol *8*, e1002618.

Sanes, J.R., and Lichtman, J.W. (1999). Development of the vertebrate neuromuscular junction. Annu. Rev. Neurosci. *22*, 389–442.

Sanes, J.R., and Yamagata, M. (2009). Many Paths to Synaptic Specificity. Annu. Rev. Cell Dev. Biol. *25*, 161–195.

Schindelin, J., Arganda-Carreras, I., Frise, E., Kaynig, V., Longair, M., Pietzsch, T., Preibisch, S., Rueden, C., Saalfeld, S., Schmid, B., et al. (2012). Fiji: an open-source platform for biological-image analysis. Nat. Methods *9*, 676–682.

Schmidt, K.-G., Bergert, H., and Funk, R.H.. (2008). Neurodegenerative Diseases of the Retina and Potential for Protection and Recovery. Curr. Neuropharmacol. *6*, 164–178.

Schmitt, E.A., and Dowling, J.E. (1999). Early retinal development in the zebrafish, Danio rerio: Light and electron microscopic analyses. J. Comp. Neurol. *404*, 515–536.

Schroeter, E.H., Wong, R.O., and Gregg, R.G. (2006). In vivo development of retinal ON-bipolar cell axonal terminals visualized in nyx:: MYFP transgenic zebrafish. Vis. Neurosci. *23*, 833–843.

Semmelhack, J.L., Donovan, J.C., Thiele, T.R., Kuehn, E., Laurell, E., and Baier, H. (2014). A dedicated visual pathway for prey detection in larval zebrafish. eLife *3*.

Sernagor, E., Eglen, S., Harris, B., and Wong, R. (2006). Retinal Development (Cambridge: Cambridge University Press).

Sherpa, T., Fimbel, S.M., Mallory, D.E., Maaswinkel, H., Spritzer, S.D., Sand, J.A., Li, L., Hyde, D.R., and Stenkamp, D.L. (2008). Ganglion cell regeneration following whole-retina destruction in zebrafish. Dev. Neurobiol. *68*, 166–181.

Singh, M.S., Charbel Issa, P., Butler, R., Martin, C., Lipinski, D.M., Sekaran, S., Barnard, A.R., and MacLaren, R.E. (2013). Reversal of end-stage retinal degeneration and restoration of visual function by photoreceptor transplantation. Proc. Natl. Acad. Sci. *110*, 1101–1106.

Skaggs, K., Goldman, D., and Parent, J.M. (2014). Excitotoxic brain injury in adult zebrafish stimulates neurogenesis and long-distance neuronal integration: Brain Repair in Adult Zebrafish. Glia *62*, 2061–2079.

Sotelo, C., Alvarado-Mallart, R.M., Gardette, R., and Crepel, F. (1990). Fate of grafted embryonic Purkinje cells in the cerebellum of the adult "Purkinje cell degeneration" mutant mouse. I. Development of reciprocal graft-host interactions. J. Comp. Neurol. *295*, 165–187.

Soto, F., Ma, X., Cecil, J.L., Vo, B.Q., Culican, S.M., and Kerschensteiner, D. (2012). Spontaneous Activity Promotes Synapse Formation in a Cell-Type-Dependent Manner in the Developing Retina. J. Neurosci. *32*, 5426–5439.

Stenkamp, D.L. (2011). The rod photoreceptor lineage of teleost fish. Prog. Retin. Eye Res. *30*, 395–404.

Stenkamp, D.L., and Cameron, D.A. (2002). Cellular pattern formation in the retina: retinal regeneration as a model system. Mol. Vis. *8*, 280–293.

Sterling, P., and Matthews, G. (2005). Structure and function of ribbon synapses. Trends Neurosci. *28*, 20–29.

Strettoi, E., Mears, A.J., and Swaroop, A. (2004). Recruitment of the rod pathway by cones in the absence of rods. J. Neurosci. Off. J. Soc. Neurosci. *24*, 7576–7582.

Suzuki, S.C., Bleckert, A., Williams, P.R., Takechi, M., Kawamura, S., and Wong, R.O.L. (2013). Cone photoreceptor types in zebrafish are generated by symmetric terminal divisions of dedicated precursors. Proc. Natl. Acad. Sci. *110*, 15109–15114.

Swaroop, A., Kim, D., and Forrest, D. (2010). Transcriptional regulation of photoreceptor development and homeostasis in the mammalian retina. Nat. Rev. Neurosci. *11*, 563–576.

Takechi, M., Hamaoka, T., and Kawamura, S. (2003). Fluorescence visualization of ultraviolet-sensitive cone photoreceptor development in living zebrafish. FEBS Lett. *553*, 90–94.

Takechi, M., Seno, S., and Kawamura, S. (2008). Identification of cis-Acting Elements Repressing Blue Opsin Expression in Zebrafish UV Cones and Pineal Cells. J. Biol. Chem. *283*, 31625–31632.

Thomas, J.L., Nelson, C.M., Luo, X., Hyde, D.R., and Thummel, R. (2012). Characterization of multiple light damage paradigms reveals regional differences in photoreceptor loss. Exp. Eye Res. *97*, 105–116.

Thomas, J.L., Ranski, A.H., Morgan, G.W., and Thummel, R. (2016). Reactive gliosis in the adult zebrafish retina. Exp. Eye Res. *143*, 98–109.

Thummel, R., Kassen, S.C., Enright, J.M., Nelson, C.M., Montgomery, J.E., and Hyde, D.R. (2008). Characterization of Müller glia and neuronal progenitors during adult zebrafish retinal regeneration. Exp. Eye Res. *87*, 433–444.

Tian, N., and Copenhagen, D.R. (2003). Visual stimulation is required for refinement of ON and OFF pathways in postnatal retina. Neuron *39*, 85–96.

Tsukamoto, Y., and Omi, N. (2014). Some OFF bipolar cell types make contact with both rods and cones in macaque and mouse retinas. Front. Neuroanat. *8*, 105.

Turner, D.L., and Cepko, C.L. (1987). A common progenitor for neurons and glia persists in rat retina late in development. Nature *328*, 131–136.

Turner, D.L., Snyder, E.Y., and Cepko, C.L. (1990). Lineage-independent determination of cell type in the embryonic mouse retina. Neuron *4*, 833–845.

Ueki, Y., Wilken, M.S., Cox, K.E., Chipman, L., Jorstad, N., Sternhagen, K., Simic, M., Ullom, K., Nakafuku, M., and Reh, T.A. (2015). Transgenic expression of the proneural transcription factor Ascl1 in Müller glia stimulates retinal regeneration in young mice. Proc. Natl. Acad. Sci. U. S. A. *112*, 13717–13722.

Venugopalan, P., Wang, Y., Nguyen, T., Huang, A., Muller, K.J., and Goldberg, J.L. (2016). Transplanted neurons integrate into adult retinas and respond to light. Nat. Commun. *7*, 10472.

Vihtelic, T.S., and Hyde, D.R. (2000). Light-induced rod and cone cell death and regeneration in the adult albino zebrafish (Danio rerio) retina. J. Neurobiol. *44*, 289–307.

Vihtelic, T.S., Doro, C.J., and Hyde, D.R. (1999). Cloning and characterization of six zebrafish photoreceptor opsin cDNAs and immunolocalization of their corresponding proteins. Vis. Neurosci. *16*, 571–585.

Vitorino, M., Jusuf, P.R., Maurus, D., Kimura, Y., Higashijima, S.-I., and Harris, W.A. (2009). Vsx2 in the zebrafish retina: restricted lineages through derepression. Neural Develop. *4*, 14.

Wan, L. (2005). Two ribeye Genes in Teleosts: The Role of Ribeye in Ribbon Formation and Bipolar Cell Development. J. Neurosci. *25*, 941–949.

Wan, J., Ramachandran, R., and Goldman, D. (2012). HB-EGF is necessary and sufficient for Müller glia dedifferentiation and retina regeneration. Dev. Cell *22*, 334–347.

Wan, Y., Almeida, A.D., Rulands, S., Chalour, N., Muresan, L., Wu, Y., Simons, B.D., He, J., and Harris, W.A. (2016). The ciliary marginal zone of the zebrafish retina: clonal and time-lapse analysis of a continuously growing tissue. Dev. Camb. Engl. *143*, 1099–1107.

Wang, Y., Dakubo, G.D., Thurig, S., Mazerolle, C.J., and Wallace, V.A. (2005). Retinal ganglion cell-derived sonic hedgehog locally controls proliferation and the timing of RGC development in the embryonic mouse retina. Dev. Camb. Engl. *132*, 5103–5113.

Wässle, H. (2004). Parallel processing in the mammalian retina. Nat. Rev. Neurosci. *5*, 747–757.

Watanabe, T., and Raff, M.C. (1990). Rod photoreceptor development in vitro: intrinsic properties of proliferating neuroepithelial cells change as development proceeds in the rat retina. Neuron *4*, 461–467.

Wetts, R., and Fraser, S.E. (1988). Multipotent precursors can give rise to all major cell types of the frog retina. Science *239*, 1142–1145.

Wong, K.Y., and Dowling, J.E. (2005). Retinal bipolar cell input mechanisms in giant danio. III. ON-OFF bipolar cells and their color-opponent mechanisms. J. Neurophysiol. *94*, 265–272.

Wong, K.Y., Cohen, E.D., and Dowling, J.E. (2005). Retinal bipolar cell input mechanisms in giant danio. II. Patch-clamp analysis of on bipolar cells. J. Neurophysiol. *93*, 94–107.

Wood, J.P.M., McCord, R.J., and Osborne, N.N. (1997). Retinal protein kinase C. Neurochem. Int. *30*, 119–136.

Yang, H.-J., Ratnapriya, R., Cogliati, T., Kim, J.-W., and Swaroop, A. (2015). Vision from next generation sequencing: multi-dimensional genome-wide analysis for producing gene regulatory networks underlying retinal development, aging and disease. Prog. Retin. Eye Res. *46*, 1–30.

Yoshimatsu, T., Williams, P.R., D'Orazi, F.D., Suzuki, S.C., Fadool, J.M., Allison, W.T., Raymond, P.A., and Wong, R.O. (2014). Transmission from the dominant input shapes the stereotypic ratio of photoreceptor inputs onto horizontal cells. Nat. Commun. *5*.

Yoshimatsu, T., D'Orazi, F.D., Gamlin, C.R., Suzuki, S.C., Suli, A., Kimelman, D., Raible, D.W., and Wong, R.O. (2016). Presynaptic partner selection during retinal circuit reassembly varies with timing of neuronal regeneration in vivo. Nat. Commun. *7*, 10590.

Young, T.L., and Cepko, C.L. (2004). A role for ligand-gated ion channels in rod photoreceptor development. Neuron *41*, 867–879.

Zhao, X.-F., Ellingsen, S., and Fjose, A. (2009). Labelling and targeted ablation of specific bipolar cell types in the zebrafish retina. BMC Neurosci. *10*, 107.